FABRICATION AND WETTABILITY STUDY OF METAL OXIDE PHOTOCATALYST FILMS FOR OIL-WATER SEPARATION

BY

MUHAMMAD SUBKHI SADULLAH

A Thesis Presented to the
DEANSHIP OF GRADUATE STUDIES

KING FAHD UNIVERSITY OF PETROLEUM & MINERALS

DHAHRAN, SAUDI ARABIA

In Partial Fulfillment of the
Requirements for the Degree of

MASTER OF SCIENCE

In

PHYSICS

KING FAHD UNIVERSITY OF PETROLEUM & MINERALS

DHAHRAN- 31261, SAUDI ARABIA

DEANSHIP OF GRADUATE STUDIES

This thesis, written by **MUHAMMAD SUBKHI SADULLAH** under the direction his thesis advisor and approved by his thesis committee, has been presented and accepted by the Dean of Graduate Studies, in partial fulfillment of the requirements for the degree of **MASTER OF SCIENCE IN PHYSICS.**

M. A. Gondal

Prof. M.A. Gondal
(Advisor)

Dr. Abdul-Aziz Al-Jalal
Department Chairman

Dr. Z.H. Yamani
(Member)

Dr. Salam A. Zummo
Dean of Graduate Studies

Dr. M.M. Faiz
(Member)

5/6/14

Date

عمادة الدراسات العليا
DEANSHIP OF GRADUATE STUDIES

Dedication

This thesis work is dedicated to my parents and family, who have spent years raising me with their kind love and care, who support and believe in my dreams.

ACKNOWLEDGMENTS

All praise is for Allah SWT who gave me strength, power, health to finish this thesis work. I acknowledge that without His will and power, I would not be able to achieve what I have accomplished in my life. In addition, I would also like to thank all people who helped me to complete my M.S degree in physics at KFUPM.

Firstly, I am pleased to thank to my thesis advisor, Prof. Mohammed A. Gondal for his guidance, patience, motivation, and encouragement to become a good scientist., I feel proud to be his student and I am thankful to him for his guidance, instigating novel ideas, never ending support, long discussions and patience which lead me to accomplish successfully my goals and pursuits under his supervision.

I would also like to thank Dr. Zain H. Yamani for giving me inspiration about many aspects including teaching, research, and attitude. I am very happy that he was one of my thesis committee members.

My deep thanks to Dr. Mohammed M. Faiz for his attention and constructive feedback as a committee member in my thesis research.

I would like to extend my thanks to the chairman of the Physics Department for giving me a chance to join KFUPM and work in strong research and scientific oriented conducive environment.

Special thanks are due to Mr. Dastageer for technical help and guidance during my stay at laser research group and developing writing skills.

I thank to Center for Clean Water and Clean Energy at MIT & KFUPM for supporting my visit to MIT during my thesis work. I also would like to thank to our collaborators at MIT, Prof. John Lienhard, Prof. Kripa K. Varanasi, Ronan McGovern, Adam Wiener, and especially Prof. Gareth H. McKinley and Divya Panchanathan who supervised me during my visit.

Many thanks to all Laser Research Group members including Dr. Muhammad Ashraf Ali, Mr. Rashid G. Siddique, Mr. Pillai and Mr. Xiaofeng Chang.

I would like to thank to faculty members who taught me physics courses, Dr. Thamer Al-Aithan, Dr. Fatah Z. Khiari, Dr. Khalil A. Ziq, and Dr. Mohammed S. Abdulmonem.

I also thank to my fellow students in the Department including Talal, Yasin, Hasan, Faris, Ismail, Salman, Hendi. And I praise Allah for acquainting me with noble personalities like Ammar Musa and Hussam Walwil.

Special thanks to my roommate Yusri Syahrir, to the predecessors of Indonesian students at KFUPM, Muhammad Iqbal, Fuady and Dr. Farid Fadhilah and to current students at KFUPM, Fandi, Syarif, Ghazi, Sudibyo, Bagus, Rhoma and everyone else.

The last but not the least, I would like to thank to my all family members(father, mother, brother and sisters) for their patience, love, support and prayers during these years.

TABLE OF CONTENTS

LIST OF TABLES

LIST OF FIGURES

ABSTRACT

Full Name : Muhammad Subkhi Sadullah

Thesis Title : Fabrication and Wettability Study of Metal Oxide Photocatalyst Films for Oil-Water Separation

Major Field : Physics

Date of Degree : May, 2014

This thesis work mainly concerned about the study of physical phenomena of oil-water separation using superhydrophilic material. For this purpose, photocatalytic materials were used due to their excellent superhydrophilic nature. Oil water separation has attracted the interest of many researchers from different fields due to its importance for industrial application and environmental issue such as waste water treatment and oil spills. In this work, superhydrophilic-superoleophobic mesh has been applied as an effective gravity driven oil-water separator having high separation efficiency, 98.4 ± 0.6%. Such mesh was fabricated using single step spray deposition of metal oxides such as TiO_2, ZnO, and WO_3 nanoparticle dispersion on stainless steel mesh. This preparation method allowed us to investigate in detail and study the physical phenomena which govern the oil-water separation without dealing with delicate surface texturing process. We modeled the mechanism of oil-water separation through an approximation of the intrusion pressure. We found that the superhydrophilicity and underwater superoleophobicity were essential but not sufficient for oil water separation application. The presence of adsorbed water on the surface of the mesh and capillary bridge of water are found to be the determining factors for the oil water separation.

ملخص الرسالة

الاسم الكامل : محمد صبحى سعدالله

عنوان الرسالة: إنتاج ودراسة تبلل أغشيه رقيقه من أكاسيد المعادن ذات تحفيز ضوئي وإستخدامها لفصل الزيت عن الماء

التخصص: فيزياء

تاريخ الدرجة العلمية: مايو 2014

هذه الأطروحه العلميه تهدف بشكل أساسي إلى دراسة الظواهر الفيزيائية لفصل الزيت عن الماء باستخدام مواد ذات قابليه عاليه للماء. لهذا الغرض، استخدمت مواد لها خاصية التحفيز الضوئي نظرا لأن قابليتها للماء عاليه وممتازه . إن فصل الماء عن الزيت قد جذب اهتمام العديد من الباحثين من مختلف المجالات نظرا لأهميته في التطبيقات الصناعية والمشاكل البيئية مثل معالجة مياه الصرف الصحي وتسرب النفط. في هذه الدراسه، تم توظيف شبكة من- مواد ذات قابليه عاليه للماء وأخرى ذات رفض كبير للماء- كفاصل للماء عن الزيت بشكل فعال والذي يمتلك كفاءة فصل عالية, 98.4 ± 0.6٪. هذه الشبكة تم تصنيعها باستخدام تقنية ترسيب الرذاذ بخطوة واحدة من أكاسيد المعادن مثل التيتانيا، أكسيد الزنك، وأكسيد التنجستن ذات الجسيمات المتناهية الصغر(نانويه) على شبكة من الفولاذ المقاوم للصدأ. إن طريقة التحضير هذه تسمح لنا بفحص ودراسة الظواهر الفيزيائية التي تحكم فصل الزيت عن الماء بالتفصيل ودون التعامل مع عملية التركيب السطحي الدقيق. لقد قمنا بعمل نموذج أوتمثيل لآلية فصل الماء عن الزيت من خلال تقريب ضغط الإسترساب. وجدنا أن القابليه العاليه والرفض الكبير للماء ضرورية لكنها غير كافية لتطبيق فصل الماء عن الزيت. إن وجود الماء على سطح الشبكه والجسرالدقيق من الماء يشكلان العوامل المحددة لفصل الزيت عن الماء.

CHAPTER 1

INTRODUCTION

Wetting phenomena have been studied extensively due to numerous application in industrial and environmental applications. Surfaces having extreme wettability such as superhydrophilic (water-loving) or superhydrophobic (water-hating) surfaces are of interest to many research groups due to the richness of the physics behind the interfacial phenomena and the promising applications. In this thesis, we harnessed superhydrophilic surfaces for oil-water separation application.

1.1 Challenge in the Treatment of Oil-Water Mixture

Petrochemical industries and environmental protection agencies encounter challenges in the science and technology of oil water separation, because an enormous amount of oil easily gets blended into the water and the water bodies during the production processes, by accidents and by human activities. The oil drilling companies inject a large amount of water into oil wells to recover maximum amount of oil from the reservoirs, and this leads to the production of huge quantity of oil mixed water (produced water) reaching the production wells [1,2]. In early days, this produced water was disposed in large evaporation ponds, which is now deemed environmentally unacceptable, as the produced water is considered as industrial waste. Moreover, with the growing scarcity of water globally, the oil producers are now bound to recycle this produced water [3,4].

In addition, oil spills have become a dangerous environmental issue. Every year millions of barrels of crude oil and refined petroleum products are intentionally and accidentally spilled into the seas and oceans by tankers, offshore platforms, drilling rigs, oil cargo ships and of course by wars and sabotage [5], causing extensive damage to marine ecosystem. In addition, the cleaning up of the oil spill is quite laborious, costly, time consuming and depends on many factors like nature of oil, temperature, weather and geographical location etc. Development of an effective and reliable oil water separation method is essential to meet the ecological, economical, and industrial needs and challenges.

1.1.1 Conventional Oil-Water Separation Methods

Many oil-water separation methods such as air flotation, bioremediation, skimming, centrifuging and dispersing have been developed using combined physical, chemical, and biological approaches. Certain mechanical processes are often needed to assist the process of the oil-water separation [6]. These methods have been widely used for industrial application as well as for oil spill cleanup to prevent further environmental damage. In some extreme cases, controlled burning were applied for removing oil from the body of water.

One of the most prominent method for removing oil from oil-water mixture is oil skimming. The system consists of a large tank for containing oil-water mixture, engines, rotational belt for collecting the oil, trimmer for removing the adsorbed oil from the belt and oil container for collecting the separated oil. This system works by taking advantage of the stickiness of the oil and the oil-wettable nature of the belt as an oil collector. Oil

from the mixture will be adsorbed by the belt and conveyed to the trimmer. The oil will then be removed by the trimmer and transfered to the oil collector [6].

Another useful technique is gravity separation method which works by stabilizing the oil-water mixture by resting the mixture undisturbed. Oil-water mixture will settle if it is given enough time. This method can be applied for larger quantity of oil-water mixture. In fact, it needs very large volume for the separation process since oil-water mixture normally needs some time to settle down. The more viscous the oil, the longer it needs to settle down. The separating process harnessing the difference of the specific gravity between oil and water so that oil will be accumulated on top for the collecting mechanism. The system is also equipped with mechanism which allows passive sedimentation of the other contaminants, producing much cleaner water to come out from the outlet [6].

Similarly to the gravity separation process, dissolved air flotation method is also used for oil-water separation and wastewater treatment in general. Using this method, not only oil but also suspended water pollutants such as solids and debris will be brought to the surface for further removal mechanism. In the treatment process, micro air bubbles are sprayed inside the wastewater basin. These micro bubbles will then adheres with the pollutants and increase the buoyant force of the pollutants so that it rises to the surface of water. The floating pollutants then can be removed easily by skimming mechanism [6].

Those oil-water separation methods have been widely used as industrial processes. However, because these methods require long separation process, high power consumption and large area of deployment, considerable amount of cost is needed for

developing this facility. In addition, the risk of oil fouling may reduce the separation efficiency and increase the cost for the maintenance. Another drawback is the flaw in the separation performance. Some amount of water is often found in the oil phase after the separation which is dangerous since even small amount of water can lead to engine failure in combustion process [7]. Therefore, smart, cost effective and excellent performance oil-water separation method is needed to satisfy the need for the waste water treatment in industry and for oil spill cleanup.

1.1.2 Oil-Water Separation Based on the Surface Wettability of Material

Since oil-water mixture is an interfacial phenomenon, an effective method for the separation can be approached by studying the interfacial properties of a matter. By using a material which has preferential wetting, i.e. the material which is wettable by either oil or water phase and non-wettable by the other, one can remove one phase from the mixture and leave the other. Such method can be accomplished using so called hydrophobic-oleophilic materials. This type of materials is wettable by oil but non-wettable by water. Two separation methods can be applied by using this type of material; that is, oil adsorbing and oil filtering method. This type of material is relatively easy to prepare, by reducing the solid surface energy of the material through some surface modification such that the surface energy of the material is smaller than the surface tension of water (γ_{wv} ~ 72 dyne/m) but larger than the surface tension of oil (γ_{ov} ~ 30 dyne/m) [8-12].

Hydrophobic-oleophilic materials are available in nature in form of rubber, kapok, milkweed, cotton and wool [13]. These materials have been proposed as effective media for oil removal without further modification [14-16]. Synthetic materials are also widely

used as this purpose. For example, silica aerogel can be used for an excellent oil adsorbent due to its oloephilicity and its very large surface area. It was reported that silica aerogel can adsorb oil as much as 237 times of its weigh [17,18]. Using surface modifications to increase the hydrophobicity, inexpensive materials such as polyurethane foam and filter paper can also be used as oil adsorbents [19]. The biggest limitation of this method is that it can only remove limited amount of oil. After adsorbing a certain amount of oil phase, the surface will saturate and the adsorbing performance significantly decreased. If the cleaning or recycling mechanism is not available, the materials become secondary pollutant and need further treatment. This is also a great disadvantage if the fabrication of the material is costly.

A more clever method is using this type of material for oil filtration by applying it to porous material such as fabric or mesh. This filtration method allows oil phase to pass through the filter and retains water phase at the same time. Feng et al. firstly reported the use of polytetrafluoroethylene (PTFE) or Teflon coating on stainless steel mesh for oil water separation [11]. Later, Wang et al. used electrochemical deposition to deposit copper nanoparticle on copper mesh to create superhydrophobic-superoleophilic surface for oil water separation [12]. However, this type of separation process is prone to fail since the specific gravity of the oil is generally smaller than that of the water. In this case, water phase tend to accumulate in the lower position and form a column of water during the separation process and block the oil phase from permeating to the other face of the filter. This method is more difficult to be implemented in industrial application.

Another oil water separation method which involve preferential wetting is using hydrophilic-oleophobic material. This type of material has the opposite wetting properties

of the material discussed earlier. By applying this material on porous material, such as stainless steel mesh, one can achieve gravity driven oil-water separation where water will be permeated through the mesh while the oil will be retained on the other face of the mesh. Since the material is wettable by water, the water permeation through the mesh comes naturally without any assistance from external forces. However, this type of material is very rare and difficult to prepare [20]. Theoretically, this type of surface cannot be achieved just by lowering the surface energy of the materials. Usually, this type of material is a superomniphobic material (nonwettable by any type of liquid) which can respond to external trigger such as electric field, temperature, humidity, and the pH of the environment [21-23]. This type of material opens new gate of controllable oil-water separation.

1.1.3 Capillarity Based Gravity Driven Oil-Water Separation Using Superhydrophilic and Underwater Superoleophobic Materials

Both filtration methods, i.e. using hydrophobic-oleophilic mesh and hydrophilic-oleophobic mesh, work by taking advantages of the nature of two different capillary forces between the liquids and solid surface. The direction of the capillary force of wetting liquid phase is pointing downward, which is in the opposite direction for that of the non-wetting liquid phase as illustrated in Figure 1-1. Therefore, the wetting liquid phase tends to permeate through the mesh, while the other tends to be retained and sitting on the mesh. Because the simplicity yet super effective oil-water separation method, many research groups have been trying to develop a surface having superoleophobic-superhydrophilic property. However, due to the difficulty of preparing this type of material, researchers look for the new possibility of harnessing superomniphilic (wettable

by any type of liquid) material as an alternative for the application of oil-water separation.

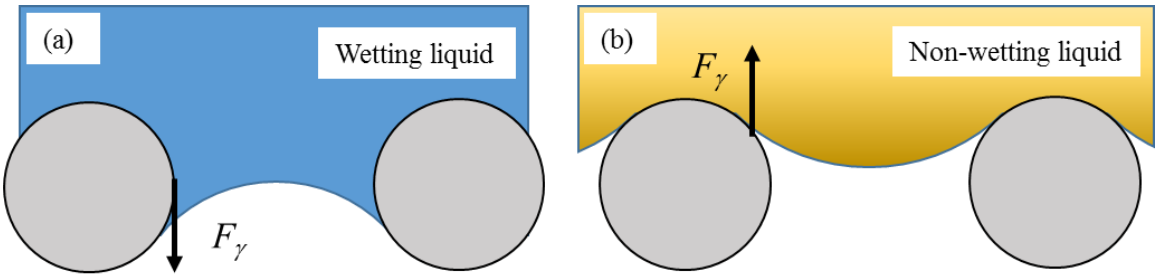

Figure 1- 1. Illustration of the direction of the capillary force for (a) wetting liquid and (b) non-wetting liquid.

Lie Jiang discovered the new option of selecting material for gravity driven oil-water separation after observing the wetting behavior of fish scale [24]. He pointed out that fish scale is superomniphilic in air but when it is immersed in water it becomes an extreme oil repellent (underwater superoleophobic surfaces). He also discovered that the secret of this extreme underwater oil repellency is the surface structure of the fish scale which display double scale roughness i.e. micro and nano scale. The trapped water within its roughness create solid-liquid composite interface which is repulsive to oil. Later, he prepared hydrogel coated stainless steel mesh, which is superhydrophilic and superoleophobic in water, for oil water separation [25]. The prepared mesh can selectively separate water from oil-water mixture effectively. Much research has been conducted to harness this behavior for oil-water separation application [26-31]. The outcomes were very successful and show high performance and high separation efficiency.

1.2 The Need for This Research

The first report discussing superhydrophilic-underwater superoleophobic surfaces for oil-water separation was presented in 2011 [32]. Since then, various preparation methods such as layer-by-layer coating, polymerization, sol gel method, hydrothermal process, direct oxidation, and chemical vapor deposition, have been employed, and various material such as hydrogel, silicate, TiO_2, silica gel, zeolite, and ZnO, have been tried [26-31] to achieve superhydrophilic surface which is also having an extreme underwater oil repellency. However, most of the preparation methods often require long and multiple processes, delicate sample preparation, exotic materials and chemicals and extreme condition. Also, most of the current research only focused on what materials and what preparation methods can be used to fabricate the surfaces for this application, while the mechanism and the prediction are poorly discussed. Therefore, study of factors which govern the separation of oil and water using this type of surface need to be carried out to help us have better understanding on the oil water separation process.

We employed the spray deposition of nanoparticle dispersions technique to fabricate the surfaces for capillary based gravity driven oil-water separation. Spray deposition technique was chosen because of its simplicity for preparing hierarchical surface for special wettability application [33,34]. The morphology of the surfaces was characterized and the wettability of the films was studied. The results of this research inform us about the general requirements for the capillarity based gravity driven oil water separation. This information also leads us to know what the best method and what attempts are required for fabricating surfaces for oil-water separation application.

1.3 Objectives

The main objective of this thesis is to study the wetting properties of metal oxide photocatalyst films prepared using spray deposition technique and apply the films for oil-water separation application. The objectives can be divided to several parts as the following:

1. To fabricate, characterize, and study the wetting properties of the metal oxide photocatalyst films prepared by spray deposition technique.
2. To apply the films for oil water separation.
3. To study the physics and identify the important factor and general requirements of the separating medium.

CHAPTER 2

LITERATURE REVIEW

The main purpose of this chapter is to review the theory related to this research including some fundamental concepts. Most of the discussion is related to the physics of fluids and fluid statics. In addition, photocatalysis process and the relation of this research is also discussed.

2.1 Liquid Contact Angle and Wetting Phenomena on Solids

2.1.1 Surface Tension and Surface Energy

In the physics of solids, the molecules on the surface have higher energy than the molecules in the bulk of materials. Every molecule inside the bulk is connected with the neighborhood molecules through molecular interaction such as metallic bonding, ionic bonding, and covalent bonding. However, the molecules at the surface of solids are bond with fewer molecules than that of inside the bulk. As a consequence, the molecules at the surface have higher potential energy. This additional energy is called surface energy (γ) and is measured in energy per unit area (J/m^2). In liquids, the term of surface energy is usually called surface tension which has unit of force per unit length (N/m). The total energy (W_{tot}) of a system with interface is defined as surface energy times the surface area of the system, as in equation (1). Any system tends to achieve the state where the total energy is minimal. For example, undisturbed water droplet tends to have spherical shape when it is airborne (neglecting the effect of gravity) since sphere has the lowest surface area for a given volume.

$$W_{\text{tot}} = \gamma \times A_{\text{tot}} \quad (1)$$

The effect of the surface tension can also be noticed in the rise of liquid surface in capillary tube. The origin of surface tension is intermolecular attractive forces inside the liquid. The attractive force may come from Van der Waal's force, hydrogen bonding, and or electrostatic force and cumulatively become cohesion force. The surface tension is defined as the work associated with the increasing surface area. Since the force created from surface tension depends on the contact line while the weight force depend on the volume of liquid, we can compare the effect of the weight force with the capillary force as the following:

$$\frac{F_\gamma}{F_g} \sim \frac{L}{L^3} = \frac{1}{L^2}$$

The important observation can be made here is that when the length scale is sufficiently small, the effect of surface tension is much greater than the effect of gravity. On the other hand, when the length scale is large, the effect of surface tension is negligible. Therefore, in narrow tube, water can rise up in absence of external pressure until the height where the weight force and the capillary force are balanced. A characteristic length or dimension of liquid beyond which the effect of gravity become dominant is called capillary length, λ. It is defined as $\lambda = \sqrt{\gamma/\rho g}$ where ρ and g is liquid density and gravitational acceleration respectively. The value of λ for water is 2.7 mm.

2.1.2 Wetting

Solid liquid interfacial phenomena are often called wetting. Study of wetting is important in many disciplines including physics, surface science, microfluidics devices, physical

chemistry, and biomimetics. Some of the applications of the study of wetting phenomena are superhydrophobic surfaces, superhydrophilic surfaces, self-cleaning surfaces, and so on.

Fundamentally, wetting phenomena is determined by liquid surface tension and solid surface energy as well as interfacial energy of solid and liquid. The wettability of solid by a probe liquid is usually observed by measuring the contact angle, from which solid surface energy may be examined. The contact angle represents three lines of forces which can be explained using Young's contact angle equation, as given in equation (2), where γ_{sv}, γ_{lv}, and γ_{sl} are solid surface energy, liquid surface tension and solid-liquid interfacial tension respectively. Even though the surface tension is a scalar quantity, the force caused by it is a vector quantity which has direction parallel or tangential to the interface [35].

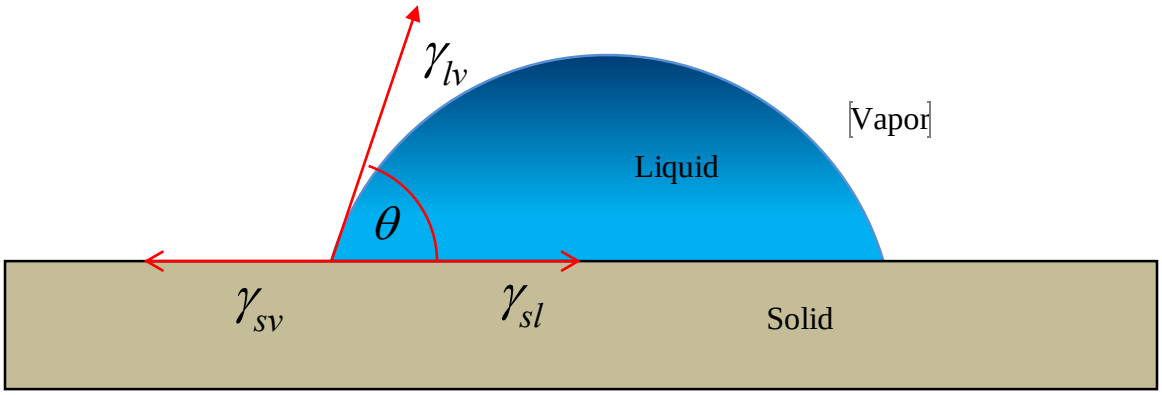

Figure 2- 1. Wetting phenomena and contact angle formation.

$$\cos\theta = \frac{\gamma_{sv} - \gamma_{sl}}{\gamma_{lv}} \qquad (2)$$

The solid surfaces can be categorized by mean of the contact angle of liquid. Surfaces which have water contact angle, θ_{water}, larger than 90° are called hydrophobic surfaces.

Surfaces which have θ_{water} smaller than 90° are called hydrophilic surfaces. Superhydrophobic surfaces are surfaces which have θ_{water} larger than 150°, while surperhydophilic surfaces are surfaces which have θ_{water} smaller than 5°. Similarly, oleophobic and oleophilic surfaces are characterized using the same range of oil contact angle on the solid surface, θ_{oil}, with that of for θ_{water} [36].

2.1.3 Contact Angle from Thermodynamic Point of View

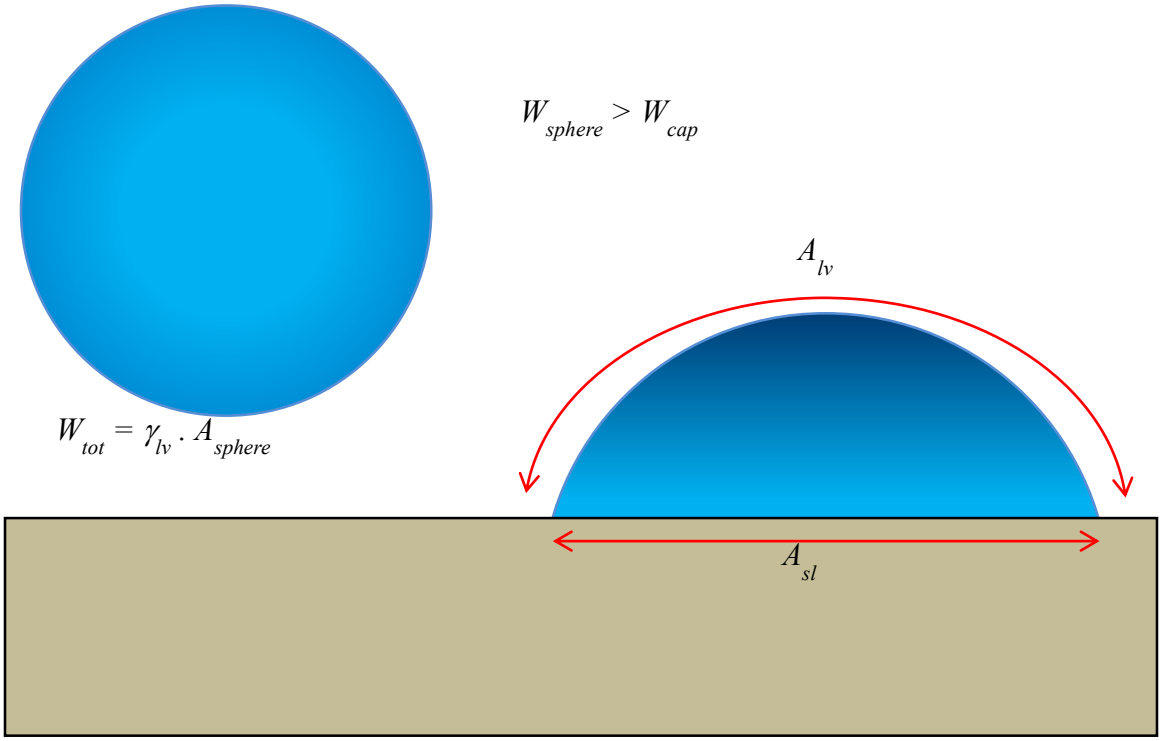

Figure 2- 2. Water droplet change shape when in contact with solid by minimizing the total energy of the system.

Young's equation of contact angle can be derived by analyzing the total energy of the system. Water droplet tends to have spherical shape as it corresponds to the state where the total energy is minimal. Upon contact with solid, water droplet will create solid liquid interface and become a spherical cap if, and only if, the total energy can be reduced, as in

Figure 2-2, where A_{lv} and A_{sl} are surface area of liquid vapor interface and surface area of solid liquid interface respectively. The new total energy of the system now can be expressed as in equation (3) where w_a is the work of adhesion.

$$W_{tot} = \gamma_{lv}(A_{sl} + A_{lv}) - w_a A_{sl} \quad (3)$$

Work of adhesion is the amount of energy required to separate liquid and solid in vapor medium. The work of adhesion can be calculated as the difference of solid liquid interfacial energy and the surface energies created by separation process, as expressed in equation (4).

$$w_a = \gamma_{sv} + \gamma_{lv} - \gamma_{sl} \quad (4)$$

By substituting (4) to (3) one can define the new total energy in term of surface energy and the surface area of the system as in (5).

$$W_{tot} = \gamma_{lv}(A_{sl} + A_{lv}) - (\gamma_{sv} + \gamma_{lv} - \gamma_{sl})A_{sl}$$

$$W_{tot} = (\gamma_{lv}A_{sl} + \gamma_{lv}A_{lv}) - (\gamma_{sv}A_{sl} + \gamma_{lv}A_{sl} - \gamma_{sl}A_{sl})$$

$$W_{tot} = \gamma_{lv}A_{lv} - (\gamma_{sv} - \gamma_{sl})A_{sl} \quad (5)$$

The equilibrium shape of the system is achieved when the surface energy is minimum by minimizing surface area.

$$0 = dW_{tot} = \gamma_{lv}dA_{lv} - (\gamma_{sv} - \gamma_{sl})dA_{sl}$$

$$\gamma_{lv}dA_{lv} = (\gamma_{sv} - \gamma_{sl})dA_{sl}$$

$$\frac{dA_{lv}}{dA_{sl}} = \frac{(\gamma_{sv} - \gamma_{sl})}{\gamma_{lv}} \quad (6)$$

Geometrically, dA_l/dA_{sl} is equal to $cos\ \theta$ as illustrated in Figure 2-4. Thus by substituting dA_l/dA_{sl} with $cos\ \theta$, one can obtain the Young's contact angle equation as in equation (2) [38,39].

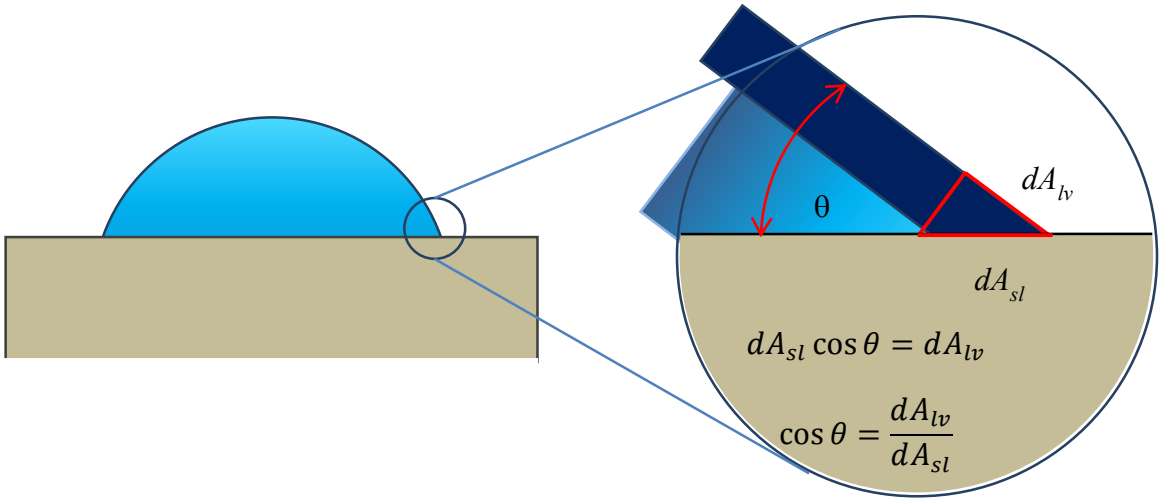

Figure 2- 3. Geometrical representation of dAlv/dAsl.

2.1.4 Young-Laplace Equation and the Applications

Another effect of the surface tension is the presence of meniscus of liquid surface in the container such as capillary tube. The meniscus happens due to the presence of pressure difference across the surface. By reviewing the definition of the surface tension, the pressure difference across the surface can be calculated using Young-Laplace equation as the following

$$\Delta P = P_{in} - P_{out} = \gamma\left(\frac{1}{R_1} + \frac{1}{R_2}\right) \quad (7)$$

where P_{in} and P_{out} are the pressure inside and outside the curvature, while R_1 and R_2 are the principal radius of curvatures. For spherical shape, $R_1 = R_2$. Therefore, the pressure difference can be written as $\Delta P = 2\gamma/R$.

Consider a liquid in capillary tube having contact angle α as shown in Figure 2-4. The interface can consist of the wetting phase (such as water) and the non-wetting phase (such as air or oil). By analyzing the geometry, we can deduct that the pressure difference across the surface is

$$\Delta P = \frac{4\gamma \cos\alpha}{D} \tag{8}$$

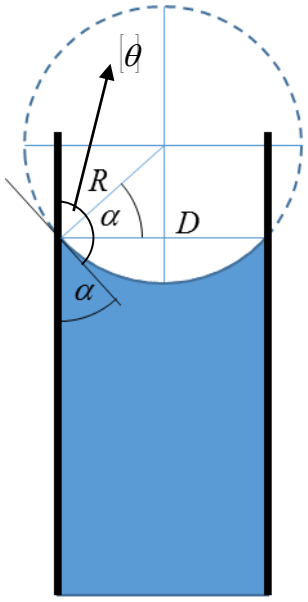

$$R\cos\alpha = \frac{D}{2}$$

$$R = \frac{D}{2\cos\alpha}$$

$$\Delta P = \frac{2\gamma}{R} = \frac{4\gamma\cos\alpha}{D}$$

Figure 2- 4. The shape of liquid-air interface in capillary tube.

where α and D are wetting angle and the diameter of the capillary tube. For most cases, the contact angle of the non-wetting phase, θ, is of interest. Knowing the fact that $\alpha = \pi - \theta$, and $\cos\alpha = -\cos\theta$, we can rewrite the equation (8) as the following equation.

$$\Delta P = -\frac{4\gamma \cos\theta}{D} \quad (9)$$

Note that γ here is the interfacial tension between two phase, i.e. oil and water, or air and water. Equation (9) is known as the Washburn equation which is normally used to determine the average pore size of a porous material in mercury porosimetry. This porosimetry works by characterizing the external pressure needed by mercury to intrude the pores of the material [37]. Since the surface tension of mercury is 480 dyne/cm in room temperature and the average contact angle θ of mercury is 140° for most of solid surfaces, the pore size of material is determined as D = 1450 kPa/P_{int} (μm) [37]. P_{int} here is the applied pressure needed by mercury to penetrate the pores of the sample. It is also called the intrusion pressure.

2.1.5 The Effect of Surface Roughness on the Wettability of Surface

The contact angle of rough surfaces can be explained by using Wenzel's model and Cassie-Baxter's model. Wenzel pointed out that surface structure may modify the wetting property of solids. Surface roughness is characterized as the ratio of the true area of the rough surface to its projection, and can be denoted as $r = A_{real}/A_{apparent}$. The value of r is always greater than 1 (r >1). Wenzel's contact angle equation is expressed in equation (10).

$$cos\,\theta_W = r\,cos\,\theta \quad (10)$$

Figure 2-5 illustrates the Wenzel's model and the calculation of the roughness factor, r [40,41]. As the consequence of the value of r the change of the contact angle, θ_W, depends on the initial contact angle on smooth surface, θ. If θ is greater than 90°, then θ_W

will be enhanced. On the other hand, if θ is smaller than 90°, then the θ_W will be diminished [40,41].

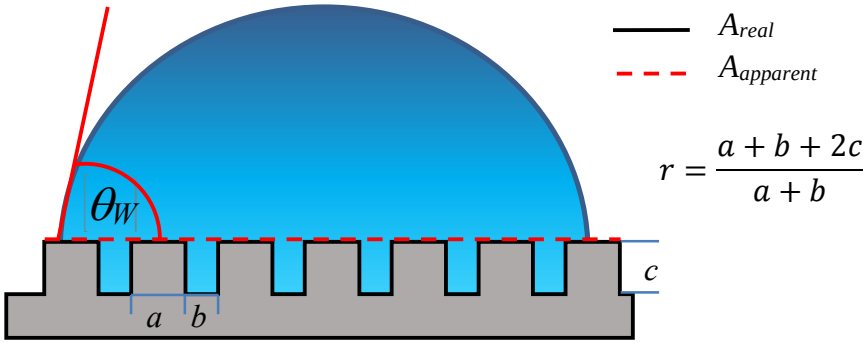

Figure 2- 5. Wenzel's model and the calculation of roughness factor *r*.

Later, Cassie and Baxter viewed rough surface as flat surface but consists of different materials of composites, that is solid and vapor, and can be characterized by their own surface energies with respective material fraction f_i on the surface with $\Sigma f_i = 1$. Therefore, the contact angle can be defined as $\cos\theta_{CB} = \sum_i^n f_i \cos\theta_i$. By realizing that the vapor phase is non-wetting phase ($\theta = 2\pi$) one can obtain the final form of Cassie-Baxter's contact angle equation, as expressed in equation (11) [40,41].

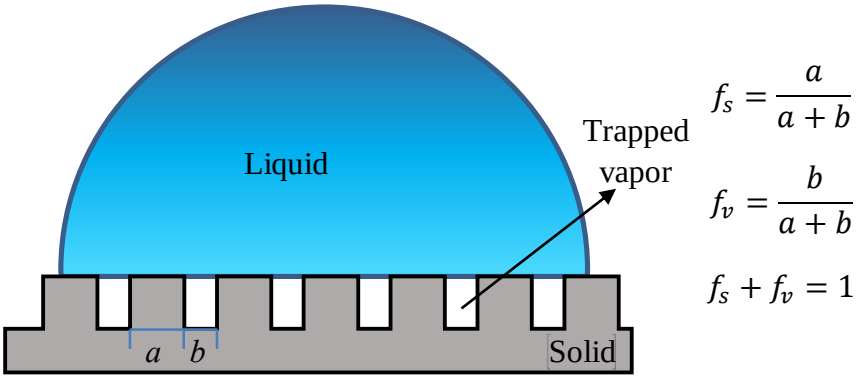

Figure 2- 6. Cassie-Baxter's model and the calculation of fraction of solid and vapor.

$$\cos\theta_{CB} = f_s \cos\theta + f_v \cos 2\pi$$

$$cos\ \theta_{CB} = f_s \cos\theta - f_v$$

$$\cos\theta_{CB} = f_s \cos\theta + f_s - 1 \qquad (11)$$

Here, f_s and f_v are fraction of solid and fraction of vapor respectively. Figure 2-6 illustrates the Cassie-Baxter's model and the calculation of f_s. When there is no trapped air, f_s is equal to r in Wenzel model. Realizing this, roughness factor r_f, defiined as the ratio of the real area of f_s to its projected area, can be included for more precise approximation. The value of r_f is equal to 1 when the surface in contact with liquid is flat such as in Figure 2-6. Figure 2-7 shows the example of the calculation of r_f and f_s in Cassie-Baxter model when the f_s is not a flat area.

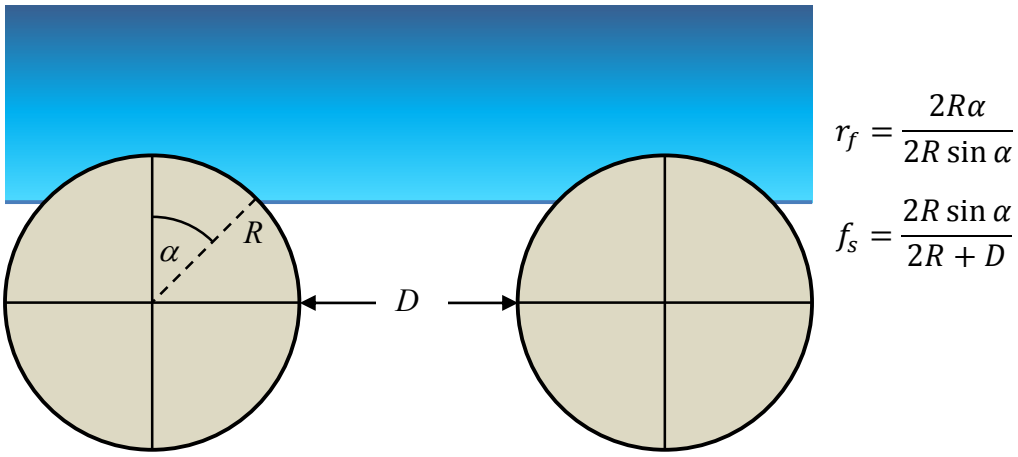

Figure 2- 7. Cassie-Baxter model for non-flat fraction of solid in contact with liquid.

Thus, the Cassie-Baxter equation can be rewritten as equation (12) [40,41].

$$\cos\theta_{CB} = r_f f_s \cos\theta + f_s - 1 \qquad (12)$$

Although both Cassie-Baxter and Wenzel equation can explain the high contact angle on rough surfaces, they have one principle difference which can be characterized by the sliding angle (SA) of water droplet. SA is the elevation angle where a droplet start moving due to inbalanced of the resultant of forces. In Cassie-Baxter state, droplet tends to have very low SA, which is normally smaller than 5°, due to very small contact area between liquid and solid. The famous example of this state is water droplet on lotus leaf [42]. On the other hand, in Wenzel state, droplet tends to have very high SA, larger than 45°, due to larger contact area between liquid and solid. This phenomena is called pinning as the droplet is still adhered to the surface even for high elevation angle. This type of surface also presence in nature such as on the petal of rose [43].

2.1.6 Wetting in Liquid Medium

In this thesis work, we are interested in the contact angle of two immiscible liquids, such as oil and water. In this case, the Young contact angle equation needs to be adjusted. Figure 2-8 shows the contact line of oil-water, solid-water, and solid-oil interfaces. Thus, the Young contact angle equation can be written as

$$\cos\theta_{ow} = \frac{\gamma_{sw} - \gamma_{so}}{\gamma_{ow}} \tag{13}$$

where θ_{ow} is the contact angle of oil in water, while γ_{sw}, γ_{so}, and γ_{ow} are solid-water, solid-oil, oil-water interfacial tension respectively.

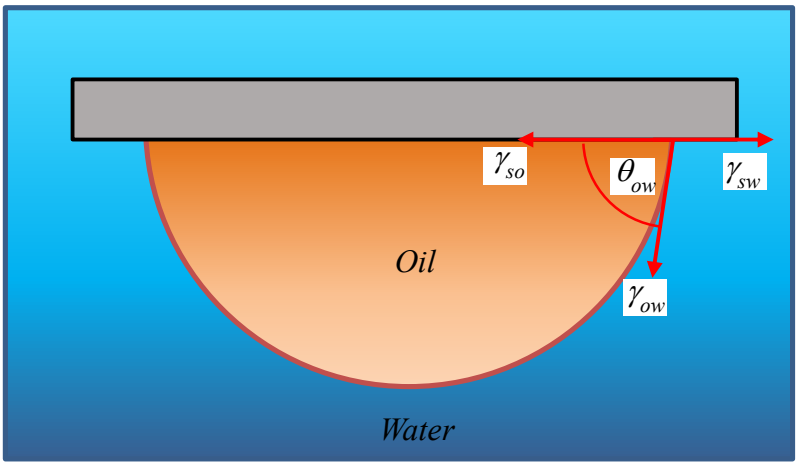

Figure 2- 8. Oil droplet on solid surface in water environment.

Normally, γ_{ow} can be measured experimentally using typical method to measure surface tension such as Wilhelmy plate method or sessile drop method tensiometer [44,45]. Unfortunately, γ_{sw} and γ_{so} are inaccessible through experiment. However, θ_{ow} can be estimated if contact angle of water in vapor, θ_{wv}, and contact angle of oil in vapor, θ_{ov}, on the same solid surface are known [46].

$$\cos\theta_{wv} = \frac{\gamma_{sv} - \gamma_{\mathrm{sw}}}{\gamma_{wv}}$$

$$\gamma_{\mathrm{sw}} = \gamma_{sv} - \gamma_{wv}\cos\theta_{wv} \tag{14}$$

$$\cos\theta_{ov} = \frac{\gamma_{sv} - \gamma_{\mathrm{so}}}{\gamma_{ov}}$$

$$\gamma_{so} = \gamma_{sv} - \gamma_{ov}\cos\theta_{ov} \tag{15}$$

Here, γ_{wv} and γ_{ov} here are water surface tension and oil surface tension respectively. By substituting (14) and (15) to (13) we can solve for $\cos\theta_{ow}$ as shown in (16) [46,47].

$$\cos\theta_{ow} = \frac{\gamma_{ov}\cos\theta_{ov} - \gamma_{wv}\cos\theta_{wv}}{\gamma_{ow}} \tag{16}$$

The observation we can make in equation (16) is that the bigger the value of $\gamma_{wv}\cos\theta_{wv}$, the bigger the value of θ_{ow}. This means that the more hydrophilic the surface the higher oil repellency underwater [47]. Based on this argument, superhydrophilic material must be chosen for the application of oil water separation.

If the environment in Figure 2-8 is reversed such that water is the testing probe and oil become the medium, one can also estimate the contact angle of water in oil θ_{wo}. By using the same approach as in equation (16), one can get the expression of θ_{wo} as given in equation (17).

$$\cos\theta_{wo} = \frac{\gamma_{wv}\cos\theta_{wv} - \gamma_{ov}\cos\theta_{ov}}{\gamma_{ow}} \tag{17}$$

2.2 Photocatalytic Processs and Superhydrophilicity

Photocatalysis is an accelerated process of chemical reaction under light irradiation in the presence of photo-active material as a catalyst. TiO_2 is an important photocatalyst material which has a lot of industrial applications. For instance, the photoinduced enhanced process can be used for degradation of organic pollutants, reduction of heavy metals, water splitting for hydrogen production, and conversion of chemical compounds [48-51]. There are two types of photochemical reaction on TiO_2 surface under UV irradiation. The first one is the photo-induced redox reaction of adsorbed substances, and the second one is photo-induced superhydrophilicity [52]. The first reaction is due to charge separation on TiO_2 surface under UV irradiation as shown in equation (18).

$$\mathrm{TiO_2} + hv \rightarrow e^- + h^+ \qquad (18)$$

Most of the applications of photocatalytic process such as removal of organic and inorganic pollutants are achieved by incorporating this reaction. The second reaction is superhydrophilicity of TiO_2 surface under UV irradiation. Figure 2-9 shows the change in contact angle of TiO_2 surface under the exposure of UV irradiation [52].

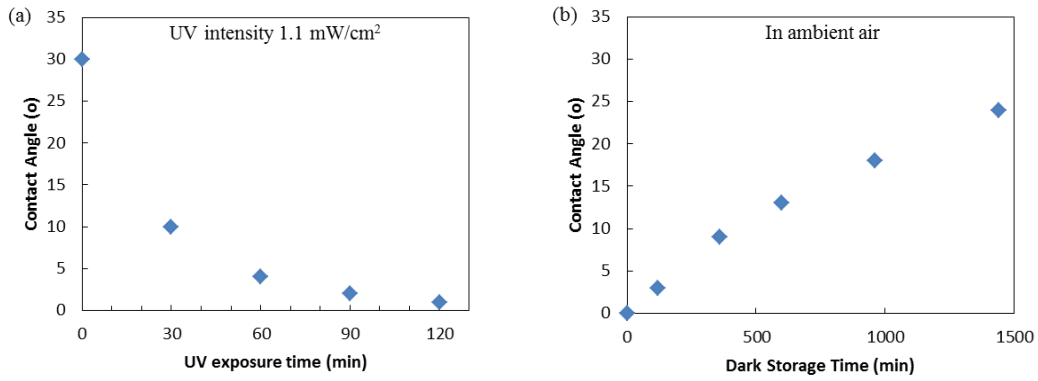

Figure 2- 9. The change of water contact angle on TiO_2 surface versus time (a) under UV irradiation and (b) after dark storage [52].

This phenomenon is still being studied and under debate for two hypotheses. The first hypothesis suggests that the superhydrophilicity is induced by decomposition of adsorbed organic contaminants when TiO_2 surface is irradiated with UV light [53]. The second hypothesis suggests that superhydrophilicity is the consequence of the lattice oxygen defects created by UV irradiation by releasing oxygen [54]. The defects are then filled with hydroxyl group (OH) which then promotes the superhydrophilicity. Many important applications have been developed out of this phenomenon such as water harvesting net and fog free surface [55,56].

Recent study indicates that the photocatalytic organic degradation is more prominent in the contribution of the switching of wetting behavior of TiO_2 [57]. TiO_2 films were fabricated using spin coating of TiO_2 nanoparticle dispersion. The prepared sample was superhydrophilic in air and in oil environment. The films were then silanized [58] to reduce the surface energy of the sample, resulting in TiO_2 based superhydrophobic surface which has contact angle of water, θ_{wv}, as large as 153°, and sliding angle smaller than 5°. The sample was then irradiated by UV when a water was droplet sitting on top of

it. Dramatic decrease in the θ_{wv} happened after 5 minutes when the water droplet wet the sample completely, as shown in Figure 2-10. A similar experiment was performed under oil environment but there was no noticeable change in the θ_{wv} even after 20 minutes of UV irradiation. Supposedly the absence of O_2 and H_2O molecules in oil prevented the photocatalytic activity to take place [57].

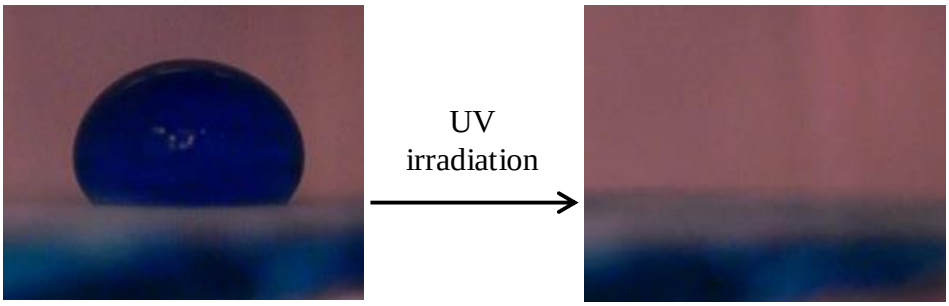

Figure 2- 10. Photo-induced wettability switching of superhydrophilic TiO_2 surface.

CHAPTER 3

EXPERIMENTAL SETUP AND CHARACTERIZATION

3.1 Films Fabrication

The materials used in this thesis work are commercially available photocatalyst materials. Tianium dioxide (TiO_2) anatase < 25 nm, zinc oxide (ZnO) < 100 nm, and tungsten oxide (WO_3) < 100 nm were purchased from Sigma Aldrich ®. The materials were deposited on stainless steel meshes, glass slides substrate and silicon wafer subtrates using spray deposition of nanoparticle dispersion. Nanoparticle form of these materials is necessary for spray deposition since the nozzle of the spray gun used is smaller than 1 mm. We found that a stable dispersion cannot be made using material with grain size larger than 100 μm. In addition, the use of nanoparticle helps on texturing the substrate and obtain larger surface area. Stainless steel meshes with pore size of 50, 102, 152 and 254 μm were purchased from TWP Inc. The samples prepared on glass slides were used for wettability study, while the sample prepared on stainless steel meshes were used for oil water separation test.

The films fabrication started by preparing the nanoparticle dispersions in tetrahydrofuran (THF). The dispersions were prepared and tested in three different concentrations to find the best concentration to be used in this work. We mixed 0.05 g, 0.10 g and 0.15 g of the nanoparticle in 10 ml of THF to obtain dispersion with concentration of 5 mg/ml, 10 mg/ml and 15 mg/ml. The mixtures were then sonicated for 1 hour to create stable dispersion for the spray coating. THF is an organic solvent which has low viscosity and

low surface tension. These properties are required to obtain optimum condition for spray deposition technique. Different solvents, such as ethanol, isopropyl alcohol, acetone, methanol, and water, were examined but only THF, isopropyl alcohol and deionized (DI) water showed stable dispersion after sonication process. In the end, THF was chosen because it has low boiling point (T_b = 66 °C) which is preferable for spray coating process as it make the solvent evaporate readily after the deposition process.

Upon deposition, the substrates were cleaned by rinsing with acetone, isopropyl alcohol and DI water. The substrates were then dried using an air blower until all the remaining water evaporated. The deposition process was done inside a fume hood as illustrated in Figure 3-1. Figure 3-2 is the pictorial view of the components for the spray coating setup. The spray gun (McMaster Carr) with nozzle diameter of 0.75 mm was used for the spray coating with the nitrogen pressure of 170 kPa. The distance between nozzle and substrate was fixed at 20 cm and the diameter of the sprayed area was 7 to 10 cm. 10 ml of the dispersion was used to coat each face of a substrate. The stainless steel mesh substrates were sprayed on both faces while for glass slides only one face was sprayed. After deposition process, the samples were annealed in air at 550 °C for 2 hours. This step is required to increase the robustness of the films attached to the substrates.

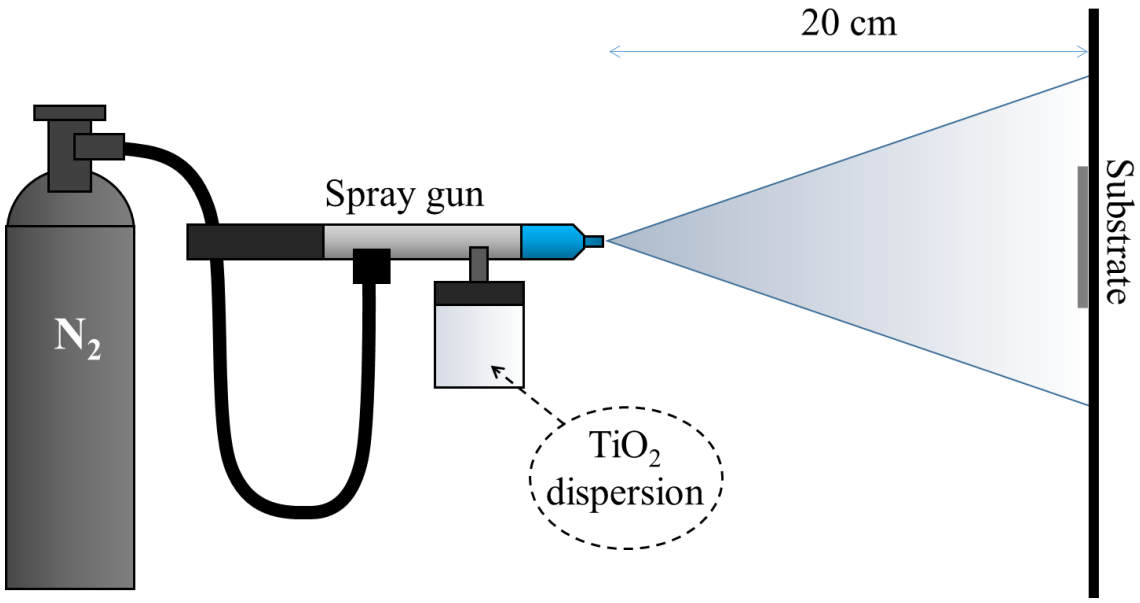

Figure 3- 1. Experimental setup of the spray deposition system.

Figure 3- 2. Photograph of the components of the spray gun.

3.2 Sample Characterizations

After annealing process, the samples underwent several characterization analysis to study the properties of the samples. The film structure and the surface morphology are characterized using X-ray diffractometer (XRD) and scanning electron microscope (SEM). The wetting properties of the samples are characterized using a goniometer.

3.2.1 X-Ray Diffraction (XRD) Analysis

The XRD was performed using Bruker D8-40kv/ 40Ma X-ray diffractometer. This analysis was performed to characterize the crystalline structure of the films after undergone annealing process. This equipment is located in Material Science Laboratory, Department of Mechanical Engineering, King Fahd University of Petroleum and Minerals. This equipment is shown in Figure 3-3.

Figure 3- 3. X-ray diffractometer Bruker D8-40kv/ 40Ma.

3.2.2 Scanning Electron Microscopy (SEM)

The SEM analysis was performed to observe the surface morphology of the samples. The scanning electron micrographs were recorded using Jeol JSM-6610LV, under 15 kV operating voltage. This equipment is located in Material Science Laboratory, Department of Mechanical Engineering, King Fahd University of Petroleum and Minerals. This equipment is shown in Figure 3-4. Field emission scanning electron microscope (FESEM), TESCAN ultra high resolution, was also used for the same analysis. This equipment is located in Center of Excellence in Nanotechnology (CENT), King Fahd University of Petroleum and Minerals.

Figure 3- 4. Scanning Electron Microscope Jeol JSM-6610LV.

3.2.3 Contact Angle Measurements

The contact angle measurements were performed to characterize the wettability of the samples. The samples were measured in air environment and in liquid (oil and water) environment as illustrated in Figure 3-5. The liquid probes for the measurement in air are DI water and hexadecane. DI water was also used as liquid probe for contact angle measurement in oil environment while the hexadecane was used as the medium. On the contrary, hexadecane was also used as liquid probe for contact angle measurement in water environment. Various oils were also tested in water environment to observe the oil repellency of the samples. The contact angle measurement was performed using Goniometer Kruss Easy Drop DSA20X. This equipment is located in Thin Film Laboratory (Building 28), Center of Excellence in Nanotechnology (CENT), King Fahd University of Petroleum and Minerals.

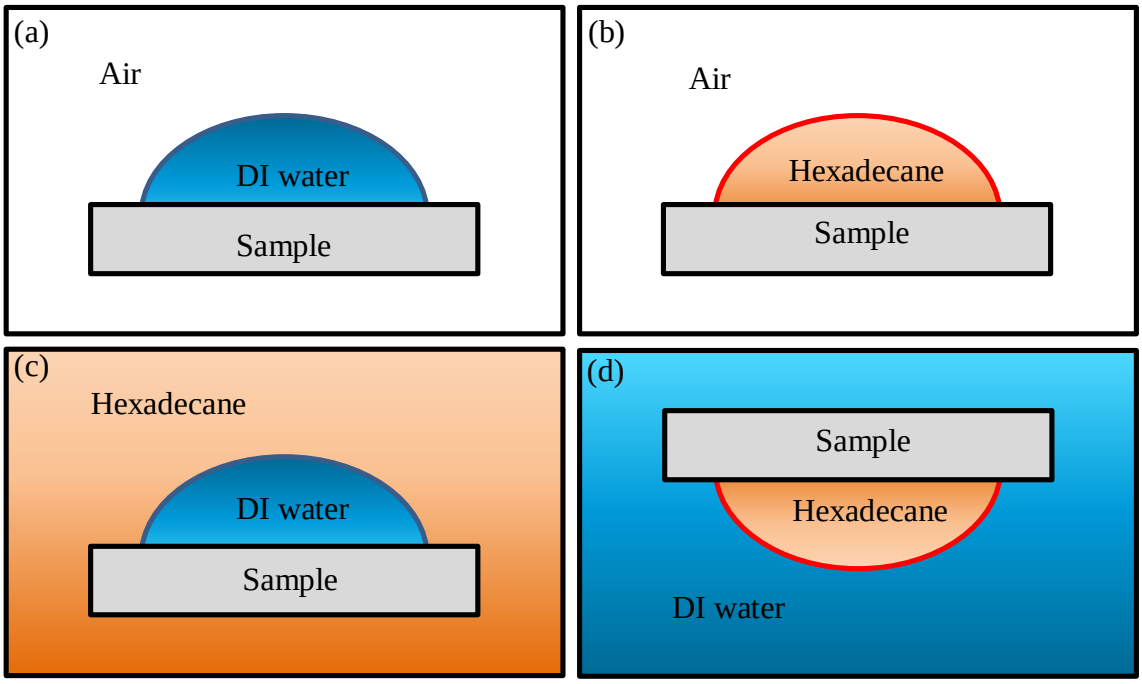

Figure 3- 5. Different cases of contact angle measurement of the samples. (a) water in air, (b) oil in air, (c) water in oil, (d) oil in water.

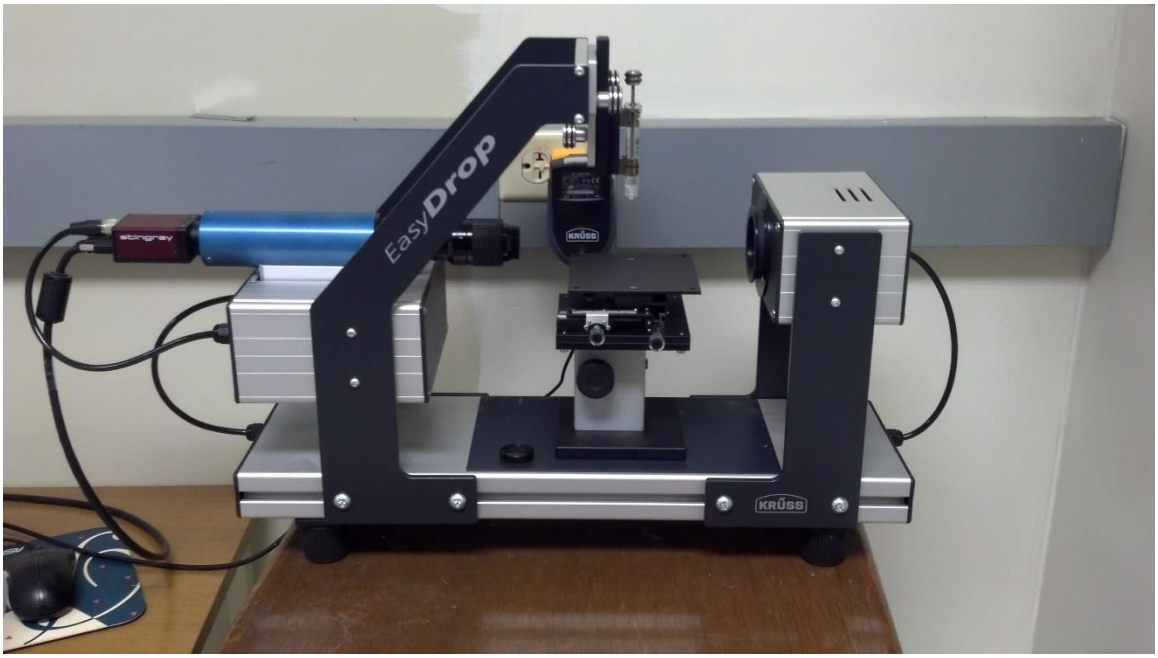

Figure 3- 6. Goniometer Kruss Easy Drop DSA20X.

3.3 Oil-Water Separation Experiment

The setup for oil-water separation was locally designed and fabricated. It consists of two pieces of Pyrex tube having diameter 1.7 cm attached to a customized Teflon coupling capable of holding the mesh between the two tubes. The oil resistant O rings were used to prevent oil leaks from the coupling. The tested mesh was wetted with water before inserting it in the oil-water separation module. The oil-water separation setup is illustrated in Figure 3-7.

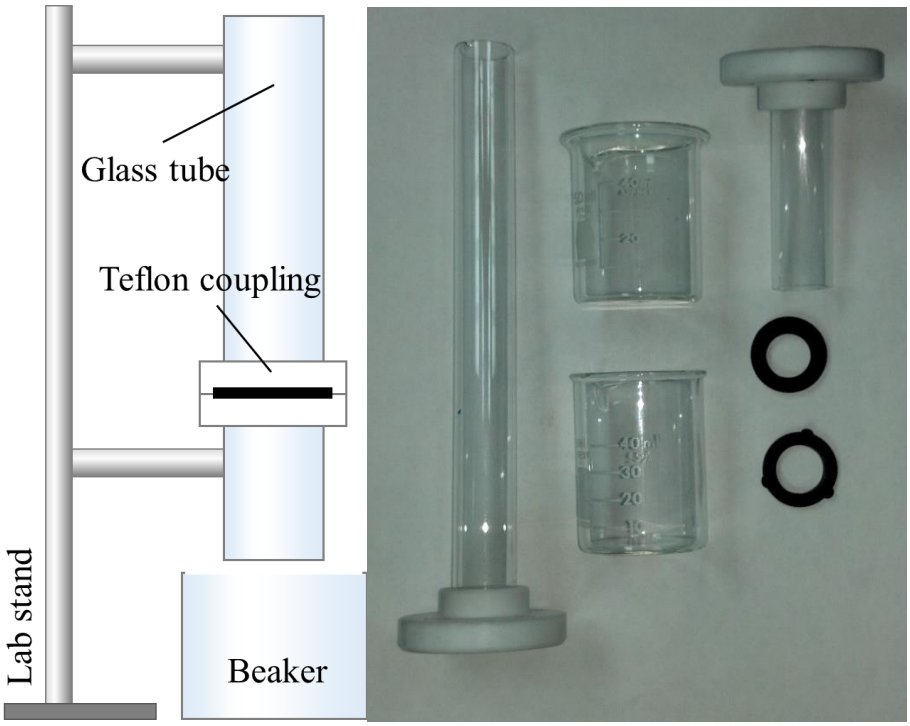

Figure 3- 7. Illustration and photograph of the components of the oil-water separation experiment.

CHAPTER 4

RESULTS AND DISCUSSION

This chapter discusses about the experimental results obtained in this thesis. Surface morphology and structure, wetting properties and oil-water separation performance of TiO_2, ZnO and WO_3 films are discussed here in detail. Eventually, the mechanism of the oil-water separation is studied by modelling the intrusion pressure and comparing with the experimental results.

4.1 TiO_2 Films

Generally metals, alloys, metal oxides, and the oxides of semiconductors exhibit superhydrophilicity due to their large surface energies. TiO_2, ZnO and WO_3 are photocatalytic materials and therefore it is expected to have excellent superhydrophilicity, which is of interest for the application of oil-water separation. In this work, we chose nano TiO_2 anatase as a benchmark because this material is stable, inexpensive, photocatalytic, in addition to its remarkable superhydrophilicity [48]. Several parameters, such as the optimum dispersion concentration and the annealing temperature were investigated by analyzing the experimental results of the synthetized films which will be elaborated in the subsequent discussion. The performance of the other materials (ZnO and WO_3) were compared to that of TiO_2.

4.1.1 Optimum Dispersion Concentration

It is important to determine the appropriate amount of material need to be used in order to know the sufficient amount of the material for the coating process. Three different

dispersion concentration were used for the spray deposition, namely 5 mg/ml, 10 mg/ml and 15 mg/ml of TiO_2 nanoparticle all of them in 10 ml of THF. The optimum dispersion concentration was determined by characterizing the surface morphology of the samples as well as the wettability of the samples in four cases, which is water in air, oil in air, water in oil and oil in water. The desired sample is the sample that is well coated by the nanoparticle. Also, it has to be superhydrophilic in air and superoleophobic in water. Figure 4-1 is the SEM image of the uncoated stainless steel mesh while Figure 4-2 to 4-7 are the SEM images of the samples prepared with different dispersion concentration. The stainless steel mesh used in this analysis is Dutch woven mesh type stainless steel with the pore size of 80 μm, and wire diameter of 0.3810 μm (TWP Inc. part number: 024X110T0100W48T).

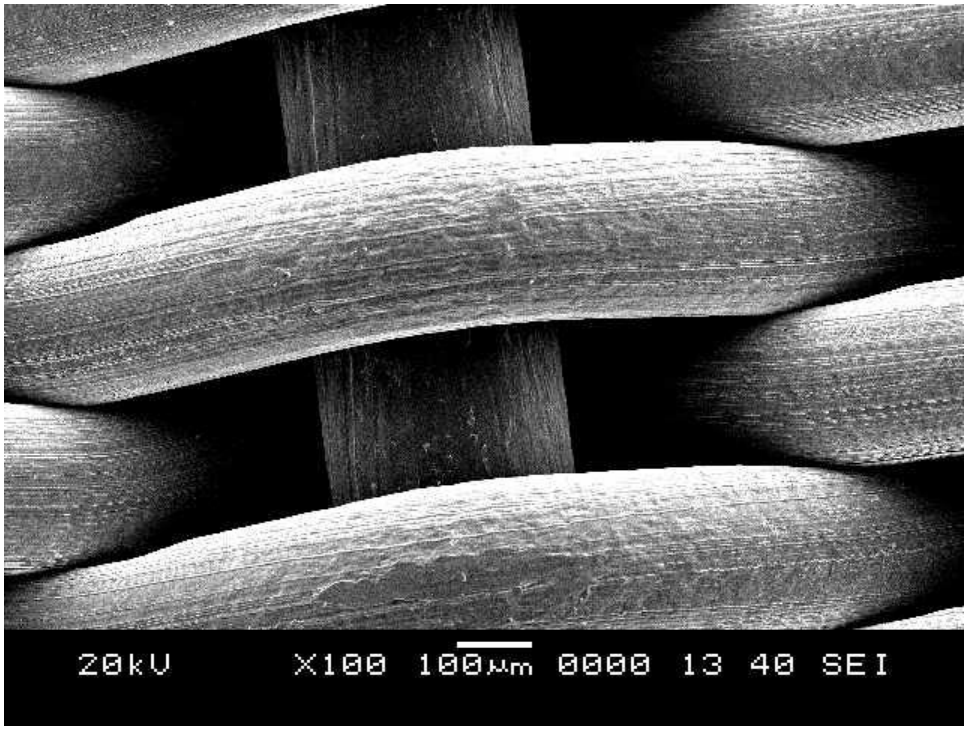

Figure 4- 1. SEM image of the uncoated mesh at 100 times magnification.

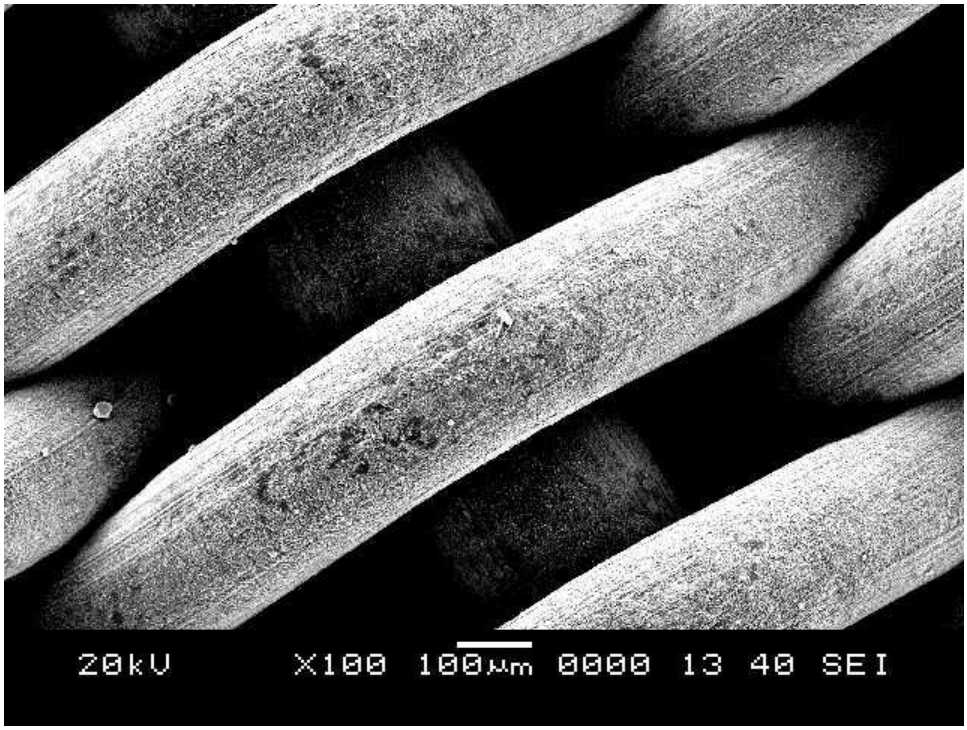

Figure 4- 2. SEM image of TiO_2 coated mesh (5 mg/ml) at 100 times magnification.

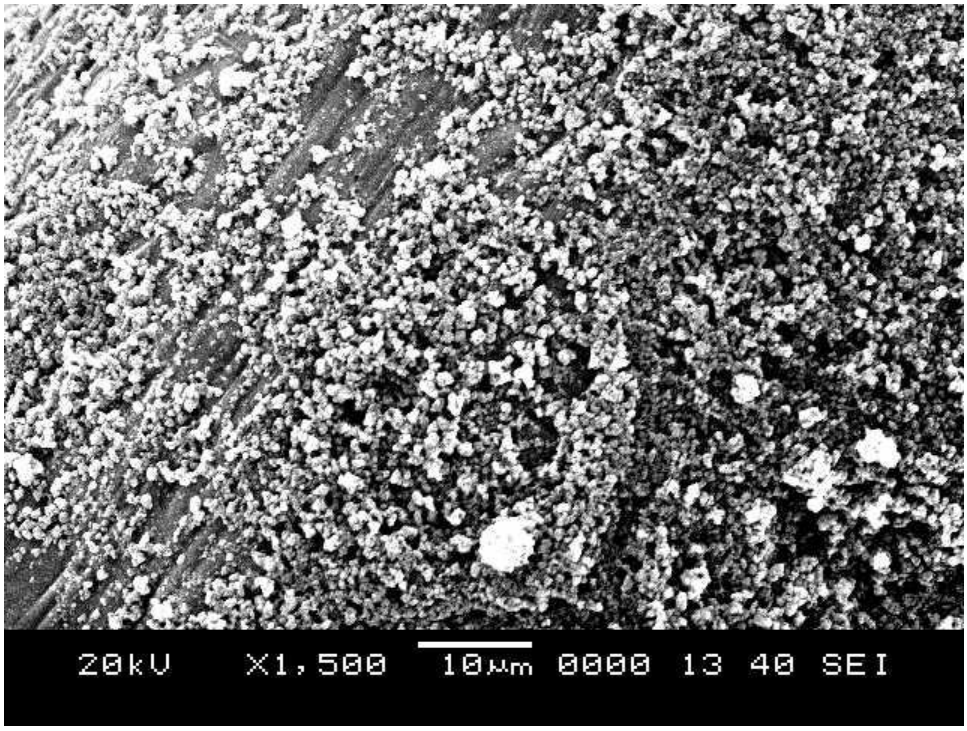

Figure 4- 3. SEM image of TiO_2 coated mesh (5 mg/ml) at 1500 times magnification.

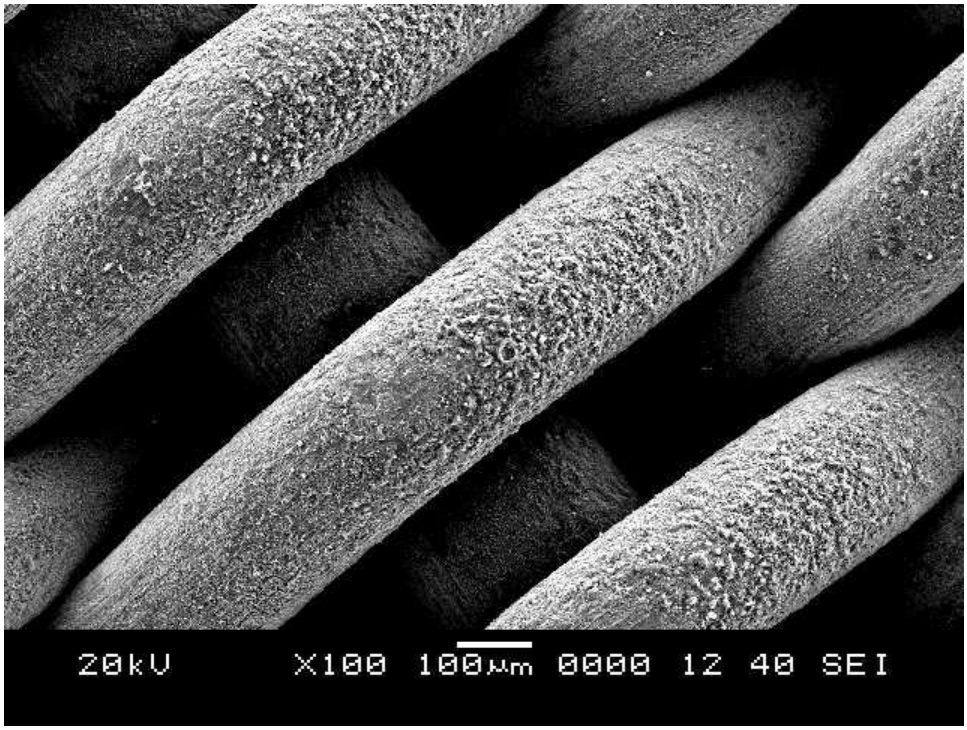

Figure 4- 4. SEM image of TiO_2 coated mesh (10 mg/ml) at 100 times magnification.

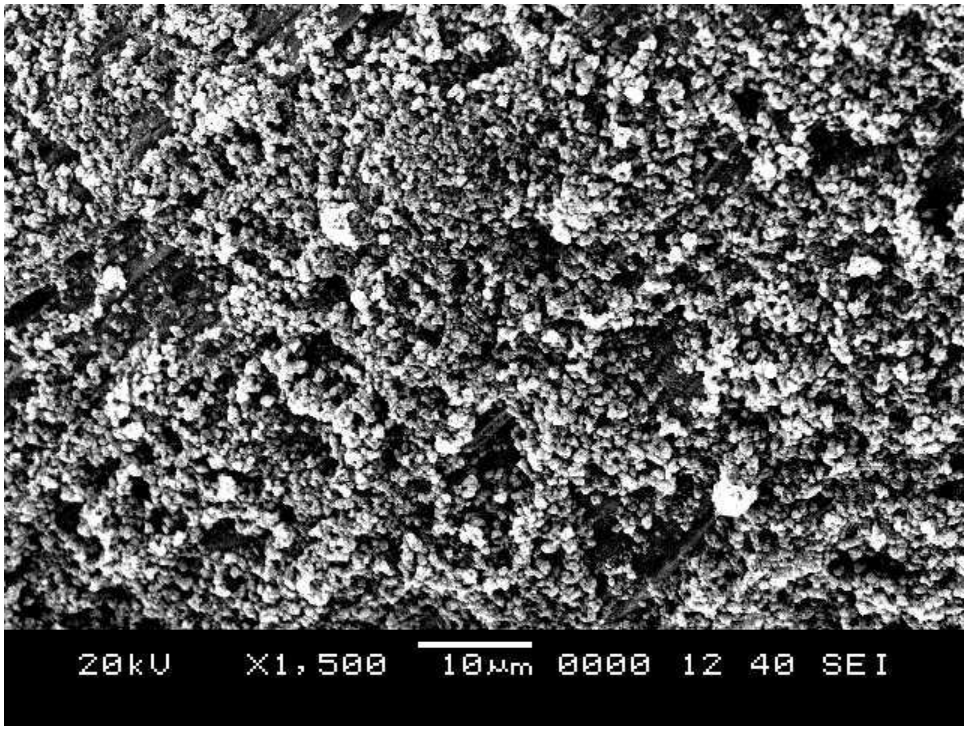

Figure 4- 5. SEM image of TiO_2 coated mesh (10 mg/ml) at 1500 times magnification.

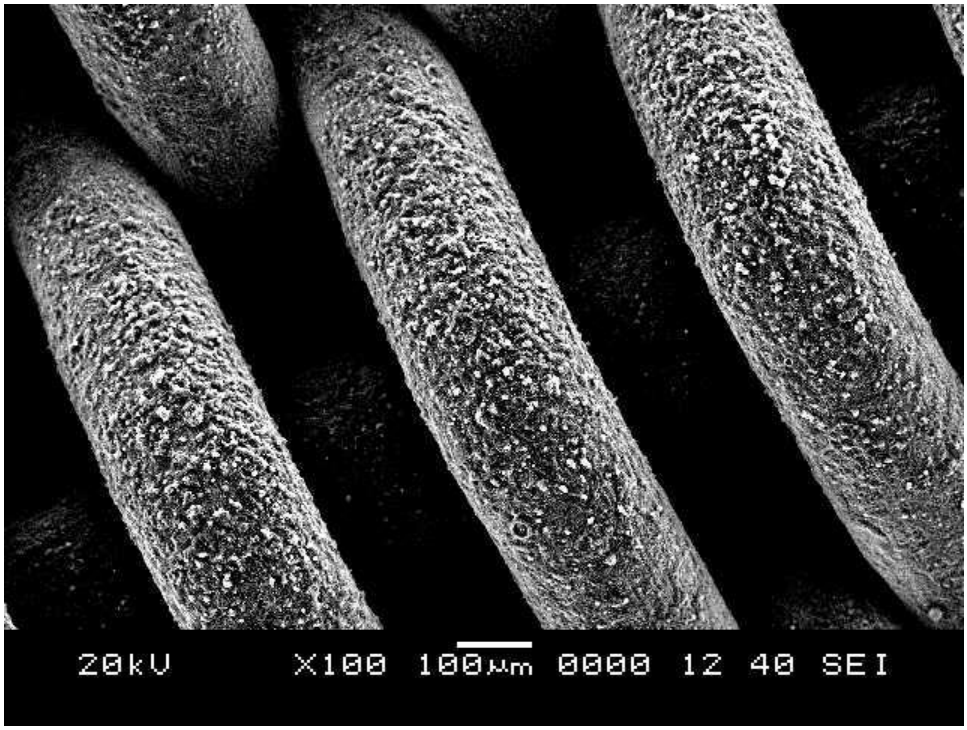

Figure 4- 6. SEM image of TiO_2 coated mesh (15 mg/ml) at 100 times magnification.

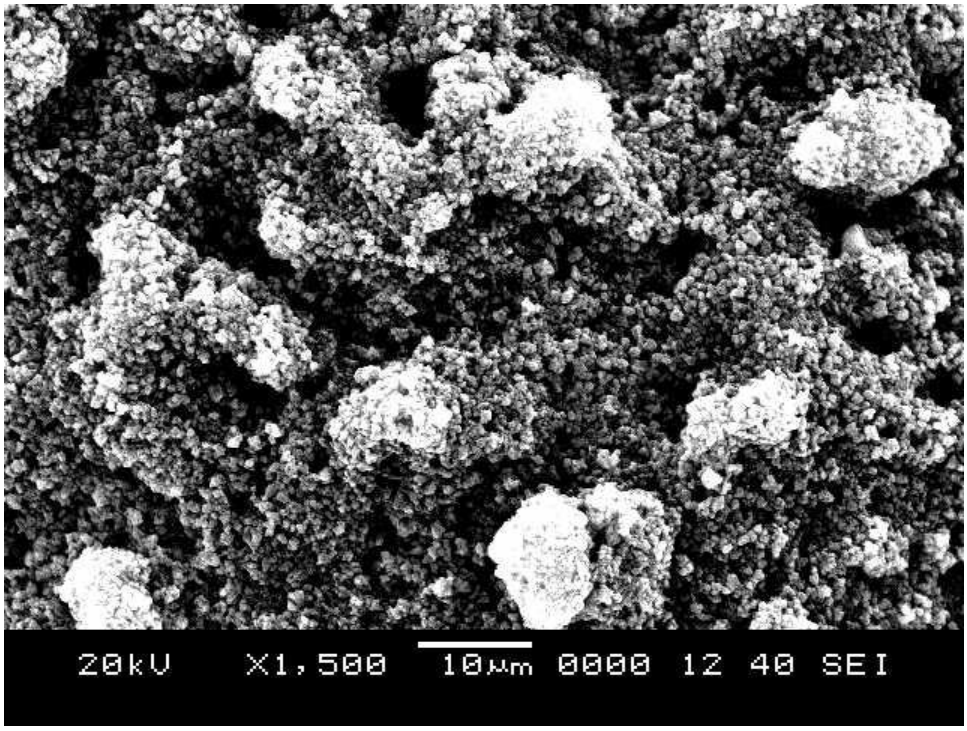

Figure 4- 7. SEM image of TiO_2 coated mesh (15 mg/ml) at 1500 times magnification.

From the SEM images, we can see that TiO_2 nanoparticle are dispersed over the whole surface. However, the sample prepared with 5 mg/ml of TiO_2 dispersion shows some uncoated parts leaving the stainless steel surface exposed. On the contrary, the sample prepared with 15 mg/ml of TiO_2 dispersion seems excessively thick where the stainless steel surface is over-coated with the nanoparticle. The sample prepared with 10 mg/ml of TiO_2 dispersion have medium thickness of the coating yet most of the stainless steel is well coated with the nanoparticle. Knowing this result, 10 mg/ml of nanoparticle dispersion in 10 ml of THF was chosen as the optimum dispersion concentration for the spray deposition.

4.1.2 Effect of Annealing Temperature

Annealing process is an important step in the films fabrication using spray deposition of nanoparticle dispersion. This step increases the robustness of the films such that the nanoparticle is well attached to the stainless steel substrate. The films were prepared in glass slide substrates using the dispersion of 0.10 g of TiO_2 nanoparticle in 10 ml THF. The samples were annealed at 550 °C and 1100 °C for 2 hours. The SEM images of the samples are depicted in Figure 4-8 to Figure 4-11.

Figure 4-8 and 4-9 are the sample which was annealed at 550 °C for 2 hours. There is no appreciable change in the surface structure of the films with the one which is not annealed. However, the robustness has greatly improved. The robustness test was carried out by putting the samples in ultrasonic bath for 10 minutes. The film on the sample which was not annealed was completely removed during this process. On the contrary, the film on the annealed sample was still intact after the sonication process.

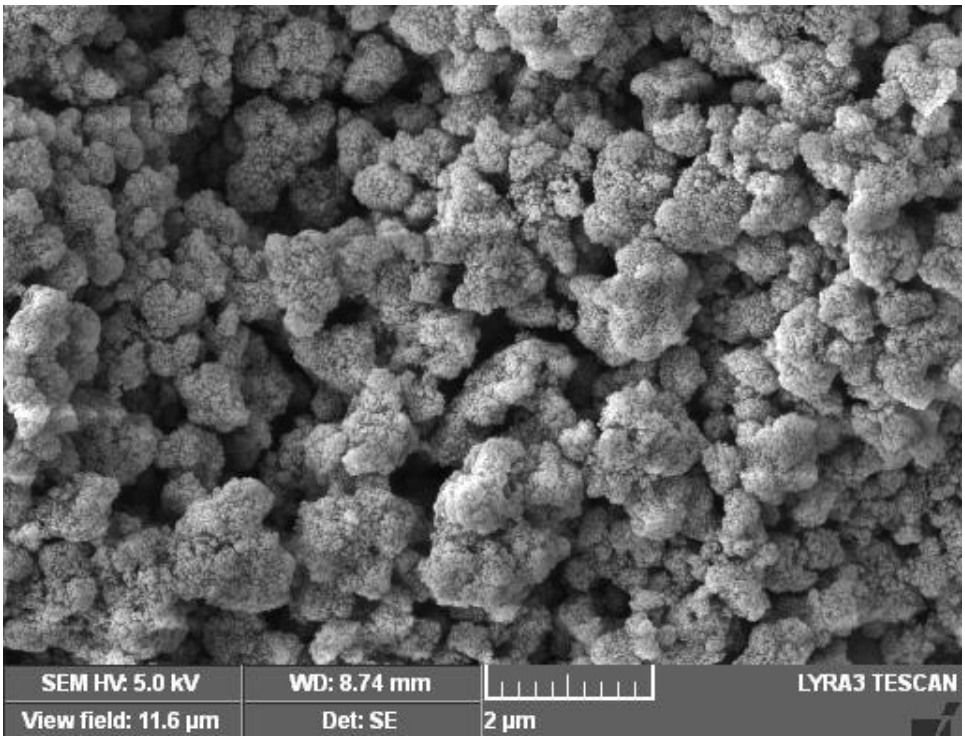

Figure 4- 8. SEM image of TiO_2 (10 mg/ml) coated mesh annealed at 550 °C at 12.5k times magnification.

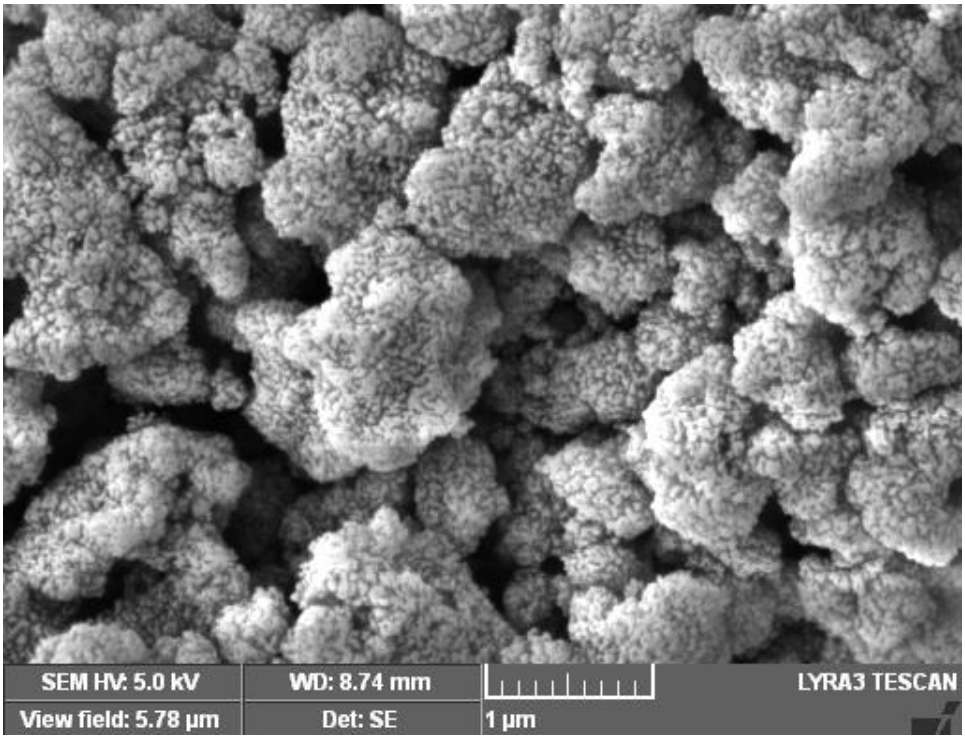

Figure 4- 9. SEM image of TiO_2 (10 mg/ml) coated mesh annealed at 550 °C at 25.0k times magnification.

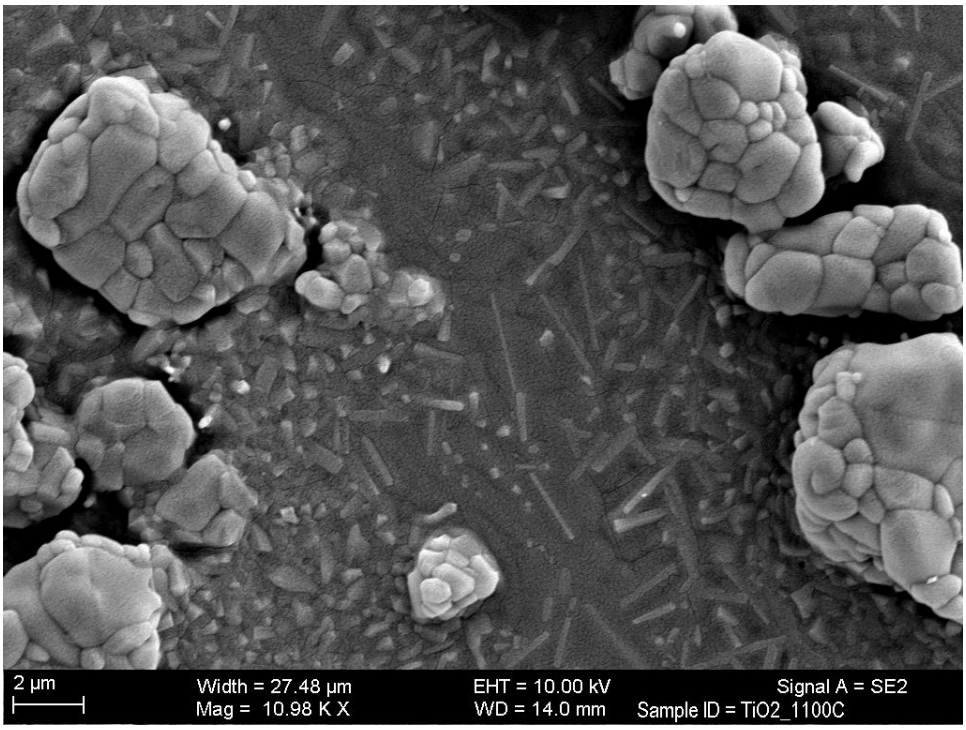

Figure 4- 10. SEM image of TiO_2 (10 mg/ml) coated mesh annealed at 1100 °C at 11k times magnification.

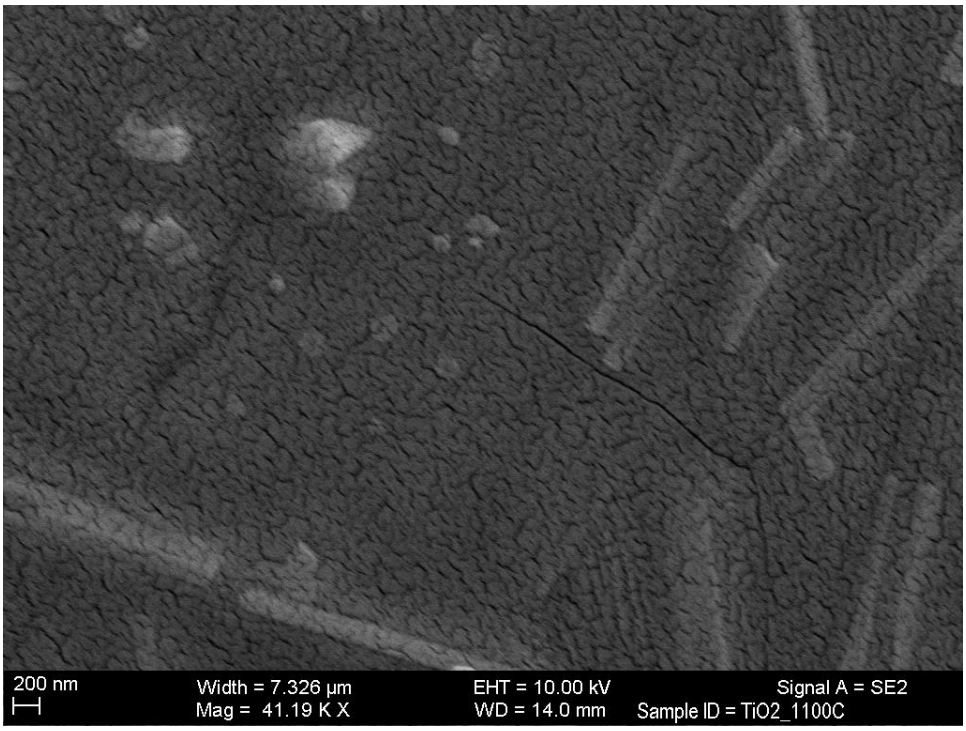

Figure 4- 11. SEM image of TiO_2 (10 mg/ml) coated mesh annealed at 1100 °C at 41k times magnification.

Figure 4-10 and 4-11 are the samples which were annealed at 1100 °C for 2 hours. Dramatic change occurred in this sample. The initial powder-like structure was changed into bar-like formation. The high temperature of annealing process made the TiO_2 nanoparticle rearrange its crystalline structure. XRD analysis was carried out in order to observe the crystalline structure of the sample which are not annealed, annealed at 550 °C and annealed at 1100 °C. The XRD 2θ pattern is shown in Figure 4-12.

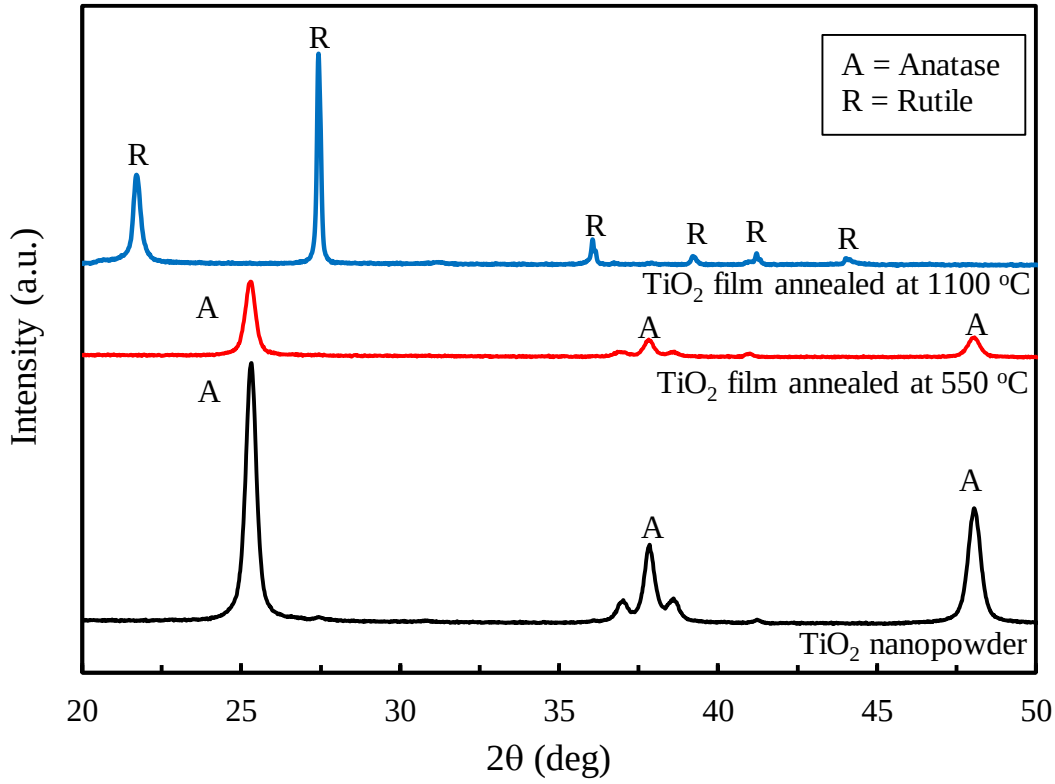

Figure 4- 12. XRD 2θ patterns from TiO_2 nanopowder, TiO_2 film calcined at 550 °C and 1100 °C.

The samples which were annealed at 1100 °C are then characterized as rutile phase of TiO_2 while the samples which were annealed at 550 °C are still in anatase form. TiO_2 anatase is a metastable state and has larger surface area than that of rutile. Thus, by giving it enough energy, TiO_2 anatase tends to transform into rutile form to minimize

surface area [59]. The impact of this transformation is not only reducing the surface roughness of the TiO_2 films but also weakens the photocatalytic property of TiO_2 nanoparticles which is undesired in this work [59]. Thus, annealing treatment at 550 ^oC is more preferable.

4.1.3 Wettability of TiO_2 Films

The wetting properties of TiO_2 films were studied by measuring the contact angle using goniometer. The contact angles were measured in 4 different conditions, which is water in air, oil in air, water in oil and oil in water. The oil used was hexadecane (HD). The experimental data is shown in Table 4-1 and depicted in Figure 4-13.

Table 4- 1. Contact angle measurement of TiO_2 films.

Dispersion concentration (mg/ml)	Air		Air		HD		Water	
	Water θ_{wa} (°)	SD	HD θ_{oa} (°)	SD	Water θ_{wo} (°)	SD	HD θ_{ow} (°)	SD
5	0	0	0	0	38.7	4.5	163.5	2.0
10	0	0	0	0	29.3	3.8	162.8	1.5
15	0	0	0	0	33.7	4.9	167.9	2.2

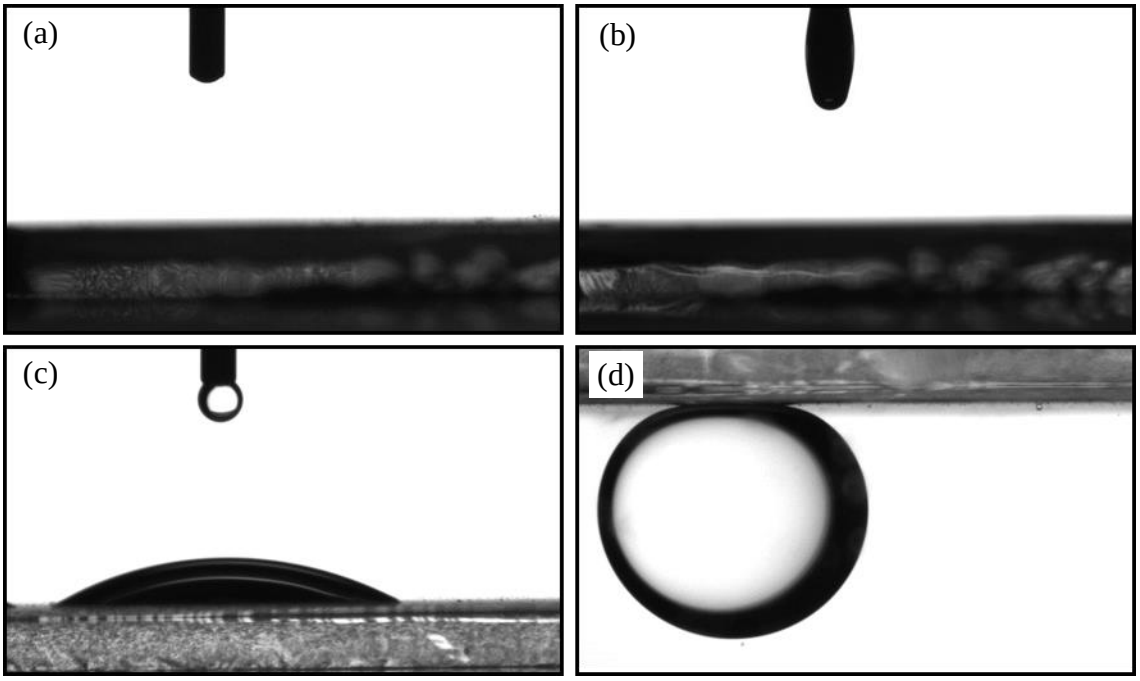

Figure 4- 13. Contact angle measurement of TiO2 films (a) water in air, (b) oil in air, (c) water in oil, (d) oil in water.

We observed that the TiO_2 films prepared by spray deposition using three different dispersion concentration are superomniphobic in air as showing 0 value of contact angle for θ_{wa} and θ_{oa}. Also, it is superoleophobic in water as shown in Figure 4-13 (d). Since the value of θ_{wa} and θ_{oa} are known, we can calculate the theoretical value of θ_{wo} and θ_{ow} using equation (16) and (17). The comparison of the experimental value and the theoretical value of θ_{wo} and θ_{ow} is shown in Table 4-2 and Figure 4-14. The γ_{wa}, γ_{oa} and γ_{ow} used in the calculation is obtained from the reference [45]. We can see that the experimental value and the theoretical value in a pretty good agreement. The higher experimental value than the predicted value of θ_{wo} is expected as the oil droplet is in Cassie state, i.e. the water is trapped in the porous surface of the TiO_2 film. The low value of θ_{wa} and θ_{wo} is convincing that the TiO_2 films have strong affinity toward water molecules and thus encourages the oil droplet to be in Cassie state where water is trapped

in the porous of the surface. This was also confirmed by the sliding angle (SA) measurement which resulting (SA < 2°) as shown in Figure 4-15.

Table 4- 2. The comparison of experimental and theoretical value of the contact angle measurement on TiO_2 films

Contact Angle Measurement	Water in oil	Oil in water
Theoretical	32.1	147.9
Experimental	29.3	165.0
SD	3.8	2.2

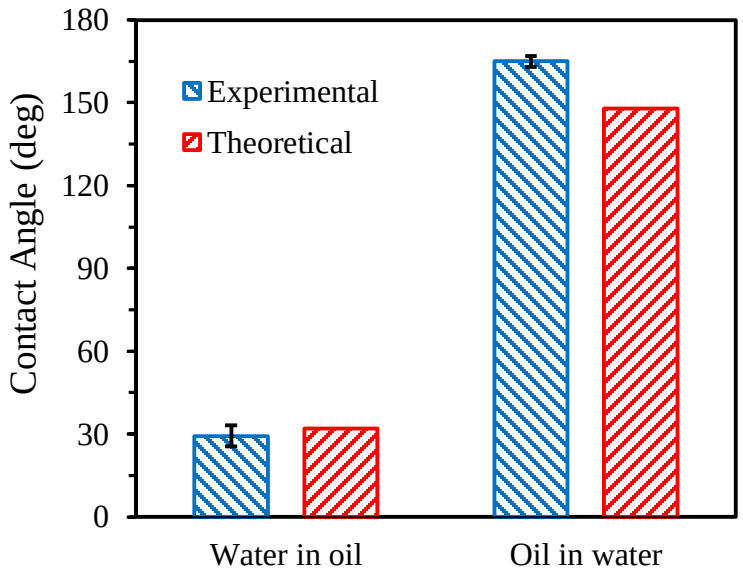

Figure 4- 14. The comparison of experimental and theoretical value of the contact angle measurement on TiO_2 films

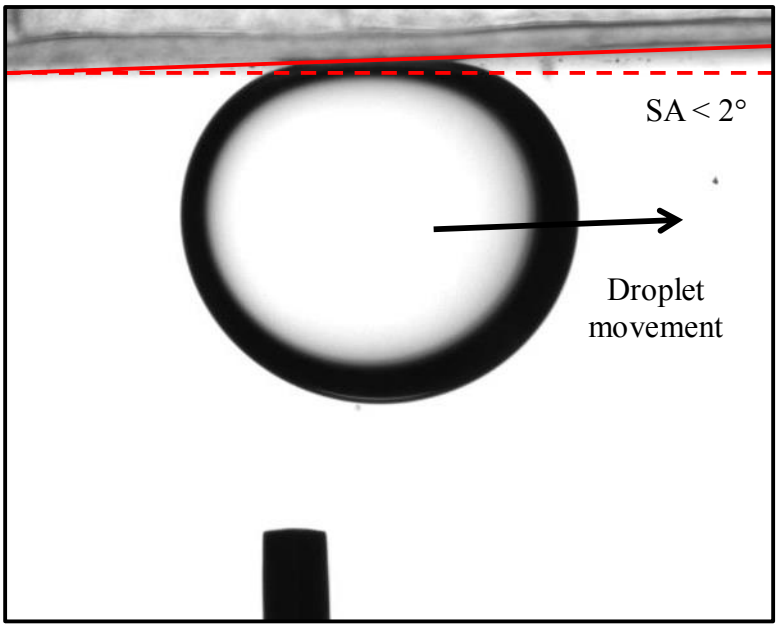

Figure 4- 15. Sliding angle of oil droplet on TiO_2 films in water environment.

The measurement of θ_{ow} for different type of oils was also conducted to calculate the average value of θ_{ow} for most oils. From the experimental result (Figure 4-16) we found the value of oil contact angle in water is as big as θ_{ow} = 162.9° ± 6.3°. In summary, the fabricated TiO_2 films are oil repellent for most of the oil underwater. This type of wetting property is considered as an important factor for the application of oil-water separation. Having this wetting property, the risk of oil fouling will be greatly reduced as the oil phase will barely be in contact with the coated surface.

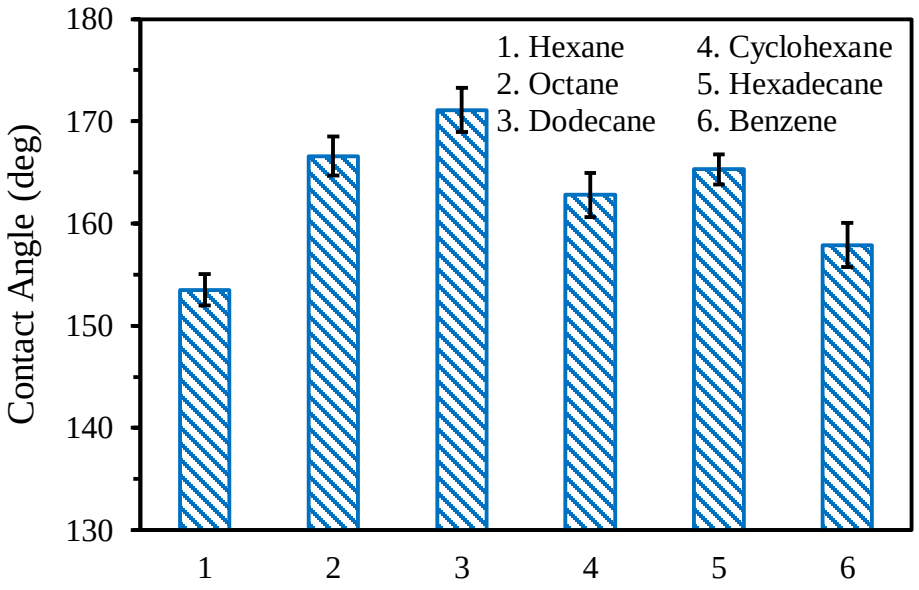

Figure 4- 16. The underwater contact angle measurement of various oils on TiO_2 films.

Further to see the effect of the TiO_2 coating, we carried out the typical contact angle and sliding angle measurement to characterize the wetting properties of TiO_2 coated glass surfaces and uncoated stainless steel substrates (annealed and unannealed). Figure 4-17 point (1-3) shows the θ_{ow} for TiO_2 coated glass surface, unannealed stainless steel, and the one annealed at 550 °C. For all the three cases the θ_{ow} were more than 150° and the values are very close to one another. The result of the contact angle measurements indicate that these surfaces are superoleophobic and the difference among themselves in terms of their oil wettability can be understood by measuring their oil in water sliding angle, which are also depicted in Figure 4-17. For TiO_2 coated on glass, the oil droplet starts sliding at 1.7°, and the same for the annealed stainless steel is more than 3°. However, for the case of unannealed stainless steel, the sliding angle was not observed.

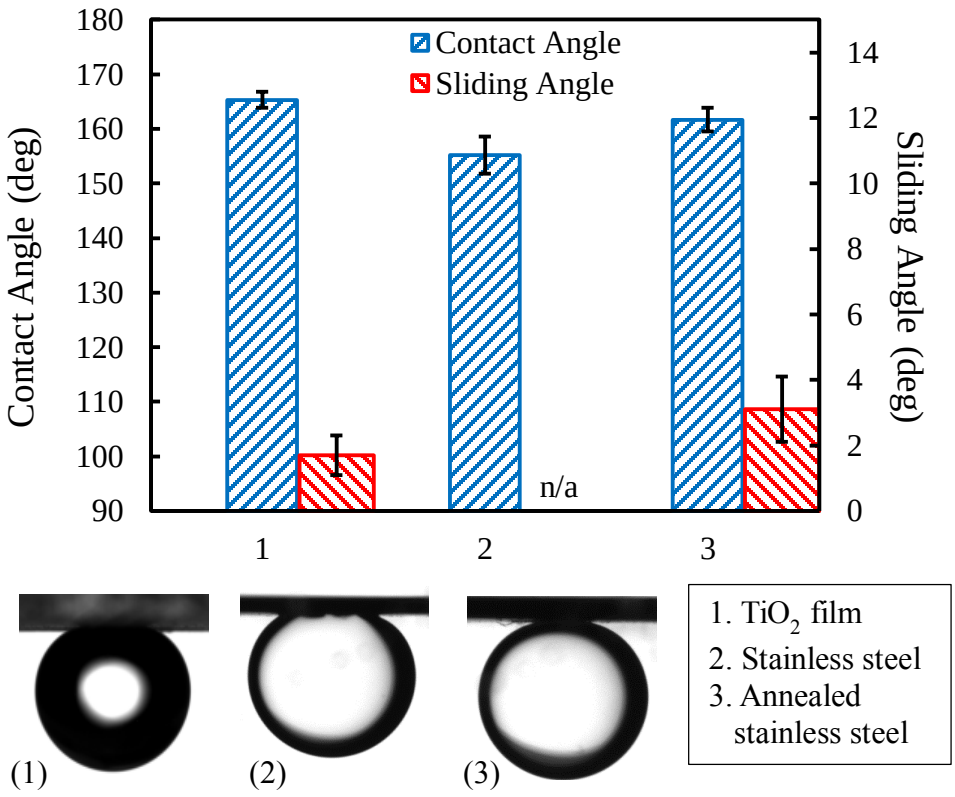

Figure 4- 17. Underwater contact angle and sliding angle measurement of oil on various samples.

From these contact angle and sliding angle measurements, it is quite evident that the annealed stainless steel mesh exhibits underwater superoleophobicity. It will be clear from the subsequent discussions, that the underwater oil repellency of stainless steel mesh is just a prerequisite, but is not sufficient for a stainless steel mesh to be a good filtering medium for oil-water separation. Also from these results, it is quite obvious that the TiO_2 coated on the glass surface has a strong affinity toward water molecules. Even when the oil is in contact with TiO_2 surface, a small volume of water can easily replace the oil in the porous surface of the coating, resulting in zero contact angle of water in oil as shown in Figure 4-13 (c). This result is quite important because the water needs to be

channeled through the mesh while retaining the oil in the process of oil-water separation using TiO_2 coated stainless steel mesh.

Prior to the actual application and study of oil-water separation using TiO_2 coated mesh, we carried out oil in water contact angle θ_{ow} measurements of different alkanes for TiO_2 coated and uncoated stainless steel mesh. Figure 4-18 compares the θ_{ow} of five different oils on the TiO_2 coated and uncoated stainless steel mesh and it is evident that the TiO_2 coating significantly improves the oil repellency of the SS mesh invariably for all the oil samples under study. Also the sliding angle for the TiO_2 coated mesh is very small while for the uncoated mesh, the sliding angle was not observed even when tilted at 30° as depicted in Figure 4-19.

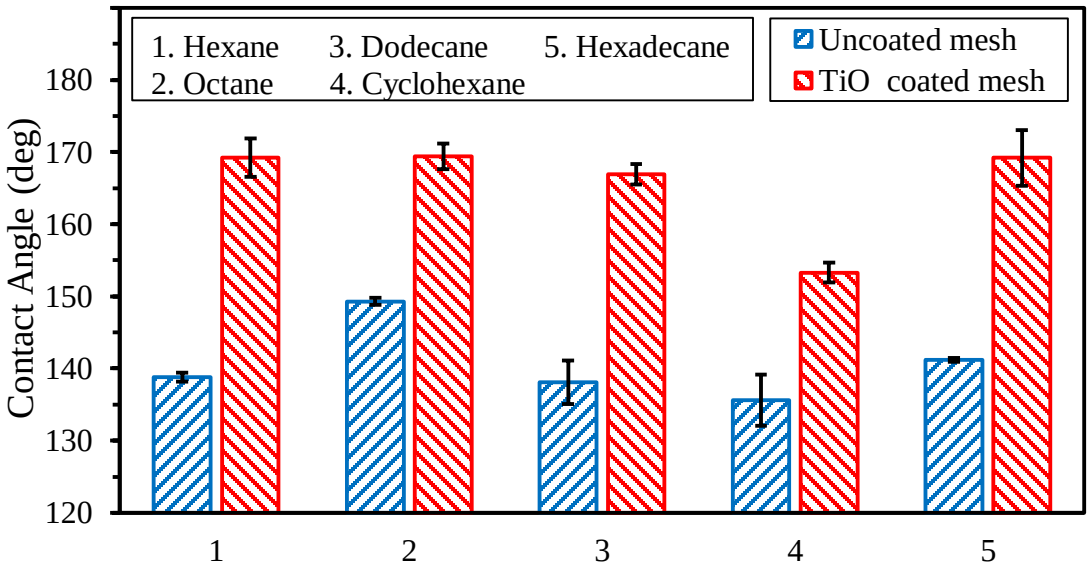

Figure 4- 18. The comparison of the contact angle on TiO_2 coated mesh with the uncoated mesh.

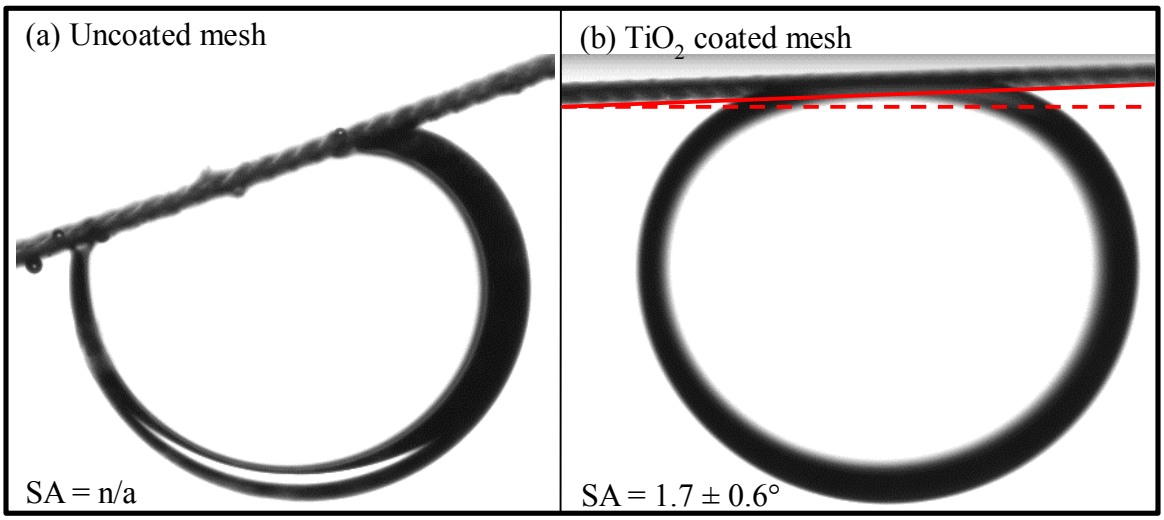

Figure 4- 19. The underwater sliding angle measurement of oil on (a) uncoated mesh and (b) TiO_2 coated mesh.

4.1.4 Oil-Water Separation Test

To understand the mechanism of oil-water separation, it is important to start the test using a mesh which has simpler geometry than the Dutch woven mesh. Simple woven mesh was chosen since it has relatively simple geometry and good homogeneity and periodicity. Simple woven stainless steel mesh with various micro scale pore sizes and wire diameters are commercially available. Figure 4-20 and Figure 4-21 show the uncoated mesh with 254 μm pore size. The TiO_2 coated mesh is shown in Figure 4-22 and 4-23. Figure 4-24 shows the cross sectional view of TiO_2 film on silicon substrate.

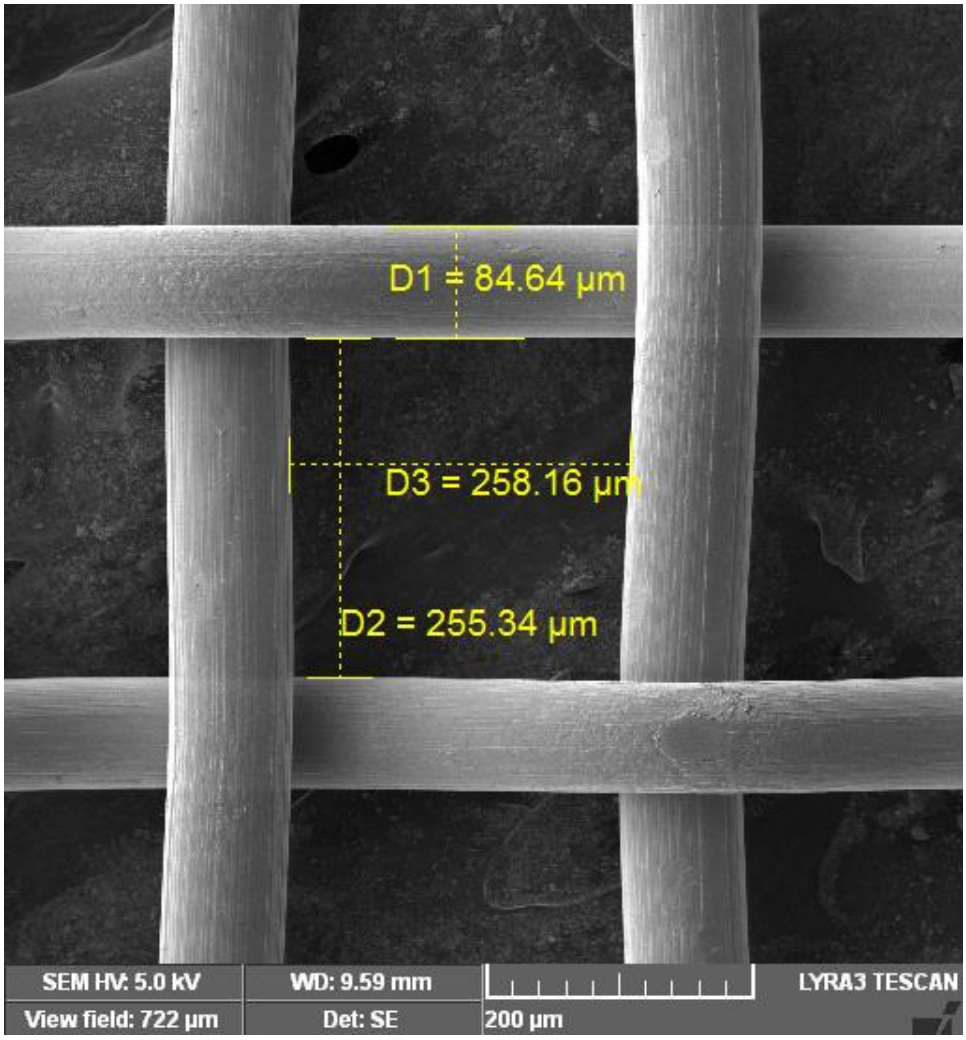

Figure 4- 20. The SEM image of the uncoated stainless steel mesh with pore size of 254 µm at 200 times magnification.

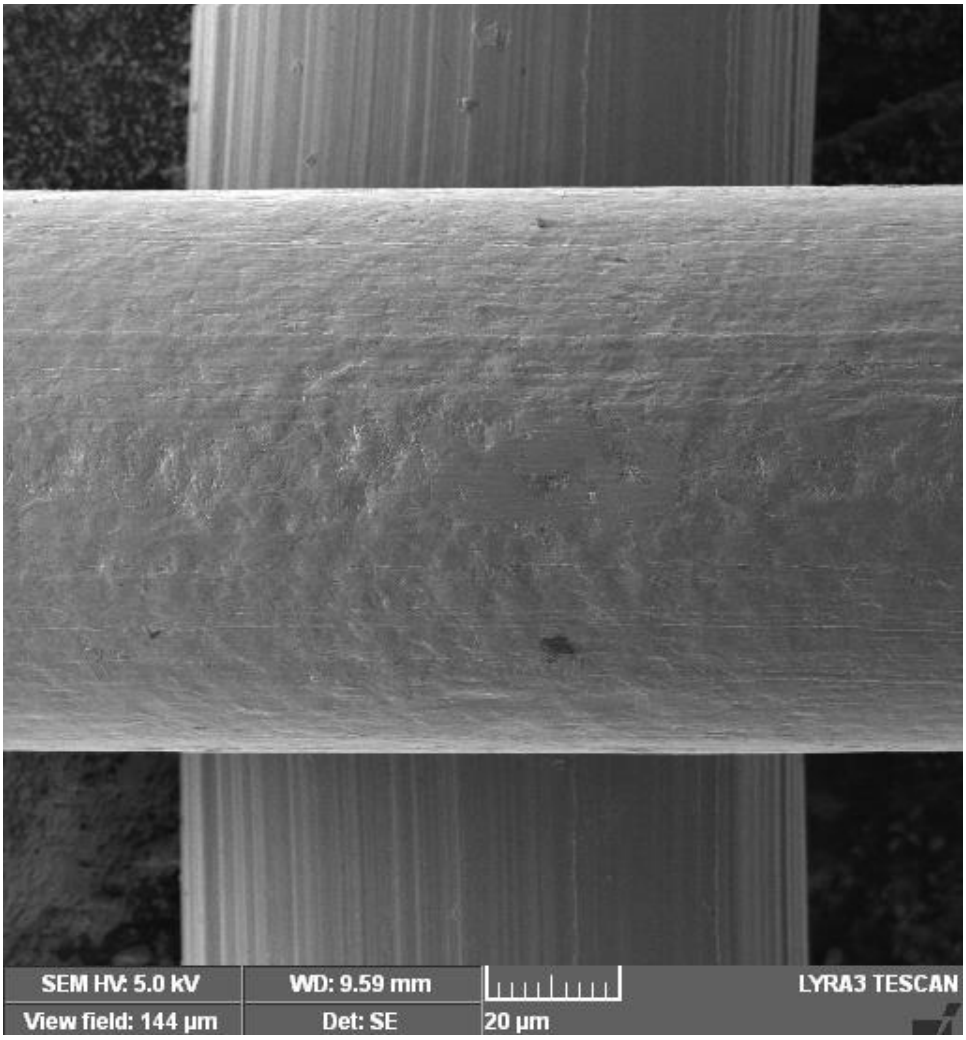

Figure 4- 21. The SEM image of the uncoated stainless steel mesh with pore size of 254 µm at 1000 times magnification.

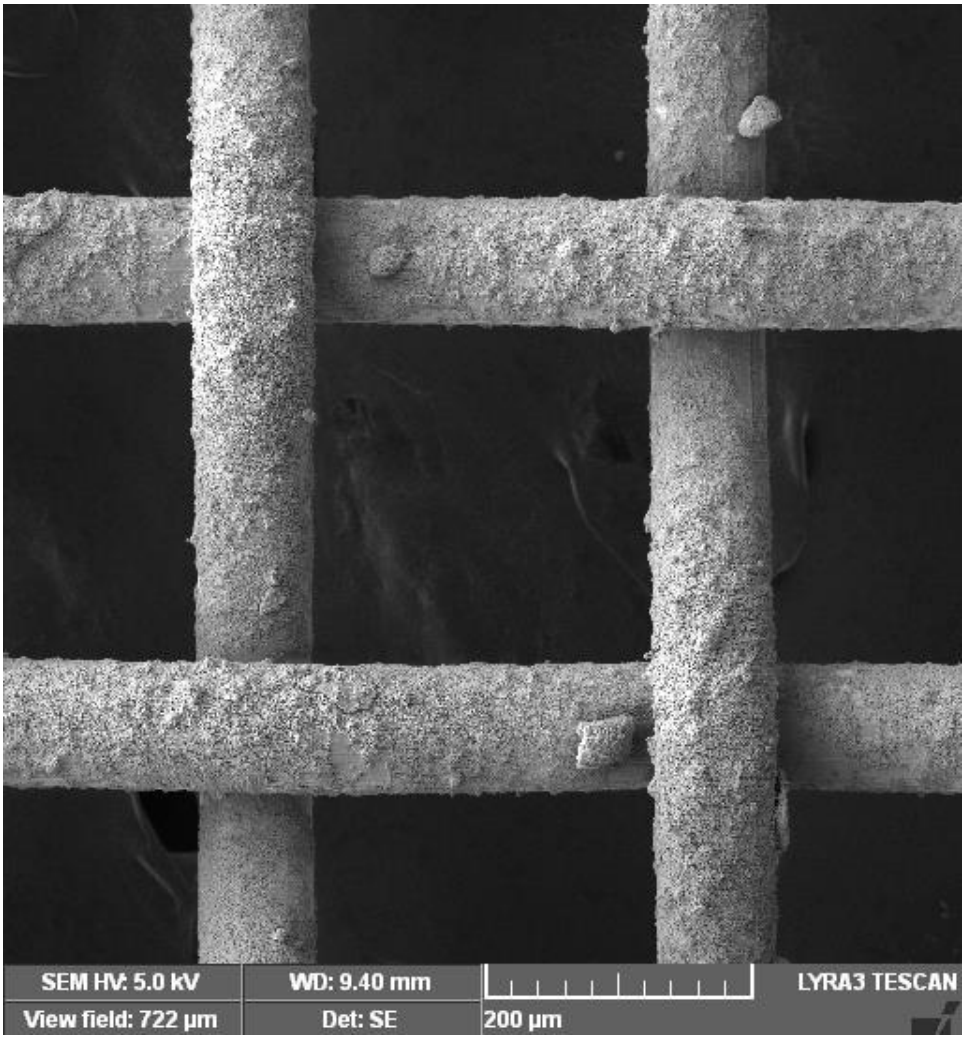

Figure 4- 22. The SEM image of the TiO_2 coated stainless steel mesh with pore size of 254 µm at 200 times magnification.

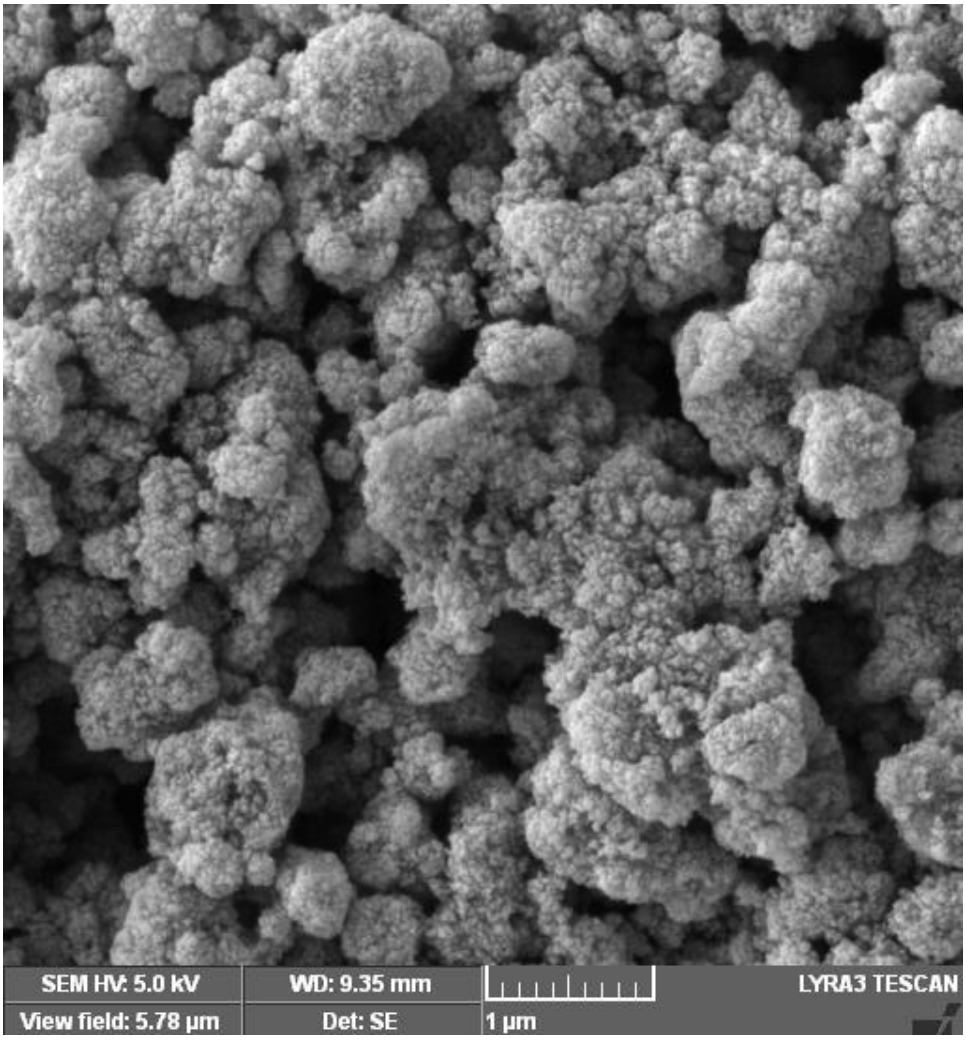

Figure 4- 23. The SEM image of the TiO_2 coated stainless steel mesh with pore size of 254 µm at 25k times magnification.

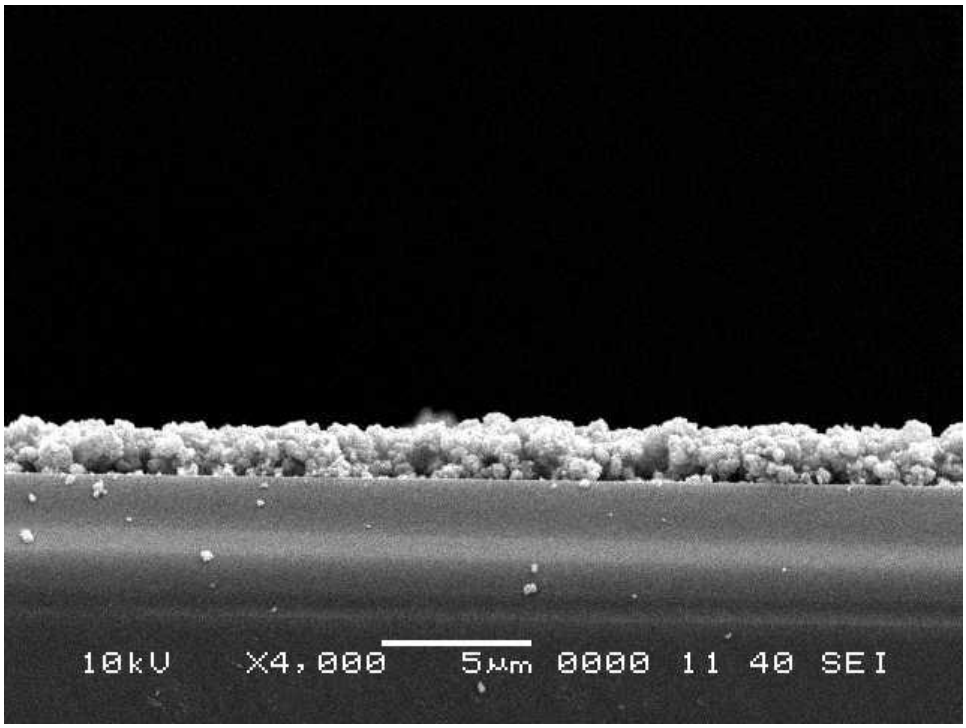

Figure 4- 24. Cross sectional image of the TiO_2 films.

As shown in Figure 4-20 and 4-21, the surface of the uncoated mesh is relatively smooth. Although macroscopically the color darkens after annealing, microscopically there is no appreciable difference compared to the surface morphology of the uncoated mesh. Figure 4-22 shows that the stainless steel mesh has been coated with TiO_2 nanoparticle. Higher magnification is shown in Figure 4-23, revealing the microscale and nanoscale surface roughness of the film. This double scale roughness is an important property for surface with special wettability. To approximate the thickness of the films, a cross sectional image of the film was taken and measured, as depicted in Figure 4-24. The thickness of the film is measured at 2 to 3 μm.

In order to see the effect of TiO_2 coating, we tested uncoated mesh and TiO_2 coated mesh for oil water separation. Pictorial view of the oil-water separation system developed locally for this study is shown in Figure 4-25, along with the SEM images of coated and uncoated stainless steel meshes of pore size 104 micron. The oil water mixture is poured on the top glass tube, and the permeate (water) is collected in a beaker underneath the bottom tube and the oil stays on the top glass tube. The oil-water separation efficiency was calculated using the formula shown in equation (19).

$$Eff = \left(1 - \frac{C_p}{C_o}\right) \times 100\% \tag{19}$$

where C_o and C_p are the volume/volume ratios (v/v) of the original oil-water mixture and the filtered permeate respectively. C_o and C_p were determined by measuring the volume ratio of oil with respect to the mixture (oil and water).

We first used annealed uncoated stainless steel mesh in between the glass tubes and found that both the oil and water permeated through the mesh as exhibited in Figure 4-25 (a). On the other hand, when TiO_2 coated stainless steel mesh was used in between, the water in the oil-water mixture permeated through the coated mesh leaving the oil in the top glass tube as shown in Figure 4-25 (b).

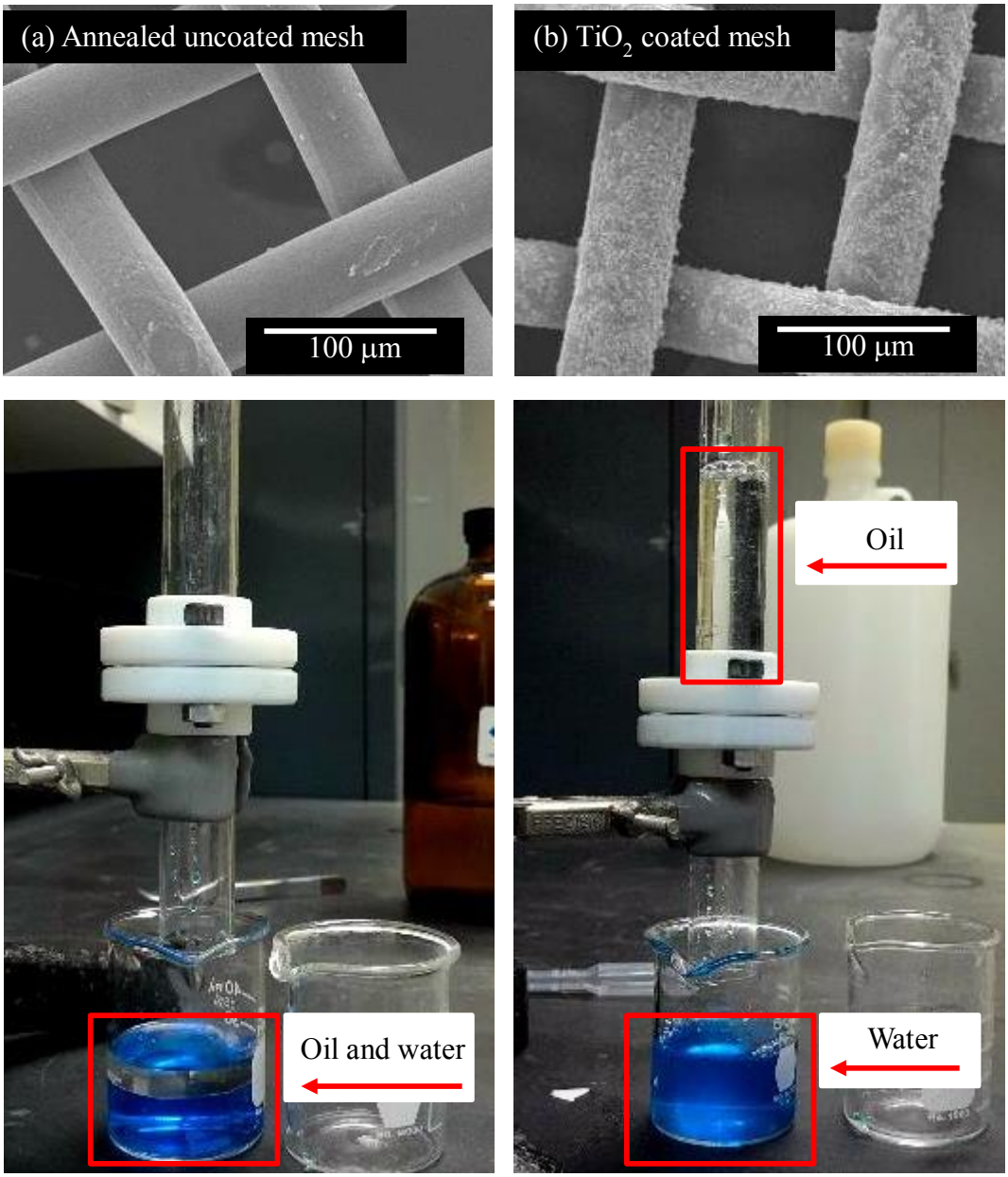

Figure 4- 25. Oil-water separation experiment using (a) uncoated mesh and (b) TiO_2 coated mesh.

Although underwater superoleophobicity is an important factor for the oil-water separation process, it is quite obvious from our experiment that it is not the only factor that governs the oil-water separation while surface roughness also plays a pivotal role. As discussed earlier in the context of Figure 4-17 point (3), superoleophobicity can be achieved simply by annealing of stainless steel. In fact, cleaned glass slides also possess superhydrophilicity and underwater oil repellency [47]. However, as it can be seen from Figure 4-25 (a), superhydrophilicity and underwater oil repellency alone are not the sufficient condition for oil water separation. Simple annealed stainless steel mesh failed in the oil-water separation as demonstrated in this work. On the other hand, the TiO_2 coated meshes of same pore sizes (50 micron and 102 micron), showed more than 98% efficiency in oil-water separation.

From the SEM image of Figure 4-23, it is quite obvious that compared to the smooth annealed stainless steel surface, TiO_2 coated mesh shows micro and nanoscale roughness. This surface roughness is another favorable factor for oil-water separation due to increased underwater oil repellency. Smooth superhydrophilic surface like annealed stainless steel tend to be in contact with water, leaving only a small area for the oil droplets, leading to high oil repellency. By introducing a roughness to the surface, superhydrophilic material can trap water within the roughness. In addition, the strong affinity of TiO_2 towards water molecules can create an adsorbed water layer such that the oil droplet is not at all in contact with the surface. This is also confirmed by the low values of sliding angle, exhibited by TiO_2 coated glass and TiO_2 coated stainless steel mesh.

Since the TiO_2 surface is also wettable by oil in air, the TiO_2 coated mesh must be wetted by water before using it for oil-water separation process so that water layer can be adsorbed by TiO_2 surface. The presence of adsorbed water layer on TiO_2 surface is an important factor for oil-water separation. The adsorbed water layer on the TiO_2 surface plays two different roles in oil-water separation: First, it prevents oil droplets to be in contact with the mesh during the separation process. Second, this layer provides paths for the water droplets from the oil-water mixture to flow to the opposite side of the coated mesh. These conditions for the oil-water separation cannot be met by annealed stainless steel mesh due to its smooth surface texture and weaker affinity toward water molecule.

4.1.5 Measuring the Oil-Water Separation Efficiency

The oil water separation experiment was performed on simple woven meshes with various pore sizes to test the pore size dependence of the oil-water separation. The meshes used have the pore size of 50, 102, 152 and 254 μm. The SEM images of these meshes are shown in Figure 4-26 to Figure 4-29.

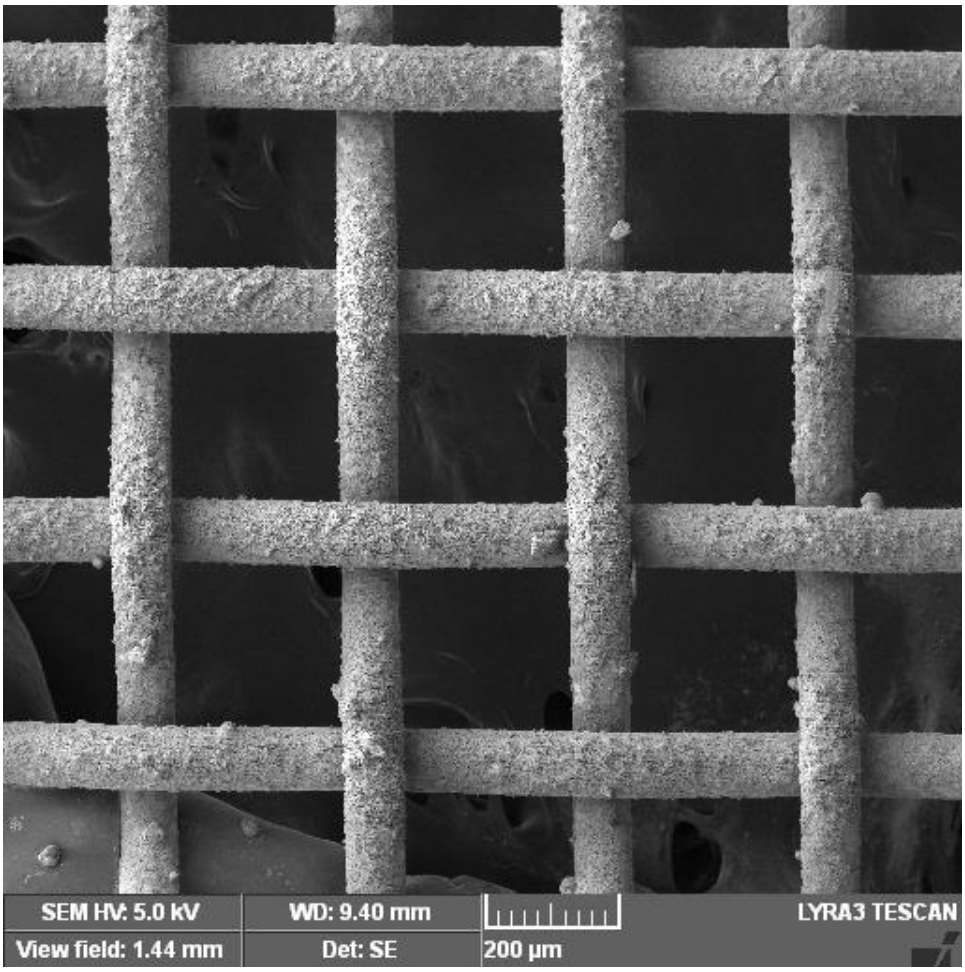

Figure 4- 26. The SEM image of TiO_2 coated mesh with the pore size of 254 µm.

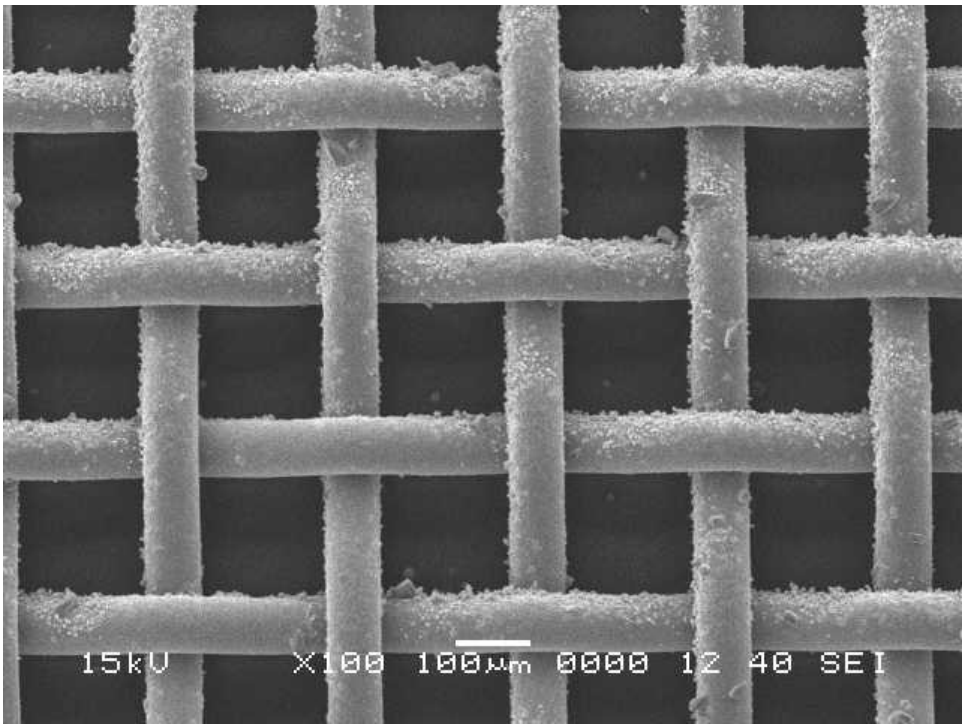

Figure 4- 27. The SEM image of TiO_2 coated mesh with the pore size of 152 µm.

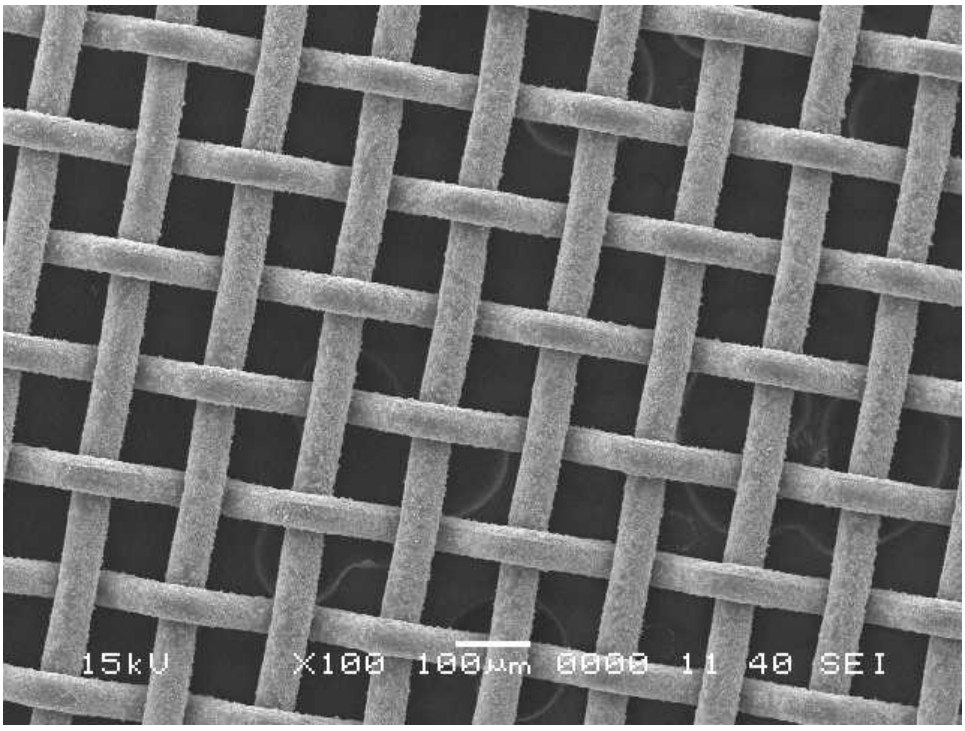

Figure 4- 28. The SEM image of TiO_2 coated mesh with the pore size of 102 µm.

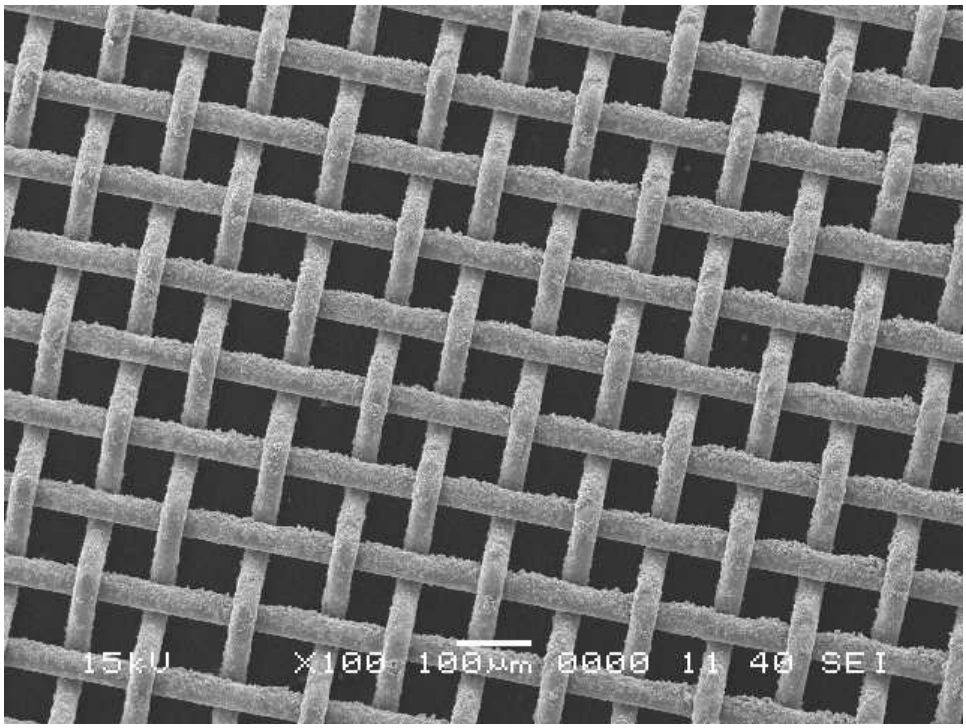

Figure 4- 29. The SEM image of TiO_2 coated mesh with the pore size of 50 µm.

In this oil-water separation system, we used TiO_2 coated stainless steel meshes of four different pore sizes and tested for three different oil samples. The oil-water separation efficiencies of all the 12 combinations of oils and pore sizes are shown in Figure 4-30. From Figure 4-30, it is clear that the TiO_2 coated stainless steel mesh of 50 micron and 104 micron achieved at around 99% oil-water separation efficiency and a very small traces of oil was found in the permeate (water). However, the TiO_2 coated stainless steel meshes of higher pore size shows poor oil-water separation efficiency.

It is clear from this study that a simple spray deposition of nanoparticle dispersion on stainless steel mesh substrates, (contrary to the cumbersome coating procedures) can be applied very well for the oil-water separation. Viscous oil like hexadecane and relatively

less viscous oil like cyclohexane were tested for oil-water separation efficiencies. We found that the separation performance is independent of the viscosity of the oil.

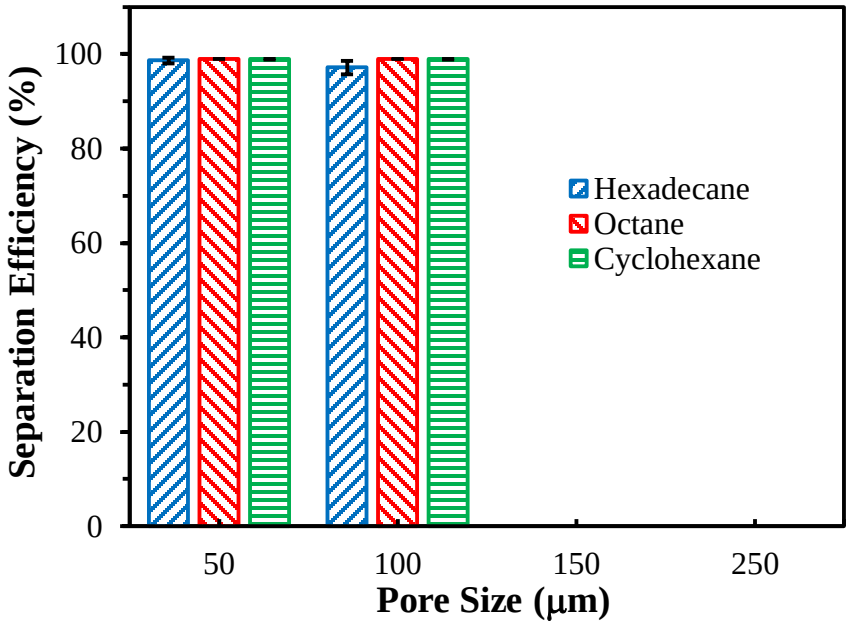

Figure 4- 30. The separation efficiency of TiO_2 coated mesh with different pore sizes.

4.2 ZnO Films

The ZnO films were fabricated using the same method as that of the TiO_2 films. The dispersion concentration used for this study was 10 mg/ml which is produced by mixing 0.10 g of ZnO nanoparticle with 10 ml of THF. The dispersion was then used to coat glass slide substrates, stainless steel mesh substrates, and silicon wafer substrates. The samples were then annealed at 550° for 2 hours. The result of the characterization of the sample is compared with that of the TiO_2 films.

4.2.1 Wettability of ZnO films

The wettability of ZnO films was characterized using the same method as explained earlier. We found that the ZnO films have different wetting behavior than that of the TiO_2 films. Table 4-3 shows the contact angle measurement of ZnO films prepared with different dispersion concentrations in 4 conditions.

Table 4- 3. Contact angle measurement of ZnO films

Dispersion concentration (mg/ml)	Air		Air		HD		Water	
	Water θ_{wa} (°)	SD	HD θ_{oa} (°)	SD	Water θ_{wo} (°)	SD	HD θ_{ow} (°)	SD
5	13.4	3.4	9.7	1.3	67.3	4.0	153.4	2.2
10	16.6	3.7	0	0	50.7	3.6	169.0	2.1
15	6.2	0.6	0	0	51.3	2.2	167.0	2.2

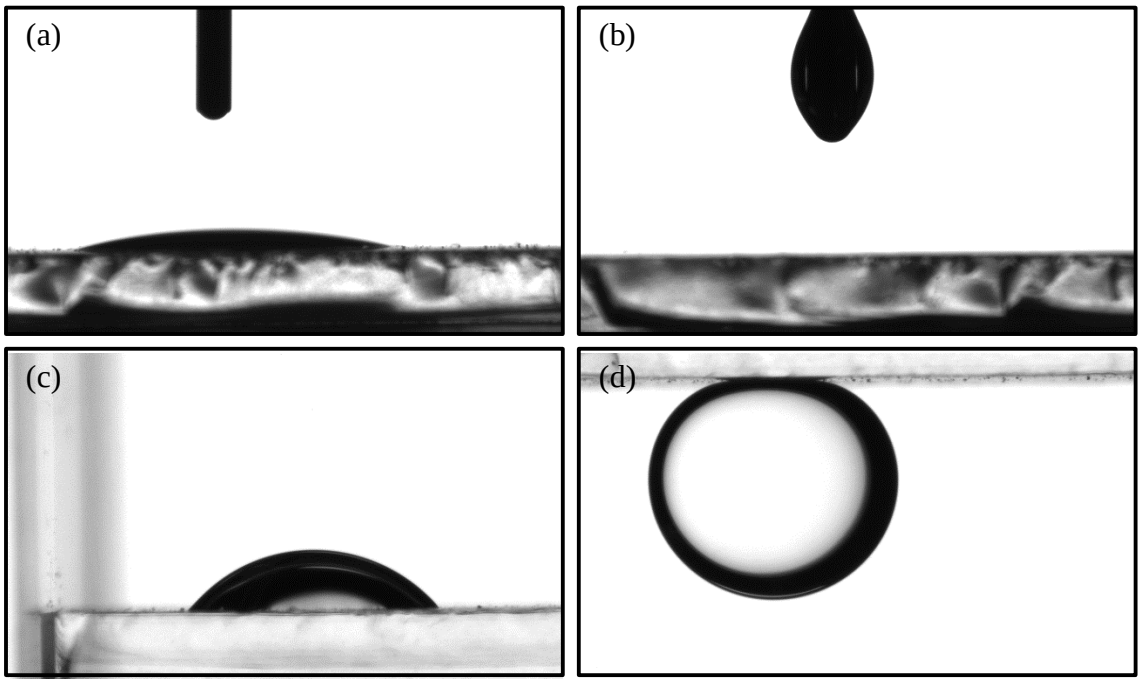

Figure 4- 31. Contact angle measurement of ZnO films (a) water in air, (b) oil in air, (c) water in oil, (d) oil in water.

The wetting property of ZnO films is slightly different than that of TiO_2 films. In Figure 4-31 we can see that the value of θ_{wa} is not 0 like in TiO_2 films. Also, the value of θ_{wo} is much higher than that of in TiO_2 films. These two facts suggest that TiO_2 films have better hydrophilicity than ZnO films. We also observed that the value of θ_{ow} is comparable with that of in TiO_2. This high value of θ_{ow} indicates that the ZnO films have potential for oil-water separation application. The comparison of the wetting properties between TiO_2 films and ZnO films is provided in Figure 4-32.

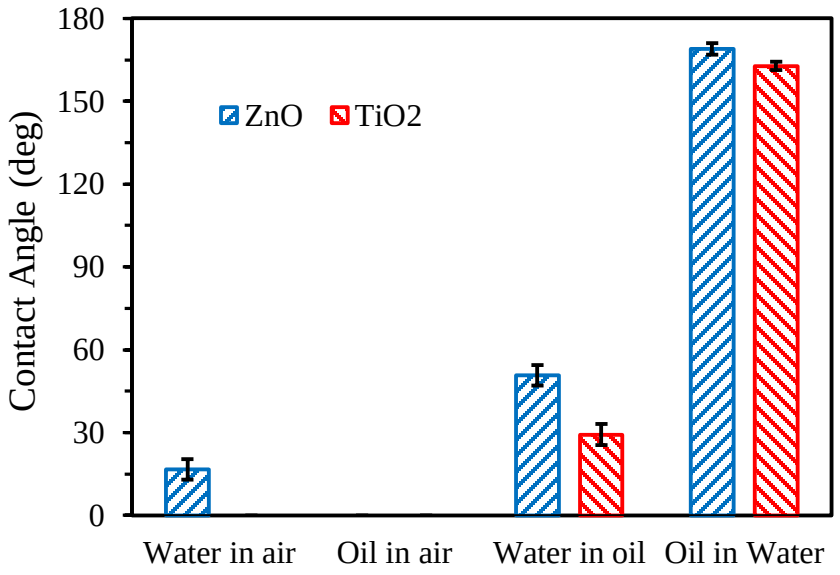

Figure 4- 32. The comparison of the contact angle of ZnO films with TiO_2 films.

4.2.2 Surface Morphology of ZnO films

The surface morphology of the films was characterized using SEM. Figure 4-33 to Figure 4-35 show the surface morphology of ZnO film deposited on stainless steel mesh substrate. Figure 4-36 shows the cross sectional view of the films deposited on silicon wafer substrates. The ZnO films seem to have finer surface morphology, better particle distribution and less clustered agglomeration than the TiO_2 films.

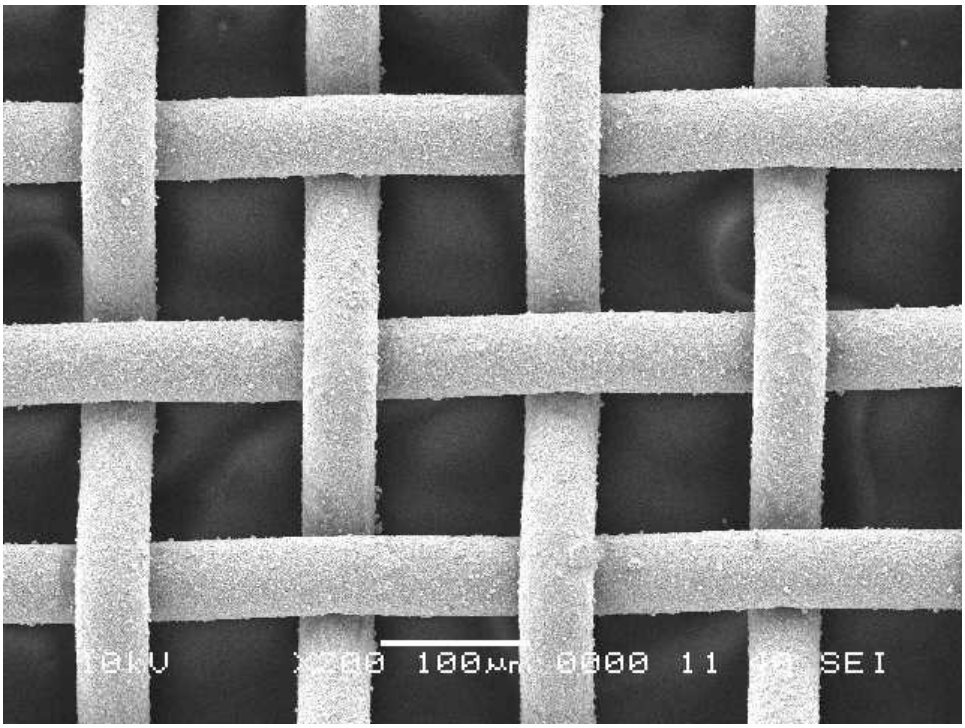

Figure 4- 33. The SEM image of ZnO coated mesh with the pore size of 102 µm at 200 times magnification.

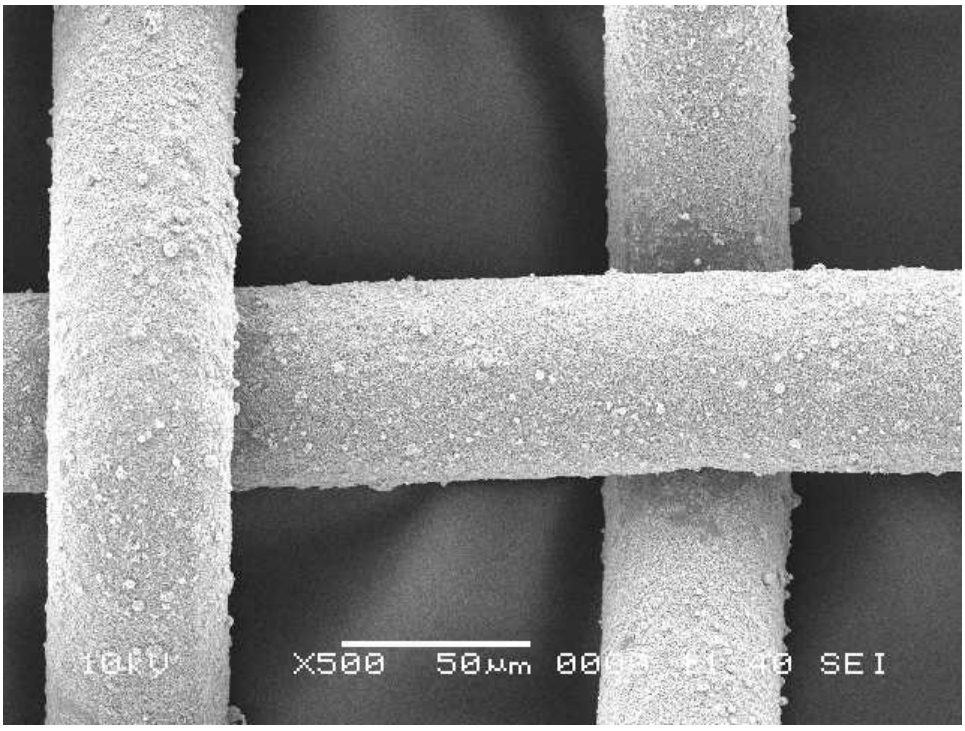

Figure 4- 34. The SEM image of ZnO coated mesh with the pore size of 102 µm at 500 times magnification.

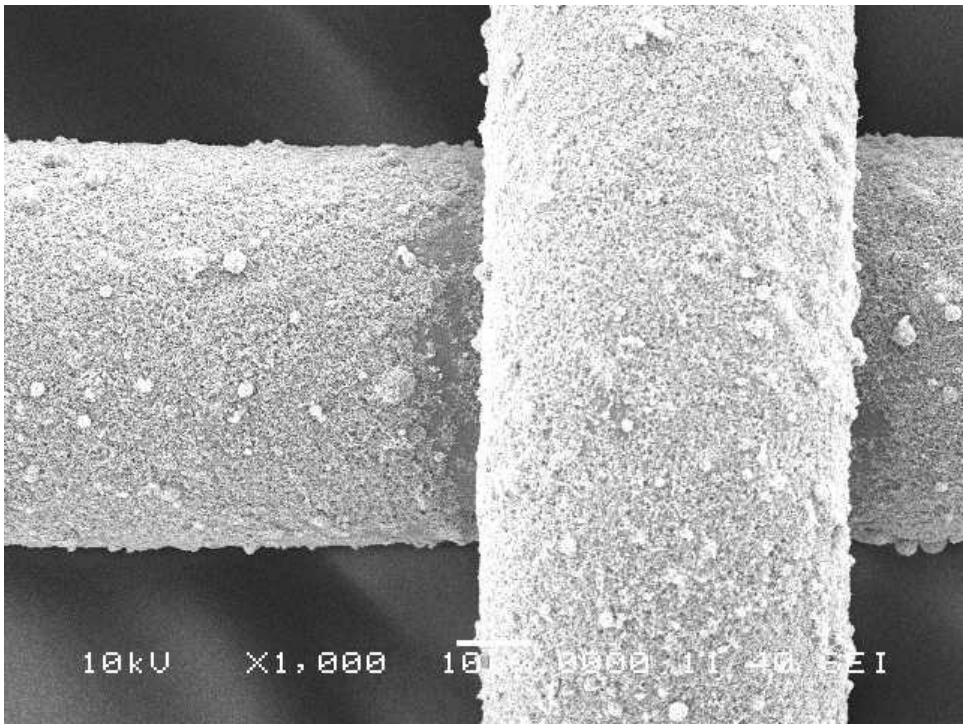

Figure 4- 35. The SEM image of ZnO coated mesh with the pore size of 102 μm at 1000 times magnification.

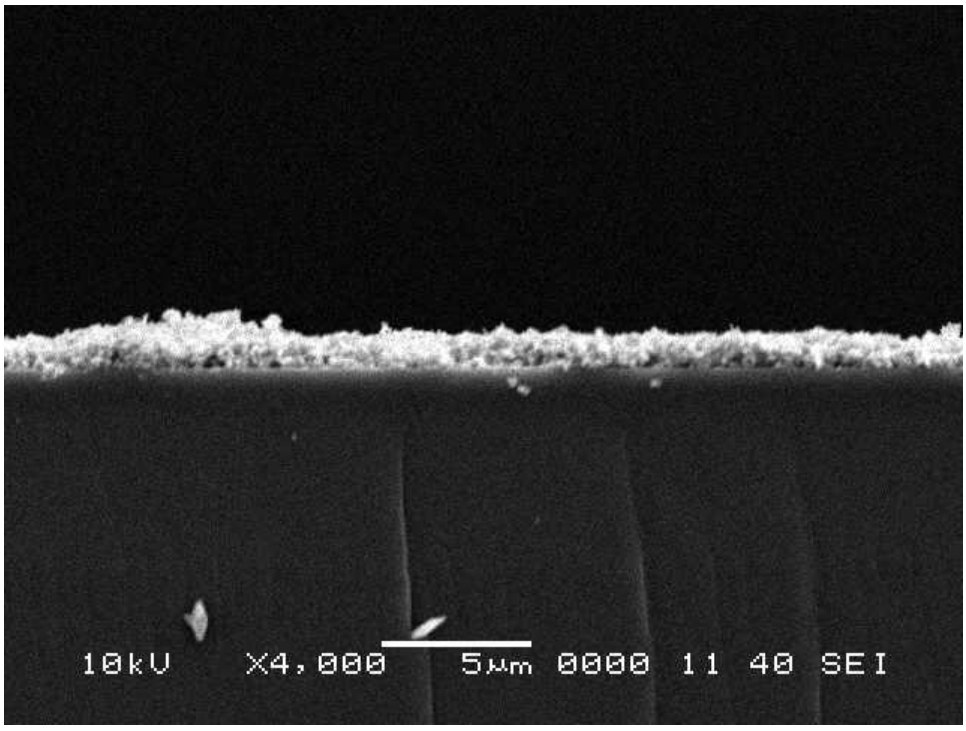

Figure 4- 36. Cross sectional view of ZnO film.

4.2.3 Oil Water Separation Test

The oil water separation test was also carried out using the ZnO coated mesh with different pore sizes. In this experiment, only octane and cyclohexane were being tested. The result was rather different than the test for TiO_2 coated mesh. While the maximum pore size in TiO_2 coated mesh for performing oil-water separation was observed at 104 μm, the maximum pore size for ZnO coated mesh was only at 50 μm. The experimental result is depicted in Figure 4-37.

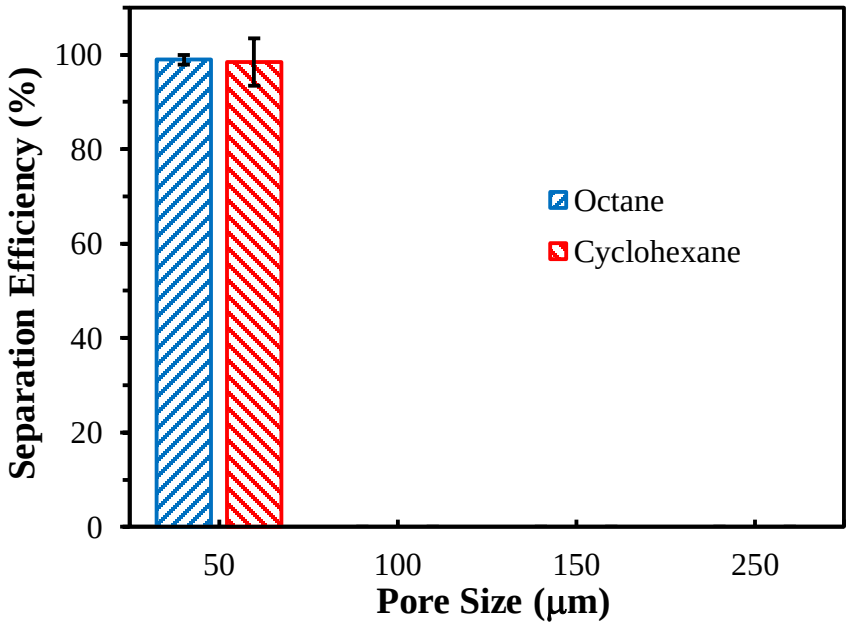

Figure 4- 37. The separation efficiency of ZnO coated mesh with different pore sizes.

4.3 WO_3 Films

The WO_3 films were fabricated using spray deposition of nanoparticle dispersion. Based on the optimum experimental parameters found in the fabrication of TiO_2 films, the WO3 films were fabricated using 10 mg/ml of the dispersion of nano WO_3 in THF. The substrates used are stainless steel mesh, glass slides, and silicon wafer substrates. The annealing temperature was 550° C set for 2 hours. The samples were then characterized and compared with the results for TiO_2 films.

4.3.1 The Wettability of WO_3 Films

Goniometric measurement was performed to assess the wettability of the WO_3 films. Table 4-4 shows the results of the contact angle measurement of WO_3 films prepared using there different dispersion concentrations. 10 mg/ml was taken to be the optimum dispersion concentration since it has excellent superhydrophilicity and underwater oil repellency. Also, higher dispersion concentration did make better results for the surface wettability. From the result shown in Figure 4-38 and Figure 4-39, we can see that the value of θ_{wo} for WO_3 films is lower than TiO_2 films while the value of θ_{ow} of the two films are comparable. These facts suggest that the WO_3 films is more hydrophilic than the TiO_2 films. This result make WO_3 favorable since for the oil-water separation application, material which has better hydrophilicity is more desired [26].

Table 4- 4. The contact angle measurement of WO_3 films.

Dispersion concentration (mg/ml)	Air		Air		HD		Water	
	Water θ_{wa} (°)	SD	HD θ_{oa} (°)	SD	Water θ_{wo} (°)	SD	HD θ_{ow} (°)	SD
5	18.2	0.9	15.7	3.5	57.7	3.7	153.2	2.3
10	0	0	0	0	16.4	2.1	163.6	2.1
15	0	0	0	0	15.3	2.3	164.7	2.3

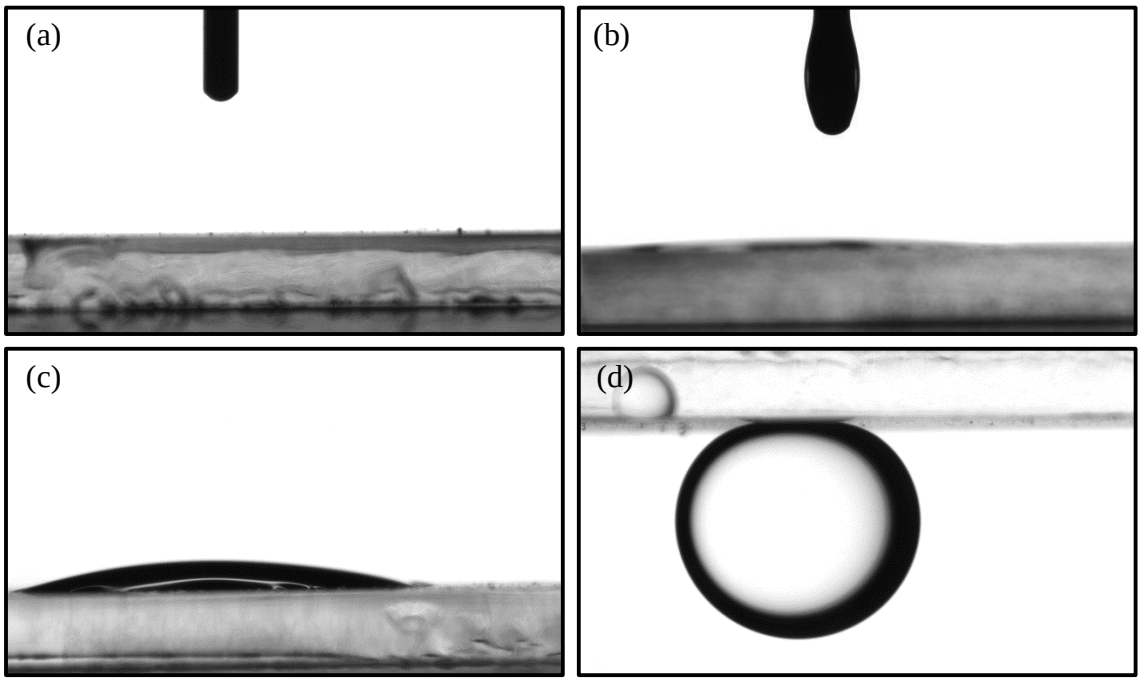

Figure 4- 38. Contact angle measurement of WO_3 films (a) water in air, (b) oil in air, (c) water in oil, (d) oil in water.

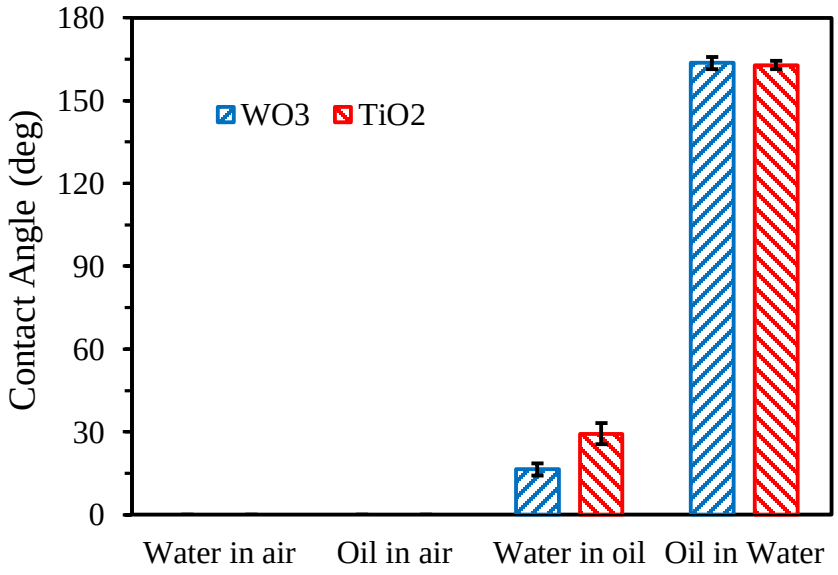

Figure 4- 39. The comparison of the contact angle of WO_3 films with TiO_2 films.

4.3.2 Surface Morphology of WO_3 Films

The surface morphology of the WO_3 films was investigated under SEM. Figure 4-40 and Figure 4-41 show the surface morphology of WO_3 film deposited on stainless steel mesh substrate. Figure 4-42 shows the cross sectional view of the films deposited on silicon wafer substrates. The nanoparticles look uniformly distributed to the whole surface of the substrate with thickness of 1 to 2 micron.

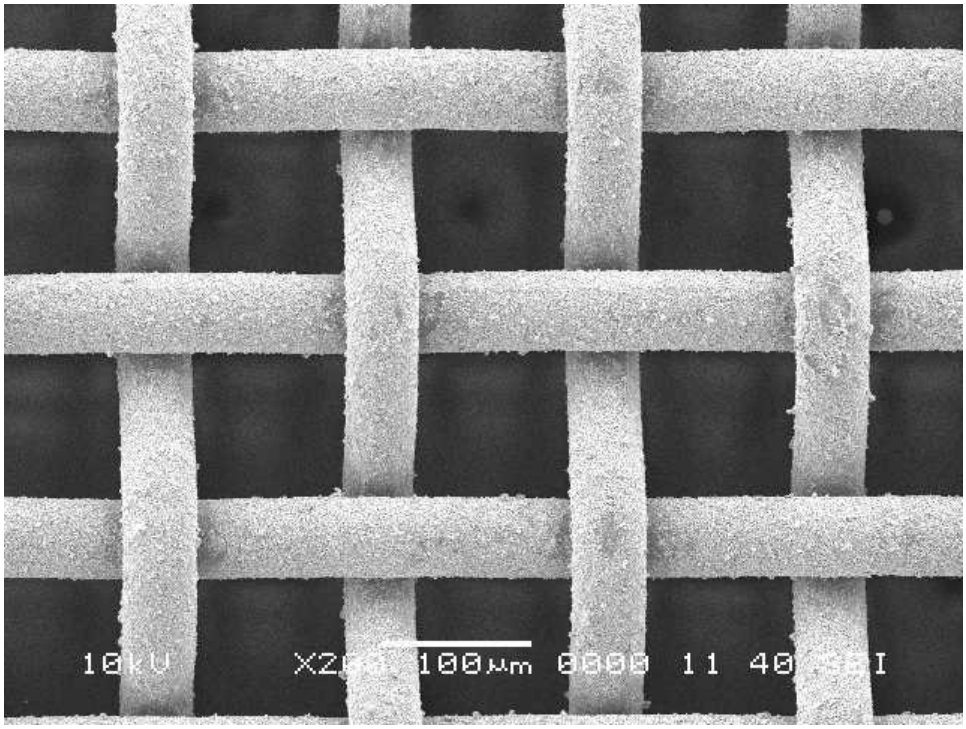

Figure 4- 40. The SEM image of WO_3 coated mesh with the pore size of 102 µm at 200 times magnification.

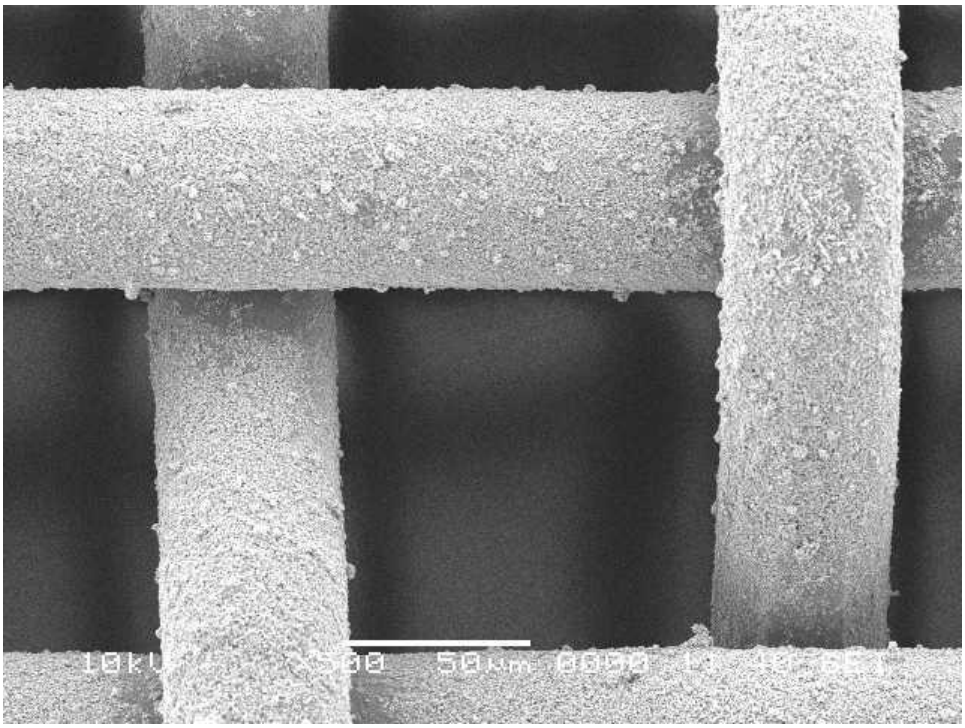

Figure 4- 41. The SEM image of WO_3 coated mesh with the pore size of 102 μm at 500 times magnification.

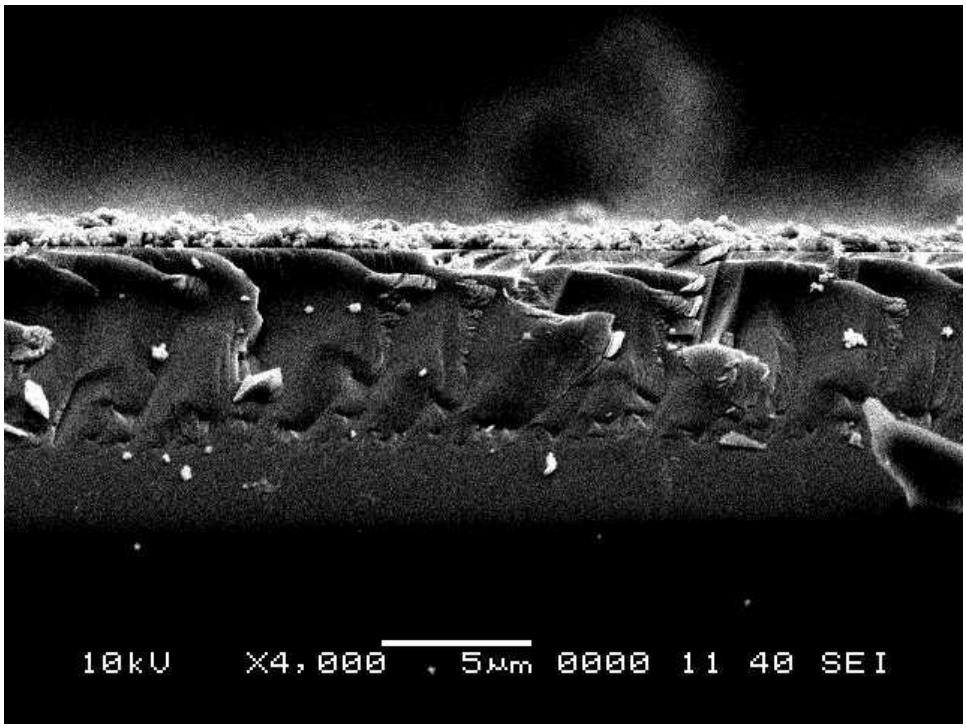

Figure 4- 42. Cross sectional view of WO_3 film

4.3.3 Oil Water Separation Test

Oil-water separation experiment was carried out to examine the performance of WO_3 coated mesh for separating water phase from the oil-water mixture. The WO_3 coated mesh seems to have better performance in the oil-water separation as compared with TiO_2 coated mesh and ZnO coated mesh. The maximum pore size can work for oil water separation is 152 μm which is bigger than that of using TiO_2 and ZnO films. The separation efficiency for pore size lower than 152 μm was higher than 98%. For the pore size as large as 254 μm, the separation failed and both oil phase and water phase are channeled to the opposite face of the coated mesh and accumulated in the beaker. From this result, we conclude that, compared to TiO_2 and ZnO, WO_3 is the best material for oil-water separation application.

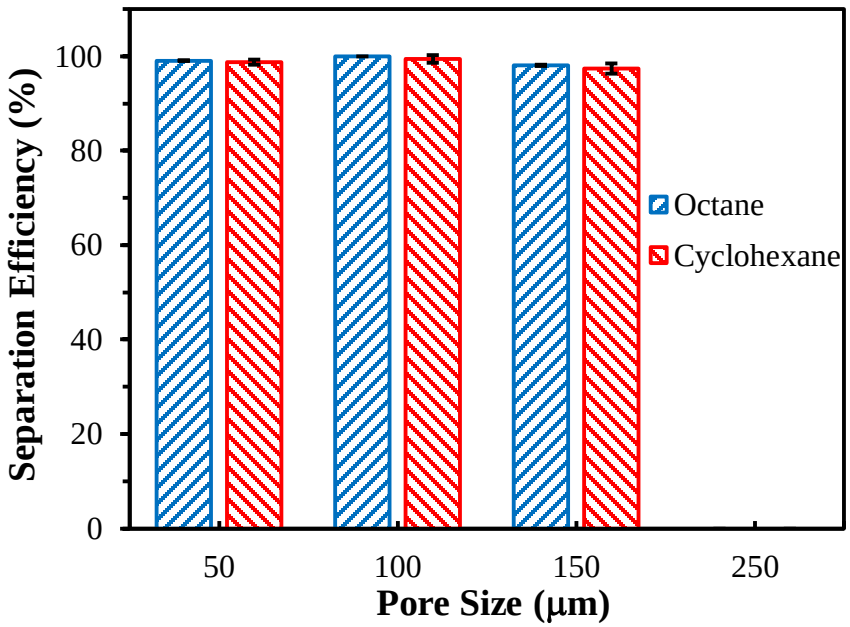

Figure 4- 43. The separation efficiency of WO_3 films with different pore sizes.

4.4 The Intrusion Pressure

We observed in Figure 4-30, 4-37, and 4-43 that the oil-water separation did not yield a desirable result when the pore size of the stainless steel mesh is more than 102 micron for TiO_2 coated mesh. However, if the oil was carefully placed on top of the coated mesh, it can withstand the pressure of the oil column as shown in Figure 4-44. At a certain height, h_{max}, the oil starts flowing down and penetrating the TiO_2 coated mesh. The intrusion pressure can be determined by calculating the maximum hydrostatic pressure which can be sustained by the mesh. It can be defined as $P_{int} = \rho g h_{max}$ where ρ is the density of oil. When the hydrostatic pressure is below the intrusion pressure, i.e. after $h < h_{max}$, we expected that the oil will stop flowing. Curiously, once the oil starts flowing, it will keep flowing until most of the oil phase is transferred to the other side of the coated mesh.

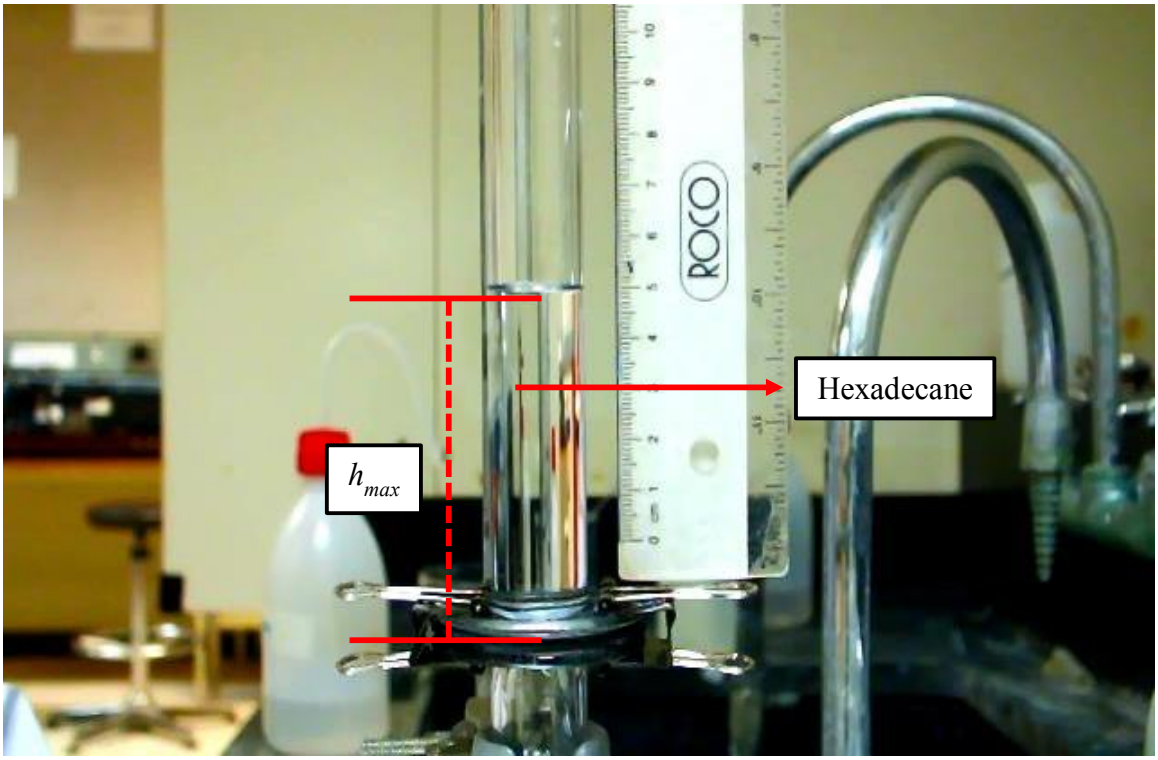

Figure 4- 44. The intrusion pressure measurement of TiO_2 coated mesh with pore size of 254 μm.

The intrusion pressure can be approximated theoretically using equation (5) where the γ and θ now are γ_{ow} and θ_{ow} since the interface is between oil and water, and D is the pore size of the coated mesh. The use of γ_{ow} and θ_{ow} here is because of the formation of capillary bridge (water-film) during the wetting process before the intrusion pressure measurement was initiated. This capillary bridge is illustrated in Figure 4-45 (a). The presence of the capillary bridge provide similar interface such as in Figure 2-1 except that the non-wetting phase is oil phase. Thus, equation (5) can be re written in equation (20).

$$P_{int} = -\frac{4\gamma_{ow}\cos\theta_{ow}}{D} \qquad (20)$$

This approximation has limitation since the geometry taken into account in equation (20) is circular or a tube as shown in Figure 2-1. However, several observation can be made using this equation. Firstly, the magnitude of the intrusion pressure is pore size dependent. The smaller the pore size is, the higher the magnitude of the intrusion pressure. This observation match with experimental result since when the pore size of the mesh used is bigger, the separation is more prone to failure. If the intrusion pressure is small, the separation may fail as the impact force of the mixture fluctuates during the separation process.

Secondly, as long as the θ_{ow} is larger than $\pi/2$, the intrusion pressure will always be positive. The intrusion pressure is actually the pressure difference between water phase and the oil phase, $P_{int} = \Delta P = P_{water} - P_{oil}$. Thus, if the value of P_{int} is positive, then the pressure of water phase is greater than the pressure of the oil phase, so that oil cannot flow through the pore of the mesh unless an external pressure is applied to overcome the pressure difference. On the contrary, if the value of P_{int} is negative, oil will channel through the mesh even without the aid of external pressure.

Thirdly, equation (20) works if and only if the interface is between oil and water so that γ_{ow} and θ_{ow} are used. This can also be proven otherwise. In the measurement of the intrusion pressure, oil phase will flow through the coated mesh when h_{max} is reached. This fact indicates that the interface within the pore of the mesh has changed.

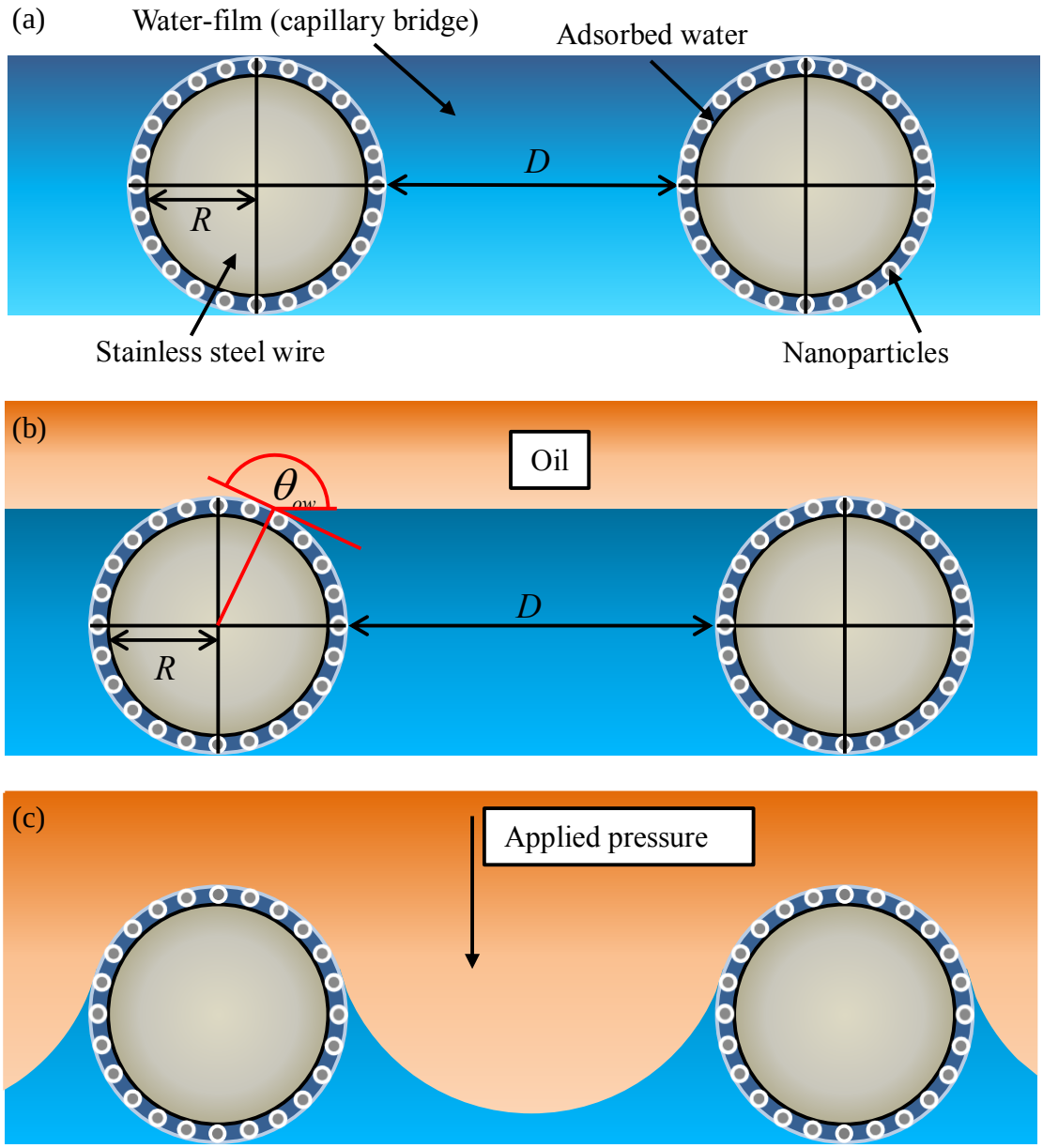

Figure 4- 45. Illustration of the interface within the pore of the mesh.

Figure 4-45 shows the illustration of the interface within the pore of the mesh. Figure 4-45 (a) is when the oil phase is absence in the interface i.e. before the oil was added to the mesh. Figure 4-45 (b) is when the oil was added to the mesh. The oil water interface is formed with the contact angle θ_{ow} is formed. When the external pressure is introduced,

the oil phase is squeezed and approaching the bottom line of the water film. If the applied pressure is higher than the intrusion pressure, the water film will break and the new interface will be formed, which is oil water and vapor interface. One then can examine the new contact angle formed using Young's equation of contact angle, as in equation (21), by imagining oil droplet sitting on water in air environment.

$$\cos\theta = \frac{\gamma_{wv} - \gamma_{\mathrm{ow}}}{\gamma_{ov}} \tag{21}$$

Since the value of γ_{wv} is generally larger than γ_{ow} in most of the case, the value of the newly formed contact angle θ is positive. As the consequence, the intrusion pressure will be negative. This is why the oil can flow through the coated mesh after the h_{max} is reached and keep flowing even after h is lower than h_{max}.

The formation of the capillary of water-film between the wires of the mesh is quite normal, because the pore size of the mesh is much smaller than the capillary length of water [60,61]. This water-film is found to be one of the most important factors that govern the oil-water separation. Failing to form the capillary bridge, oil water interface will not be formed and equation (20) cannot be applied. With this view, it is important to select porous substrate where robust capillary bridge can be formed and can sustain high external pressure.

4.5 Modeling the Oil-Water Separation Mechanism

In this work, oil-water separation medium was achieved by modifying surface wettability such that the surface is more wettable by water than by oil. Figure 4-45 (a) illustrates the complete set of the separating medium. It consists of porous substrate coated with superhydrophilic material and water film attached between the pores. The water film has role as a barrier to prevent the oil from penetrating the mesh. When the oil phase comes in contact with the coated mesh, it will be sustained by the capillary force of oil in which the direction is the opposite of the weight force. On the other hand, when water phase comes, it will be diffused with the water layer and transferred to the other phase of the mesh. In summary, the oil water separation can take place because of the difference in the direction of the capillary forces for oil and water.

The intrusion pressure can be deducted from the force balance in vertical axis, $\Sigma F_y = 0$, at the interface. The forces involved here are the force from external pressure F_P and the force from the interfacial tension, F_γ. These forces can be written as

$$F_P = \Delta P \times A \tag{22}$$

$$F_\gamma = -L\gamma_{ow}\cos\theta_{ow} \tag{23}$$

$$\Delta P = \frac{-L\gamma_{ow}\cos\theta_{ow}}{A} \tag{24}$$

where A and L here are the surface area and the contact line of the interface. The value of A and L depends on the shape or geometry of the pore. By equating (22) and (23), we then can write the expression of the intrusion pressure as in equation (24). Table 4-5 shows the expression of the intrusion pressure for some basic shapes.

Table 4- 5. The expression of the intrusion pressure of pores with different shapes.

Shape of the pore	Intrusion pressure
Square 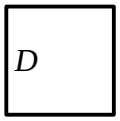	$-\frac{4\gamma_{ow}\cos\theta_{ow}}{D}$
Rectangle 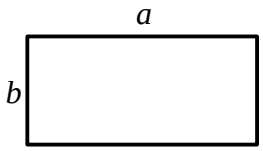	$-2\gamma_{ow}\cos\theta_{ow}\left(\frac{1}{a}+\frac{1}{b}\right)$
Circle 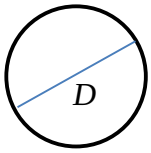	$-\frac{4\gamma_{ow}\cos\theta_{ow}}{D}$
Equilateral 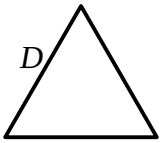	$-\frac{4\sqrt{3}}{D}\gamma_{ow}\cos\theta_{ow}$
Isosceles 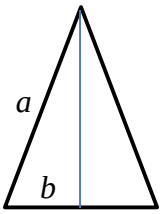	$-\frac{(2a+b)}{b(a^2-b^2)}\gamma_{ow}\cos\theta_{ow}$

Rather complex geometry is exhibited in the simple woven mesh used in this thesis work. We can approximate the shape of the pore using stack of bars parallel at same level but perpendicular at the other as shown in Figure 4-46.

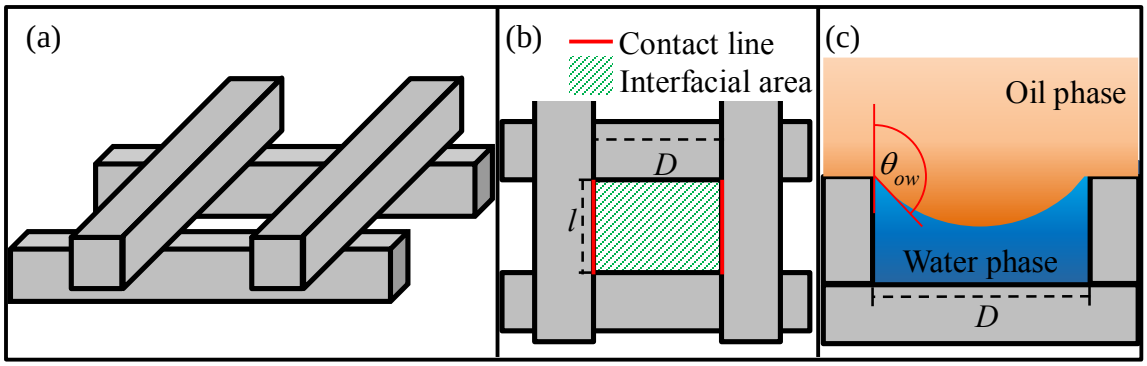

Figure 4- 46. Modeling the interface in the mesh using stack of bars.

From Figure 4-46 we can see that $A = Dl$ and $L = 2l$. Substituting these value to equation (24), we obtain the expression of the intrusion pressure for this model, which is shown in equation (25) [56].

$$\Delta P = -\frac{2\gamma_{ow}\cos\theta_{ow}}{D} \qquad (25)$$

Better approximation can be performed using stack of cylinders instead of stack of bars. This model is illustrated in Figure 4-47.

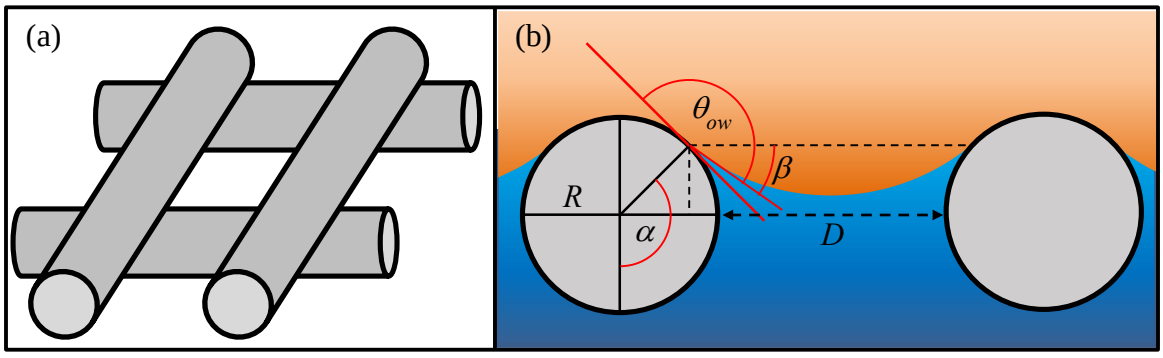

Figure 4- 47. Modeling the interface of the mesh using stack of cylinders.

The illustration for the contact area is the same with the one in Figure 4-46 (b). From Figure 4-47 we can see that the contact line, $L = 2l$. However, the contact area now is $A =$

lD^* where D^* is defined as $D^* = D + 2(R–R\ sin\ (\pi–\alpha))$. Since $sin\ (\pi–\alpha) = sin\ \alpha$, therefore, the contact area can be simplified as $A = l(D + 2R(1\text{-}sin\ \alpha))$. Knowing this fact, we can re-derive F_γ and F_P as in equation (26) and (27).

$$F_P = \Delta P \times l(D + 2R(1 - \sin\alpha) \tag{26}$$

$$F_\gamma = -2l\,\gamma_{ow} \sin\beta \tag{27}$$

In equation (27), $sin\ \beta$ is used in order to obtain the vertical component of the force caused by the interfacial tension, γ_{ow}. Here, β defined as $\beta = \theta_{ow}\text{-}\alpha$. By replacing β with $(\theta_{ow}\text{-}\alpha)$ and equating F_P and F_γ, the intrusion pressure can be expressed as in equation (28).

$$\Delta P = -\frac{2\,\gamma_{ow} \sin(\theta_{ow} - \alpha)}{(D + 2R(1 - \sin\alpha)} \tag{28}$$

All of the parameters in equation (28) are known except for α, which is the angle where the oil-water interface take place. The angle α is angle formed between the contact line and the lowest part of the mesh wire under the influence of the applied pressure. As the applied pressure increases, the value of α decreases. When there is no applied pressure, $\Delta P = 0$, then $\alpha = \alpha_0 = \theta_{ow}$ and $\beta = 0$ so that the interface will look like in Figure 4-44 (b). The intrusion pressure is overcome when ΔP is maximum, which also correspond to $\alpha = \alpha_{max}$. Thus by finding maxima of ΔP with respect to α, the expression of α_{max} can be determined [23].

$$\frac{d(\Delta P)}{d\alpha} = -\frac{2\,\gamma_{ow}((D + 2R)\cos(\theta_{ow} - \alpha_{max}) - 2R\sin\theta_{ow})}{(D + 2R(1 - \sin\alpha_{max})^2} = 0$$

$$((D + 2R)\cos(\theta_{ow} - \alpha_{max}) - 2R\sin\theta_{ow}) = 0$$

$$\cos(\theta_{ow} - \alpha_{max}) = \frac{2R \sin \theta_{ow}}{(D + 2R)}$$

$$\alpha_{max} = \theta_{ow} - cos^{-1}\left(\frac{2R \sin \theta_{ow}}{(D + 2R)}\right) \quad (29)$$

Then, the intrusion pressure in equation (28) can be written as

$$P_{int} = -\frac{2\,\gamma_{ow} \sin(\theta_{ow} - \alpha_{max})}{(D + 2R(1 - \sin \alpha_{max})} \quad (30)$$

where α_{max} is given in equation (28).

As shown in equation (29), the value of α depends on θ_{ow}. Equation (29) can be used to understand the mechanism of the oil-water separation. Figure 4-48 shows the plot of α_{max} versus θ_{ow}.

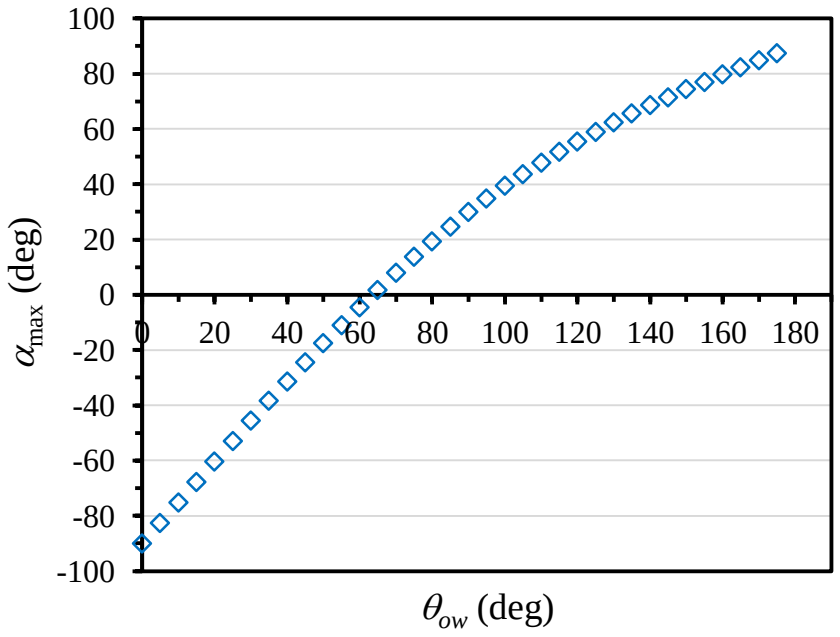

Figure 4- 48. The value of α_{max} for different value of θ_{ow}.

From Figure 4-48, we can see that when θ_{ow} is over 150°, the oil droplet needs to be squeezed to the pore until $\alpha < 90°$ in order to overcome the intrusion pressure. On the other hand, if the liquid has $\theta_{ow} = 0°$, it will immediately flow to the other face of the mesh in order to satisfy the interfacial line.

Figure 4-49 to 4-51 are the comparison of the experimental value with the calculated value of the intrusion pressure versus γ_{ow}/D for TiO_2, ZnO, and WO_3 coated meshes respectively. The measured value was determined by measuring the maximum hydrostatic pressure discussed earlier and the calculated value was obtained using equation (30). From these graphs, we can see that the experimental data is statistically in agreement with the calculated value. This result is important for selecting of correct the pore size of the mesh for oil-water separation. It is clear from equation (30) that the intrusion pressure is inversely proportional to the pore size, D. If the intrusion pressure is small, the separation may fail as the impact force of the mixture fluctuates during the separation process.

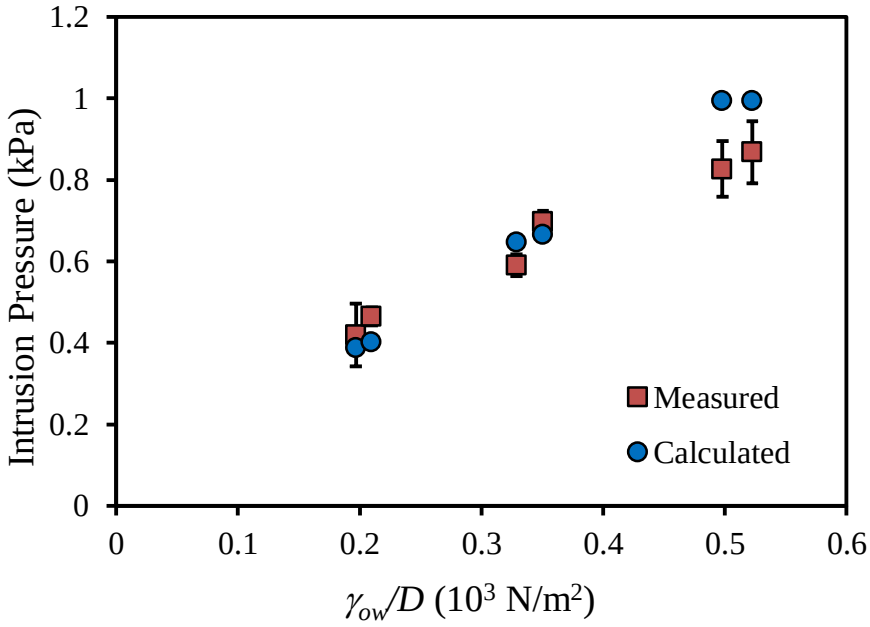

Figure 4- 49. The intrusion pressure of TiO_2 coated mesh with different pore sizes.

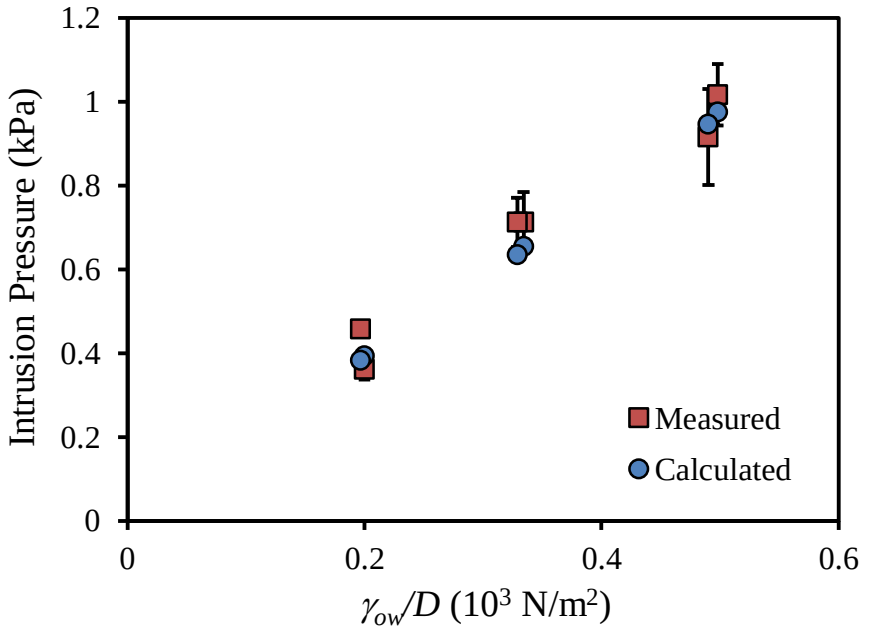

Figure 4- 50. The intrusion pressure of ZnO coated mesh with different pore sizes.

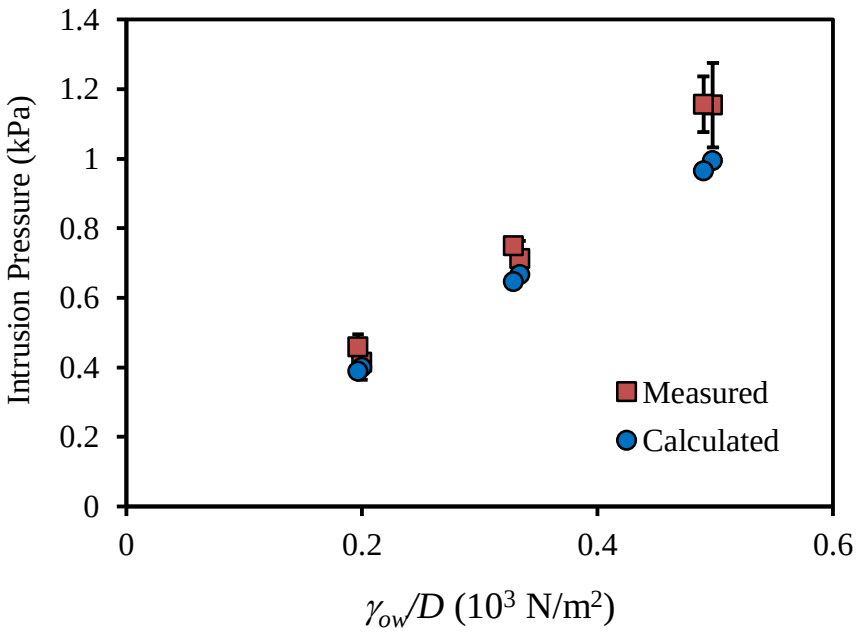

Figure 4- 51. The intrusion pressure of WO_3 coated mesh with different pore sizes.

CHAPTER 5

CONCLUSION AND RECOMMENDATION

5.1 Conclusion

We demonstrated the fabrication of the metal oxides films using spray deposition of nanoparticle dispersions. The nanoparticle used are well known photocatalytic materials such as TiO_2, ZnO and WO_3. The optimum dispersion concentration is 10 mg/ml prepared by mixing 0.10 g of nanoparticle in 10 ml of THF. The optimum annealing temperature is 550° C for 2 hours. The wettability of the TiO_2 and WO_3 films are superhydrophilic in air and oil, superoleophilic in air and superoleophobic in water. In oil environment, WO_3 films have better hydrophilicity than TiO_2 films. From the measurement of contact angle in air and in oil environment ZnO films are less hydrophilic than the other materials.

The films were applied for oil water separation with the average separation efficiency of 98.4 ± 0.6 % at the pore size of 50 μm. The maximum pore size can be used for oil water separation are different for different materials. For TiO_2 coated mesh, the maximum pore size can be applied is 102 μm, while for ZnO is 50 μm and for WO_3 is 152 μm. In this regard, further investigation need to be carried out to find out the reason for the difference of the applicable pore size for particular material. Presumably it is due to the difference in the wetting properties of the material. The more hydrophilic the material, the more robust the mesh will be for the oil-water separation.

It was revealed from this work that the oil-water separation works basically by harnessing the difference of the direction of the capillary forces of water phase and oil phase. Superhydrophilicity and underwater superoleophobicity are necessary but not sufficient criteria for oil water separation. Trapped water layer in the surface roughness plays important role for preventing the oil phase for intruding the materials. The presence of robust capillary bridge (water film) in porosity of the mesh is also essential for oil water separation. The capillary bridge acts like a semi permeable membrane which allows water phase to diffuse and permeates through the mesh and at the same time completely blocking the flow of the oil phase.

5.2 Future Work

Gravity driven oil-water separation using superhydrophilic-underwater superoleophobic mesh is considered as a new technology. To the best of our knowledge, we reported for the first time of the use of simple spray deposition of nanoparticle dispesion technique for this particular application. Also, there is no such report discussing about the utilization of WO3 for oil-water separation application. Further work is needed to explore more about this research area. The main advancement needed for this work are listed as the following.

1. Scaling up the oil-water separation system into an oil-water separator device for larger volume of the mixture.
2. The use of advanced setup which can be employed to measure high value of the intrusion pressure
3. The use of different mesh types rather than simple woven mesh and also different superhydrophilic materials which have not been tested such as F_2O_3, and Al_2O_3.

References

[1] Shannon, C.E.; , "Communication in the Presence of Noise," *Proceedings of the IRE* , vol.37, no.1, pp. 10- 21, Jan. 1949

[2] R. F. Harrington, "Effect of antenna size on gain, bandwidth, and efficiency," J. Res. Nat. Bureau Standards, vol. 64D, pp. 1–12, Jan.-Feb. 1960

[3] Gardner, W.; , "Spectral Correlation of Modulated Signals: Part I--Analog Modulation," *Communications, IEEE Transactions on* , vol.35, no.6, pp. 584-594, Jun 1987

[4] S. G. Wilson, Digital Modulation and Coding. Englewood Cliffs, NJ: Prentice-Hall, 1996.

[5] Murota, K.; Hirade, K.; , "GMSK Modulation for Digital Mobile Radio Telephony," *Communications, IEEE Transactions on* , vol.29, no.7, pp. 1044-1050, Jul 1981

Journal:

Author, A.; Author, B.; , "Title," *Journal Name* , vol.xx, no.xx, pp. xxxx-xxxx, Mon yearXXXX

Book:

A. A. Author, Title. City, State: Publisher, yearXXXX

[1.] J. M. Neff, Bioaccumulation in Marine Organisms. Effects of Contaminants from Oil Well Produced Water. Amsterdam: Elsevier Science Publisher, 2002

[2.] J. Duda, J. A. Veil, M. G. Puder, D. Elcock, & R. J. Redweik, A White Paper Describing Produced Water From Production Of Crude Oil, Natural Gas, And Coal Bed Methane. doi:10.2172/821666, 2004

[3.] Fakhru'l-Razi, A.; Pendashteh, A.; Abdullah, L.C.; Biak, D.R.A.; Madaeni, S.S.; Abidin, Z.Z.; , "Review of technologies for oil and gas produced water treatment," *Journal of hazardous materials* , vol. 170, no. 2-3, pp. 530-551. 2009

[4.] Bailey, B.; Crabtree, M.; Tyrie, J.; Elphick, J.; Kuchuk, F.; Romano, C.; and Roodhart, L.; , "Water Control," *Oilfield Review* , vol. 12, no. 1, pp. 30-51. 2000

[5.] M. Fingas, Oil Spill Science and Technology. Amsterdam: Elsevier Science Publisher, 2011

[6.] L. K. Wang, Y. T. Hung, N. K. Shammas, Advanced Physicochemical Treatment Processes. Totowa, NJ: Humana Press, 2006

[7.] A. F. Osamor, R. C. Ahlert, Oil/Water Separation: State of the Art. Cincinnati, OH: U.S. Environmental Protection Agency, 1978

[8.] Guix, M.; Orozco, J.; Garcia, M.; Gao, W.; Sattayasamitsathit, S.; Merkoči, A.; Wang, J.; , "Superhydrophobic alkanethiol-coated microsubmarines for effective removal of oil," *ACS Nano*, vol. 6, no. 5, pp. 4445-4451. 2012

[9.] Zhou, X.; Zhang, Z.; Xu, X.; Men, X.; & Zhu, X.; , "Facile fabrication of superhydrophobic sponge with selective absorption and collection of oil from water," *Ind. Eng. Chem. Res.*, vol. 52, no. 27, pp. 9411-9416. 2013

[10.] Zhu, Q.; Pan, Q.; & Liu, F.; , "Facile removal and collection of oils from water surfaces through superhydrophobic and superoleophilic sponges," *J. Phys. Chem. C*, vol. 115, no. 35, pp. 17464-17470. 2011

[11.] Feng, L.; Zhang, Z.; Mai, Z.; Ma, Y.; Liu, B.; Jiang, L.; & Zhu, D.; , "A super-hydrophobic and super-oleophilic coating mesh film for the separation of oil and water," *Angew. Chem. Int. Edit.*, vol. 43, no. 15, pp. 2012-2014. 2004

[12.] Wang, B.; & Guo, Z.; , "Superhydrophobic copper mesh films with rapid oil/water separation properties by electrochemical deposition inspired from butterfly wing," *Appl. Phys. Lett.*, vol. 103, no. 6, 2013

[13.] Choi, H.; & Moreau, J. P.; , "Oil sorption behavior of various sorbents studied by sorption capacity measurement and environmental scanning electron microscopy," *Microscopy Research and Technique*, vol. 25 no. 5-6, pp. 447-455. 1993

[14.] Wang, J.; Zheng, Y.; & Wang, A.; , "Superhydrophobic kapok fiber oil-absorbent: Preparation and high oil absorbency," *Chemical Engineering Journal*, vol. 213, pp. 1-7. 2012

[15.] Deschamps, G.; Caruel, H.; Borredon, M.; Bonnin, C.; & Vignoles, C.; , "Oil removal from water by selective sorption on hydrophobic cotton fibers. 1. study of sorption properties and comparison with other cotton fiber-based sorbents," *Environmental Science and Technology*, vol. 37, no. 5, pp. 1013-1015. 2003

[16.] Husseien, M.; Amer, A. A.; El-Maghraby, A.; & Taha, N. A.; , "Availability of barley straw application on oil spill clean up," *International Journal of Environmental Science and Technology*, vol. 6, no. 1, pp. 123-130. 2009

[17.] Reynolds, J. G.; Coronado, P. R.; & Hrubesh, L. W.; , "Hydrophobic aerogels for oil-spill clean up - synthesis and characterization." *Journal of Non-Crystalline Solids*, vol. 292, no. 1-3, pp. 127-137. 2001

[18.] Wang, D.; McLaughlin, E.; Pfeffer, R.; & Lin, Y. S.; , "Adsorption of oils from pure liquid and oil-water emulsion on hydrophobic silica aerogels," *Separation and Purification Technology*, vol. 99, pp. 28-35, 2012

[19.] Zhu, Q.; Pan, Q.; & Liu, F.; "Facile removal and collection of oils from water surfaces through superhydrophobic and superoleophilic sponges," *Journal of Physical Chemistry C*, vol. 115, no. 35, pp. 17464-17470. 2011

[20.] Yang, J.; Zhang, Z.; Xu, X.; Zhu, X.; Men, X.; & Zhou, X.; , "Superhydrophilic-superoleophobic coatings," *J. Mater. Chem.*, vol. 22, no. 7, pp. 2834-2837. 2012

[21.] Zhang, L.; Zhang, Z.; & Wang, P.; , "Smart surfaces with switchable superoleophilicity and superoleophobicity in aqueous media: Toward controllable oil/water separation," *NPG Asia Mater.*, vol. 4, no. 2, pp. 1-8. 2012

[22.] Kota, A. K.; Kwon, G.; Choi, W.; Mabry, J. M.; & Tuteja, A.; , "Hygro-responsive membranes for effective oil-water separation," *Nat. Commun.*, vol. 3, 2012

[23.] Kwon, G.; Kota, A. K.; Li, Y.; Sohani, A.; Mabry, J. M.; & Tuteja, A.; , "On-demand separation of oil-water mixtures," *Advanced Materials*, vol. 24, no. 27, pp. 3666-3671. 2012

[24.] Liu, M.; Wang, S.; Wei, Z.; Song, Y.; & Jiang, L.; , "Bioinspired design of a superoleophobic and low adhesive water/solid interface," *Adv. Mater.*, vol. 21, no. 6, pp. 665-669. 2009

[25.] Xue, Z.; Wang, S.; Lin, L.; Chen, L.; Liu, M.; Feng, L.; & Jiang, L.; "A novel superhydrophilic and underwater superoleophobic hydrogel-coated mesh for oil/water separation," *Adv. Mater.*, vol. 23, no. 37, pp. 4270-4273. 2011

[26.] Xue, Z.; Cao, Y.; Liu, N.; Feng, L.; & Jiang, L.; , "Special wettable materials for oil/water separation," *Journal of Materials Chemistry A*, vol. 2, no. 8, pp. 2445-2460. 2014

[27.] Li, H.; Li, Y.; & Liu, Q.; , "ZnO nanorod array-coated mesh film for the separation of water and oil," *Nanoscale Res. Lett.*, vol. 8 no. 1, pp. 1-6. 2013

[28.] Chen, Y.; Xue, Z.; Liu, N.; Lu, F.; Cao, Y.; Sun, Z.; & Feng, L.; , "Fabrication of a silica gel coated quartz fiber mesh for oil-water separation under strong acidic and concentrated salt conditions," *R. Soc. Chem. Adv.*, vol. 4, no. 22, pp. 11447-11450. 2014

[29.] Zhang, L.; Zhong, Y.; Cha, D.; & Wang, P.; , "A self-cleaning underwater superoleophobic mesh for oil-water separation," *Sci. Rep.*, vol. 3. 2013

[30.] Sawai, Y.; Nishimoto, S.; Kameshima, Y.; Fujii, E.; & Miyake, M.; "Photoinduced underwater superoleophobicity of TiO2 thin films," *Langmuir*, vol. 29, no. 23, pp. 6784-6789. 2013

[31.] Zeng, J.; & Guo, Z.; , "Superhydrophilic and underwater superoleophobic MFI zeolite-coated film for oil/water separation," *Colloid. Surface. A*, vol. 444, pp. 283-288. 2014

[32.] Tian, D.; Zhang, X.; Wang, X.; Zhai, J.; & Jiang, L.; , "Micro/nanoscale hierarchical structured ZnO mesh film for separation of water and oil," *Physical Chemistry Chemical Physics*, vol. 13, no. 32, pp. 14606-14610. 2011

[33.] Srinivasan, S.; Chhatre, S. S.; Mabry, J. M.; Cohen, R. E.; & McKinley, G. H.; , "Solution spraying of poly(methyl methacrylate) blends to fabricate microtextured, superoleophobic surfaces," *Polymer*, vol. 52, no. 14, pp. 3209-3218. 2011

[34.] Ogihara, H.; Xie, J.; & Saji, T.; , "Factors determining wettability of superhydrophobic paper prepared by spraying nanoparticle suspensions," *Colloids and Surfaces A: Physicochemical and Engineering Aspects*, vol. 434, pp. 35-41. 2013

[35.] S. M. Wagh, D. A. Deshpande, Essentials of Physics, Volume I. New Delhi: PHI Learning, 2013

[36.] H. J. Butt, K. Graf, M. Kappl, Physics and Chemistry of Interfaces. Weinheim: Wiley-VCH Verlag & Co. KGaA, 2003

[37.] Giesche, H.; , "Mercury porosimetry: a general (practical) overview," *Part. Part. Syst. Charact*. vol. 23, pp. 9-19. 2006

[38.] Schrader, M. E; , "Young-dupre revisited," *Langmuir*, vol. 11, no. 9, pp. 3585-3589. 1995

[39.] Gouin, H.; , "The wetting problem of fluids on solid surfaces. part 1: The dynamics of contact lines," *Continuum Mechanics and Thermodynamics*, vol. 15 no. 6, pp. 581-596. 2003

[40.] Kawase, T.; Fujii, T.; & Minagawa, M.; , "Repellency of textile assemblies. Part I: Apparent contact angle of wax-coated monofilament mesh screen," *Text. Res. J.*, vol. 57, no. 4, pp. 185-191. 1987

[41.] Michielsen, S.; & Lee, H. J.; , "Design of a superhydrophobic surface using woven structures," *Langmuir*, vol. 23, no. 11, pp. 6004-6010. 2007

[42.] Bhushan, B.; Nosonovsky, M.; & Jung, Y. C.; , "Lotus effect: Roughness-induced superhydrophobic surfaces," in B. Bhushan, *Nanotribology and Nanomechanics*, Heidelberg: Springer Berlin Heidelberg, pp. 995-1072. 2008

[43.] Feng, L.; Zhang, Y.; Xi, J.; Zhu, Y.; Wang, N.; Xia, F.; & Jiang, L.; , "Petal effect: A superhydrophobic state with high adhesive force," *Langmuir*, vol. 24, no. 8, pp. 4114-4119. 2008

[44.] Demond, A. H.; & Lindner, A. S.; , "Estimation of interfacial tension between organic liquids and water. Environmental Science and Technology," vol. 27, no. 12, pp. 2318-2331. 1993

[45.] Yoon, H.; Oostrom, M.; & Werth, C. J.; , "Estimation of interfacial tension between organic liquid mixtures and water," *Environ. Sci. Technol.*, vol. 43, no. 20, pp. 7754-7761. 2009

[46.] Good, R. J.; , "Contact angle, wetting, and adhesion: a critical review," *J. Adhes. Sci. Technol.*, vol. 6, no. 12, pp. 3-36. 1992

[47.] Grate, J. W.; Dehoff, K. J.; Warner, M. G.; Pittman, J. W.; Wietsma, T. W.; Zhang, C.; & Oostrom, M.; , "Correlation of oil-water and air-water contact angles of diverse silanized surfaces and relationship to fluid interfacial tensions," *Langmuir*, vol. 28, no. 18, pp. 7182-7188. 2012

[48.] Kawai, T.; & Sakata. T.; , "Conversion of carbohydrate into hydrogen fuel by a photocatalytic process," *Nature* vol. 286, no. 5772, pp. 474-476. 1980

[49.] Chen, D.; & Ray, A. K.; , "Removal of toxic metal ions from wastewater by semiconductor photocatalysis," *Chemical Engineering Science*, vol. 56, no. 4, pp. 1561-1570. 2001

[50.] Turchi, C. S.; & Ollis, D. F.; , "Photocatalytic degradation of organic water contaminants: Mechanisms involving hydroxyl radical attack," *Journal of Catalysis*, vol. 122, no. 1, pp. 178-192. 1990

[51.] Ni, M.; Leung, M. K. H.; Leung, D. Y. C.; & Sumathy, K.; , "A review and recent developments in photocatalytic water-splitting using TiO2 for hydrogen

production," *Renewable and Sustainable Energy Reviews*, vol. 11, no. 3 pp. 401-425. 2007

[52.] Wang, R.; Hashimoto, K.; Fujishima, A.; Chikuni, M.; Kojima, E.; Kitamura, A.; Watanabe, T.; , "Light-induced amphiphilic surfaces," *Nature*, vol. 388, no. 6641, pp. 431-432. 1997

[53.] Zhang, X.; Jin, M.; Liu, Z.; Nishimoto, S.; Saito, H.; Murakami, T.; & Fujishima, A.; , "Preparation and photocatalytic wettability conversion of TiO2-based superhydrophobic surfaces," *Langmuir*, vol. 22, no. 23, pp. 9477-9479. 2006

[54.] Hashimoto, K.; Irie, H.; & Fujishima, A.; , "TiO2 photocatalysis: A historical overview and future prospects," *Japanese Journal of Applied Physics, Part 1: Regular Papers and Short Notes and Review Papers*, vol. 44, no. 12, pp. 8269-8285. 2005

[55.] Zhang, L.; Zhao, N.; & Xu, J.; , "Fabrication and application of superhydrophilic surfaces: A review. Journal of Adhesion Science and Technology," vol. 28, no. 8-9, pp. 769-790. 2014

[56.] Zhang, J.; & Severtson, S. J.; , "Fabrication and use of artificial superhydrophilic surfaces," *Journal of Adhesion Science and Technology*, vol. 28, no. 8-9, pp. 751-768. 2014

[57.] Gondal, M. A.; Sadullah, M. S.; McKinley, G. H.; Varanasi, K. K.; & Panchanathan, D.; , "Photo-induced in situ switching of surface wettability of titania films under air and oil environment," *HONET-CNS 2013*, pp. 151-154. 2013

[58.] Bernagozzi, I.; Antonini, C.; Villa, F.; & Marengo, M.; , "Fabricating superhydrophobic aluminum: An optimized one-step wet synthesis using fluoroalkyl silane," *Colloids and Surfaces A: Physicochemical and Engineering Aspects*, vol. 441, pp. 919-924. 2014

[59.] Good, R. J.; & Islam, M.; , "Liquid bridges and the oil agglomeration method of coal beneficiation: An elementary theory of stability," *Langmuir*, vol. 7, no. 12, pp. 3219-3221. 1991

[60.] Halpegamage, S.; Tao, J.; Kramer, A.; Sutter, E.; & Batzill, M; , "Why is anatase a better photocatalyst than rutile? - Model studies on epitaxial TiO2 films," *Sci. Rep.*, vol 4, no. 4043. 2013

[61.] Chen, T. Y.; Tsamopoulos, J. A.; & Good, R. J.; , "Capillary bridges between parallel and non-parallel surfaces and their stability," *J. Colloid Interf. Sci.*, vol. 151, no. 1, pp. 49-69. 1992

[62.] Chen, P.; & Xu, Z.; , "Mineral-coated polymer membranes with superhydrophilicity and underwater superoleophobicity for effective oil/water separation," *Sci. Rep.*, vol. 3, 2013

Vita

Name	:MUHAMMAD SUBKHI SADULLAH
Nationality	:INDONESIAN
Date of Birth	:4/8/1988
Email	:muh.subkhi@gmail.com
Address	:Tembiring 06/III, Bintoro, Demak, Indonesia.
Academic Background	:B.Sc. in Physics from Diponegoro University

LIST OF PUBLICATIONS

Journal article:

Gondal, M. A., **Sadullah, M. S.**, Dastageer, M. A., McKinley, G. H., Panchanathan, D. Varanasi, K.K. Study of factors governing oil-water separation process using TiO_2 films prepared by spray deposition of nanoparticle dispersions, (2014). (Revision being submitted for *ACS Appl. Mater. Interfaces*)

Conference paper:

Gondal, M. A., **Sadullah, M. S.**, McKinley, G. H., Varanasi, K. K., & Panchanathan, D. Photo-induced in situ switching of surface wettability of titania films under air and oil environment. Paper presented at the*2013 High Capacity Optical Networks and Emerging/Enabling Technologies, HONET-CNS 2013*, 151-154 (2013).

Conference presentations and posters:

Gondal, M. A., Sadullah, M. S., McKinley, G. H., Varanasi, K. K., & Panchanathan, D. Facile method for fabrication of tio_2 films for underwater superoleophobic applications. *The Photocatalytic and Superhydrophilic Surfaces Workshop*, Manchester, United Kingdom (2013).

Sadullah, M. S., Gondal, M. A., McKinley, G. H., Varanasi, K. K., & Panchanathan, D. Photo-induced Superhydrophilicity and Underwater Oil Repellency of TiO_2 Films and Its Application for Oil Water Separation. *The Photocatalytic and Superhydrophilic Surfaces Workshop*, Manchester, United Kingdom (2013).

Sadullah, M. S., Gondal, M. A., Synthesis of superhydrophobic-oleophilic surfaces (films) for oil-water separation using solution spraying technique. The 9^{th} International Conference and Exhibition on Chemistry in Industry, Manama, Bahrain, (2013).

Working papers:

Gondal, M. A., **Sadullah, M. S.**, Dastageer, M. A., Designing gravity driven oil-water separator using WO_3 coated stainless steel mesh, (2014).

Gondal, M. A., **Sadullah, M. S.**, Dastageer, M. A., The comparison of oil-water separation performance of metal oxide (TiO_2, ZnO, and WO3) coated mesh prepared by spray deposition of nanoparticle dispersions, (2014).